From the Institute of Neuro- and Bioinformatics
of the University of Lübeck
Director: Prof. Dr. rer. nat. Thomas Martinetz

Thalamocortical dynamics and the effects of sensory stimulation during sleep

Dissertation
for Fulfillment of
Requirements
for the Doctoral Degree
of the University of Lübeck

from the Department of Computer Sciences / Engineering

Submitted by

Arne Weigenand
from Leipzig

Lübeck 2016

First referee: PD Dr. rer. nat. Jens Christian Claussen
Second referee: Prof. Dr. rer. nat. Thorsten M. Buzug
Chairman: Prof. Dr.-Ing. Alfred Mertins

Date of oral examination: 07.04.2017
Approved for printing. Lübeck, 26.10.2017

Contents

Abstract

This thesis investigates the major rhythms of the thalamocortical system during non-REM sleep – slow oscillations, K-complexes and sleep spindles. Alterations in these highly interesting dynamic phenomena are linked to many diseases and they are involved in the processes that lead to the consolidation of newly acquired memories and gist abstraction.

A promising research direction is the manipulation of these brain rhythms by external stimulation. In order to elucidate the causal role rhythms in brain function one may selectively suppress or enhance them. Models that capture the essential dynamics of slow oscillations and spindles would allow an optimization of stimulation protocols and deepen our understanding of disease mechanisms.

Here, we develop a series of models to describe the generation of the slow oscillation in brain slices in vitro and the electroencephalogram of humans during natural sleep and anesthesia. For the identification of dynamic regimes we derive a method that can estimate parameters in nonlinear stochastic dynamic systems from data.

First, the slow oscillation is regarded as phase oscillator and characterized in terms of its phase response curve. Second, a mechanistic neural mass model of the neocortex is presented that allows us to identify the dynamic determinants of K-complexes and slow oscillations. The proposed K-complex mechanism is further illustrated in a minimal model. In the following, we extend the cortical neural mass to a thalamocortical model that can generate sleep spindles and slow-wave activity and investigate its response to auditory stimulation. In particular, we reproduce EEG data from closed-loop auditory stimulation.

Finally, we used the thalamocortical model to design a new acoustic stimulation protocol which boosts slow oscillations and tested its effect on the consolidation of declarative memories in a sleep study in humans.

Zusammenfassung

Diese Arbeit untersucht die drei charakteristischsten Rhythmen des thalamokortischen Systems im Non-REM-Schlaf – langsame Oszillationen, K-Komplexe und Schlafspindeln. Viele neurologische Krankheiten sind von Veränderungen dieser interessanten dynamischen Phänomene begleitet und es wird vermutet, dass sie eine entscheidende Rolle in der Konsolidierung von neuen Gedächtnisinhalten und deren Abstraktion spielen.

Ein vielversprechender Forschungsansatz ist die Manipulation von Gehirnwellen mittels externer Stimulation. Dabei wird versucht langsame Oszillationen und Schlafspindeln selektiv zu unterdrücken oder zu verstärken um kausale Zusammenhänge zu Gehirnfunktionen herzustellen. Modelle, welche die zugrundeliegenden Prozesse abbilden, erlauben es Stimulationsprotokolle zu optimieren und einen tieferen Einblick in Krankheitsmechanismen zu erhalten.

Wir präsentieren Modelle, welche die Entstehung von langsamen Oszillationen in Hirnschnitten in vitro und im Elektroenzephalogramm des Menschen während des Schlafes und unter Anästhesie beschreiben. Um in diesen Modellen die zu den Daten passenden Schwingformen finden zu können, entwickeln wir eine Methode, welche aus Messdaten die Parameter von nichtlinearen stochastischen Systemen schätzt.

Zu Beginn approximieren wir die langsame Oszillation mit einem Phasenoszillator und bestimmen dessen Phasen-Antwort-Kurve. Wir entwickeln ein mechanistisches Feuerratenmodell des Neokortex, welches uns erlaubt die dynamischen Determinanten von K-Komplexen und langsamen Oszillationen zu identifizieren. Für den gefundenen K-Komplex-Mechanismus wird ein minmales Modell vorgeschlagen. Im Folgenden erweitern wir das Neokortex-Modell zu einem thalamokortischen System, das in der Lage ist Schlafspindeln, langsamwellige Aktivität und akustisch evozierte Potentiale zu generieren. Insbesondere gelingt es uns damit die Wirkung von phasenabhängiger akustischer Stimulation im EEG des Tiefschlafs abzubilden.

Abschließend benutzen wir das thalamokortische Modell um ein neues Stimulationsprotokoll zu entwerfen, welches langsame Oszillationen verstärkt, und untersuchen dessen Einfluss auf die Gedächtniskonsolidierung des Menschen in einer Schlafstudie.

Publications

Weigenand, A., Ngo, H.-V. V., Higgins, D., Martinetz, T., and Claussen, J. C. (2010). Switching between 'Up' and 'Down' states in a conductance-based cortex model. In *PROCEEDINGS OF BIOSIGNAL 2010*, Berlin.

Weigenand, A., Martinetz, T., and Claussen, J. C. (2012). The phase response of the cortical slow oscillation. *Cognitive Neurodynamics*, 6(4):367–375.

Weigenand, A.[1], Schellenberger Costa, M.[1], Ngo, H.-V. V., Claussen, J. C., and Martinetz, T. (2014). Characterization of K-Complexes and Slow Wave Activity in a Neural Mass Model. *PLoS Computational Biology*, 10(11):e1003923.

Schellenberger Costa, M.[1],**Weigenand, A.**[1], Ngo, H.-V. V., Marshall, L., Born, J., Martinetz, T., and Claussen, J. C. (2016). A Thalamocortical Neural Mass Model of the EEG during NREM Sleep and Its Response to Auditory Stimulation. *PLoS Computational Biology*, 12(9):e1005022.

Weigenand, A., Mölle, M., Werner, F., Martinetz, T., and Marshall, L. (2016). Timing matters: Open-loop stimulation does not improve overnight consolidation of word pairs in humans. *European Journal of Neuroscience*, 44(6):2357–2368.

---

[1]First authors

Acknowledgements

Abbreviations

DST	Digit span test
EEG	Electroencephalogram
EMG	Electromyogram
EOG	Electrooculogram
EPSP	Excitatory postsynaptic potential
FHN	Fitzhugh-Nagumo
IPSP	Inhibitory postsynaptic potential
ISI	Interstimulus interval
KC	K-complex
mPSP	Miniature postsynaptic potential
non-REM	Non-rapid eye movement
PAL	Paired-associate learning
PANAS	Positive and Negative Affect Schedule
pdf	Probability density function
PRC	Phase response curve
PSP	Postsynaptic potential
PVT	Psychomotor vigilance test
RE	Reticular
REM	rapid eye-movement
RWT	Regensburg Word Fluency Test
SF-A	Sleep questionnaire A
SO	Slow oscillation
SSS	Standford Sleepiness Scale
STD	Short-term depression
STDP	Spike-timing-dependent plasticity
SWA	Slow-wave activity
SWS	Slow-wave sleep
TC	Thalamocortical
tDCS	Transcranial direct current stimulation
TST	Total sleep time

1. Introduction

Sleep is a state of reduced responsiveness and behavioral activity. In humans it consists of three major stages, which alternate in a cyclic manner. About 50% of time asleep is spent in a light form of sleep, termed stage "N2". It generally precedes slow-wave sleep (SWS, about 20%), also called stage "N3", and rapid-eye-movement (REM) sleep (about 20%) (Figure 1.1).

Sleep stands out because it involves a reversible loss of consciousness. For some reason it is advantageous to decouple from the environment and spend one third of our lives in a vulnerable condition. Certain indispensable processes must take place that are incompatible with wake behavior or would degrade its performance (Tononi and Cirelli, 2014; Vyazovskiy and Harris, 2013).

Indeed, many studies indicate that sleep is important for the consolidation of newly acquired memories (Rasch and Born, 2013) and facilitates creative insight (Verleger et al., 2013). In particular, the consolidation of declarative memories seems to be linked to non-REM sleep, which comprises sleep stages N1, N2 and N3, and is characterized by the occurrence of sleep spindles, K-complexes and large amplitude slow oscillations (SO) in the EEG (Figure 1.2) (Yaroush et al., 1971; Fowler et al., 1973; Plihal and Born, 1997; Walker and Stickgold, 2004; Diekelmann and Born, 2010). Largely from research in amnesic patients it is known that newly acquired memories initially depend on the hippocampus and other parts of the medial temporal lobe (Squire, 2009). They only gradually become independent of this structure and transfer to a long-term store, e.g., the neocortex. In the process, memories are transformed to a gist-like, compressed representation (Winocur and Moscovitch, 2011; Dudai et al., 2015). A part of this transfer is thought to take place during slow-wave sleep and rely on the reactivation of cell assemblies that were involved in the wake experience (Wilson and McNaughton, 1994; Ji and Wilson, 2007; Ego-Stengel and Wilson, 2010; Bendor and Wilson, 2012). In the hippocampus, these reactivations occur within sharp wave-ripples, which are very fast $(100 - 300 \text{ Hz})$ oscillations in the local field potential (Buzsáki, 2015).
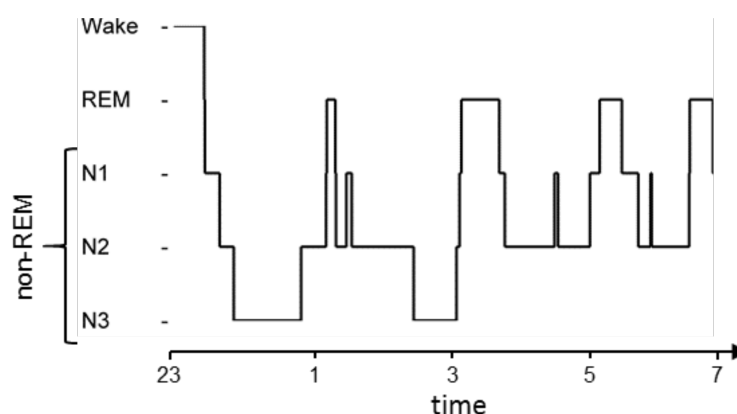
Figure 1.1.: Typical time course of sleep stages (hypnogram) of nocturnal sleep in humans. Slow-wave sleep (N3) dominates in the first half of the night, whereas REM sleep occurs mainly in the second half. Figure 1.2 shows typical EEG traces of each sleep stage.
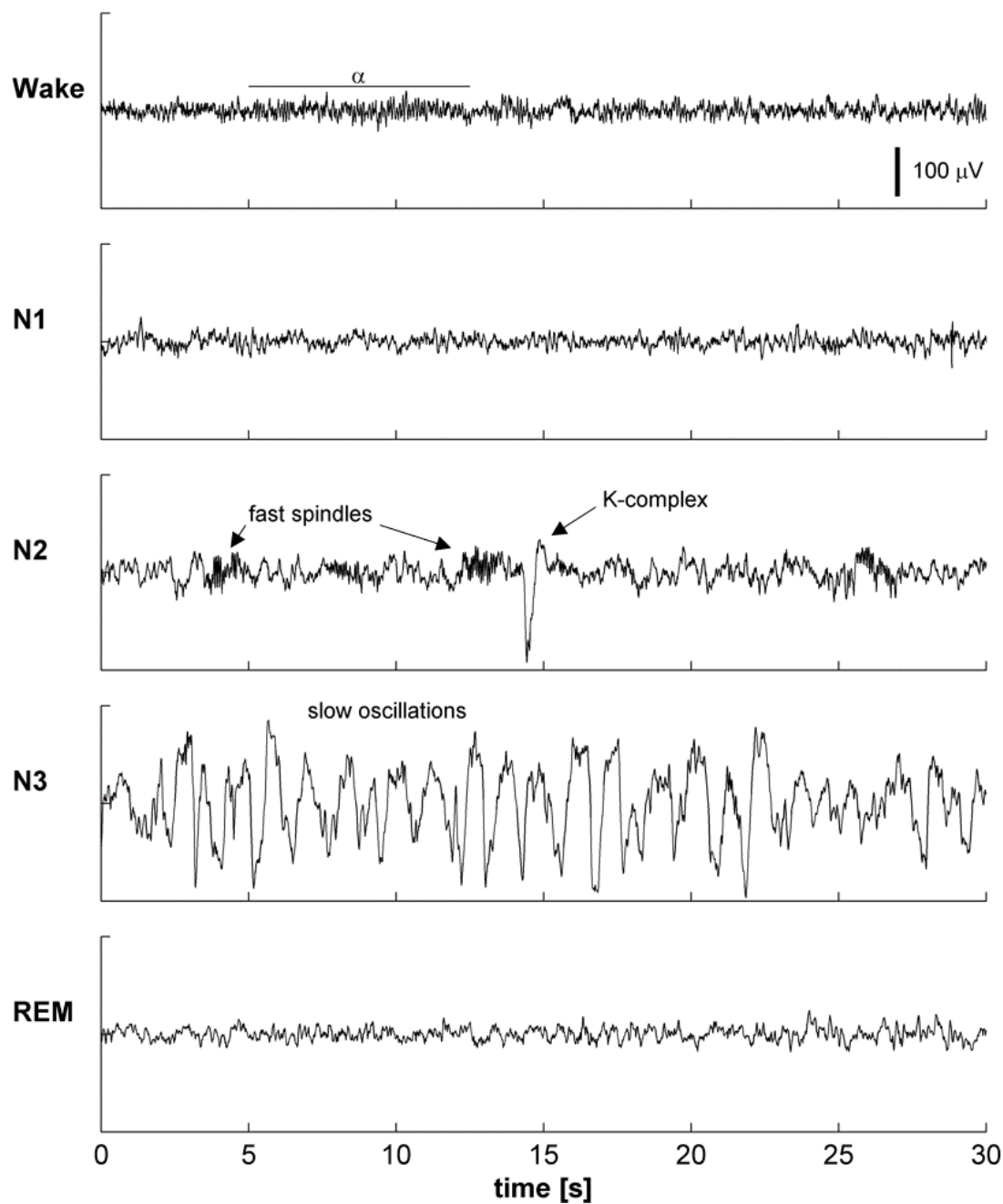
Figure 1.2.: Sleep stages in the EEG. Depicted are representative 30 second excerpts of a healthy human. Wake: low amplitude, broadband signal; with ocassional α rhyhthm. N1: less noisy appearance of the EEG and lower frequencies as compared to wake activity. N2: Further increase of low frequency components and larger amplitude as compared to N1. Appearance of spindles and large amplitude K-complexes. N3: The EEG is dominated (>20%) by large amplitude slow oscillations. Spindles are less visible due to diminished amplitude. REM: The EEG during REM is similar to wake and N1.

Several studies also report a positive correlation between the EEG signal power of spindles and overnight retention (Gais et al., 2002; Schabus et al., 2004; Fogel and Smith, 2011; Tamminen et al., 2013). Spindles and ripples can occur independently of SOs, but appear at a higher rate during the depolarized phases of SOs (Mölle et al., 2006; Clemens et al., 2007; Peyrache et al., 2011). Furthermore, ripples appear to be synchronized to the troughs of spindle oscillations (Sirota et al., 2003; Staresina et al., 2015). This temporal grouping has been suggested to be critical for hippocampus-dependent memory consolidation, as learning dependent increases in spindle activity are restricted to the SO up state (Mölle et al., 2011; Cox et al., 2012; Niknazar et al., 2015).

An interesting research direction is the manipulation of brain rhythms by external stimulation (Massimini et al., 2007; Bergmann et al., 2008; Marshall et al., 2006). In order to shed light onto the specific contributions of SOs, ripples and spindles to memory consolidation, one may selectively suppress or enhance them (Landsness et al., 2009; Girardeau et al., 2009; Ego-Stengel and Wilson, 2010). There is evidence that the efficacy of memory consolidation can be improved with oscillatory transcranial electric (Marshall et al., 2006; Antonenko et al., 2013) and auditory stimulation in synchrony with the brain's own rhythm (Ngo et al., 2013, 2015). Apart from their possible link to memory consolidation brain rhythms are interesting dynamic phenomena on their own and many diseases are linked to alterations in brain rhythms.

Much is known about the dynamics of the thalamocortical system during natural sleep, anesthesia and in slice preparations. However, its interaction with sensory stimuli is not fully understood.

Detailed knowledge of how different stimulation modalities effect critical brain rhythms would enable an optimization of stimulation protocols and consequently an advantage for experiments in basic research and clinical applications. Mathematical models and computational approaches can yield meaningful insights into the underlying dynamics as well as provide predictions for further experiments. This is the topic of the forthcoming chapters, with the focus on slow oscillations, K-complexes and spindles.

We develop a series of models to describe the generation of the slow oscillation in brain slices in vitro and the electroencephalogram of humans during natural sleep and anesthesia. For the identification of dynamic regimes we derive a method that can estimate parameters in nonlinear stochastic dynamic systems from data.

First, the slow oscillation is regarded as phase oscillator and characterized in terms of its phase response curve. Second, a mechanistic neural mass model of the neocortex is presented that allows us to identify the dynamic determinants of K-complexes and slow oscillations. The proposed K-complex mechanism is further illustrated in a minimal model. In the following, we extend the cortical neural mass to a thalamocortical model that can generate sleep spindles and slow-wave activity and investigate its response to auditory stimulation. In particular, we reproduce EEG data from closed-loop auditory stimulation. This validates our hypothesis on K-complex and slow oscillation dynamics.

Finally, we use the thalamocortical model to design a new acoustic stimulation protocol which boosts slow oscillations and tested its effect on the consolidation of declarative memories in a sleep study in humans.

1.1. Outline & main research questions

The first 5 chapters will deal with dynamics and models. The necessary theory will be introduced in the beginning of each chapter. Chapter 6 will turn to memory consolidation with an experiment.

Chapter 2: The cortical slow oscillation as phase oscillator.   How does stimulation affect the slow oscillation in brain slices in vitro? We validate a neural network and a mean-field model of slow oscillations by reproducing results of the stimulation experiment by Shu et al. (2003) and derive phase response curves, which characterize the effect of stimuli on the slow oscillation.

Chapter 3: Fitting models to time series of stochastic processes.   In this chapter, a method is presented to estimate parameters of nonlinear stochastic dynamic systems from data. This method will be used in subsequent chapters to infer dynamic regimes.

Chapter 4: A thalamocortical neural mass model of non-REM sleep.   What is a K-complex from a mathematical point of view? What is the difference between a K-complex and a slow oscillation? We find answers to these questions using neural mass models of the cortex, thalamus and the thalamocortical system. The models generate K-complexes, slow oscillations and sleep spindles and allow the investigation of responses to auditory stimulation during non-REM sleep. In particular, they reproduce EEG data from closed-loop auditory stimulation of a recent sleep study in humans (Ngo et al., 2013). We characterize K-complexes, slow oscillations and sleep spindles via bifurcation analysis.

Chapter 5: The K-complex in the Fitzhugh-Nagumo model.   What is the minimal model of a K-complex? Guided by the bifurcation structure derived in the previous chapter we show that the Fitzhugh-Nagumo model - a minimal model of canard explosions - can be regarded as such. A phase plane analysis allows novel predictions.

Chapter 6: Open-loop auditory stimulation during non-REM sleep and its effect on memory consolidation.   Can smartphones be used to boost memory? The application of auditory clicks during non-REM sleep phase-locked to the active state of the slow oscillation (closed-loop stimulation) has previously been shown to enhance the consolidation of declarative memories. We designed and applied sequences of three clicks during deep non-REM sleep to achieve a quasi-phase-dependent open-loop stimulation, without requiring the measurement of EEG signals.

Chapters 7 & 8   The thesis concludes with a summary of the main findings and directions for future work.

The remainder of this chapter will introduce the major dynamic phenomena of the thalamo-cortical system during non-REM sleep, i.e., slow oscillations, K-complexes, delta activity and sleep spindles, and their physiological basis, as this is the necessary foundation for modeling.

1.2. Slow oscillations & K-complexes

The EEG exhibits large amplitude oscillations at frequencies between 0.5 and 1 Hz during deep non-REM sleep (N3) and certain types of anesthesia, termed slow oscillations (SO). Underlying these SOs are widespread, almost synchronous, transient alternations of cortical networks between active ("up", depolarized) and silent ("down", hyperpolarized) states of activity, in which literally all cortical cells participate (Steriade et al., 1993b; Contreras and Steriade, 1995; Volgushev et al., 2006, 2011; Peyrache et al., 2012). Importantly, this phenomenon is not present in isolated cells but emerges only in large enough networks. Slow oscillations can be observed in subcortical structures, such as the thalamus, but are thought to be of cortical origin, because they are present in isolated cortical slabs in vivo (Timofeev et al., 2000), in cortical brain slices (Sanchez-Vives and McCormick, 2000; Sanchez-Vives et al., 2007), but absent in decorticated cats (Timofeev and Steriade, 1996).

Silent (down) state. Silent states are not maintained by active inhibition, but are periods of disfacilitation, i.e., there is no synaptic input anymore (Timofeev et al., 2001b). In natural sleep, they usually do not last longer than 100 - 500 ms (Chauvette et al., 2011). However, the duration can be of the order of tens of seconds under anesthesia and in slice preparations in vitro (Metherate and Ashe, 1993; Sanchez-Vives and McCormick, 2000; Cossart et al., 2003). Intracranial recordings in epileptic patients revealed a bi-modal distribution of active & silent state durations (Botella-Soler et al., 2012). As a result of active and silent states the distribution of the membrane potential becomes bimodal during non-REM sleep, whereas it is unimodal during wakefulness and REM sleep. Silent states do not occur in other states of vigilance than non-REM sleep (Steriade et al., 2001; Timofeev et al., 2001b; Mukovski et al., 2007; Rudolph et al., 2007).

Active (up) state. The active state is very similar to activity observed during wakefulness and is maintained by a balance of excitation and inhibition (Shu et al., 2003; Haider et al., 2006), which is a direct consequence of the saturating (sigmoidal) input-ouput relation of neurons (Abbott and van Vreeswijk, 1993; van Vreeswijk and Sompolinsky, 1998; Borisyuk and Kirillov, 1992). This and the bimodal membrane potential distribution lead to the view that slow oscillations reflect a bistability of cortical networks. During active states, spiking of pyramidal neurons was found to be sparse (<1 Hz) in epileptic patients and urethane anesthetized rats (Csercsa et al., 2010; Waters and Helmchen, 2006; Peyrache et al., 2012; Chen et al., 2011), but reached up to 40 Hz in naturally sleeping cats (Steriade et al., 2001) and is well above 1 Hz in the barrel cortex of naturally sleeping rats (Vijayan et al., 2010). This discrepancy stems from the layer that was recorded from and the influence of anesthetics. Neurons in superficial layers have lower firing rates than in deep layers (Sakata and Harris, 2009). On the population level, high-frequency (beta,gamma) oscillations are transiently expressed by cortical tissue during active states in natural sleep, anesthesia and in vitro (Le Van Quyen et al., 2010; Compte et al., 2008; Mukovski et al., 2007; Piantoni et al., 2013). Gamma activity has no effect on the duration of active states and is coincident with spindle oscillations during the rising phase a SO (Valencia et al., 2013; Piantoni et al., 2013; Ayoub et al., 2012). Beta activity transforms into gamma oscillation under slight membrane depolarization Steriade et al. (1996).

Both, AMPA and NMDA receptors at excitatory synapses, influence the maintenance of persistent activity, however, in a counter intuitive way. In vitro studies indicate that active states can be entirely mediated by slow NMDA-receptor excitation (Milojkovic et al., 2005, 2007; Antic et al., 2010; Castro-Alamancos and Favero, 2015). In contrast, fast AMPA excitation mainly drives feedforward inhibition, supressing active states (Favero and Castro-Alamancos,

2013). The level of both, excitatory and inhibitory, conductances decreases during an active state (Rudolph et al., 2007; Neske et al., 2015).

Transitions between active and silent states.   Several factors contributing to the switching between active and silent state have been examined in modeling and experimental studies, such as: arrival of excitation (Shu et al., 2003; Haider et al., 2006), synaptic depression (Bazhenov et al., 2002), synaptic facilitation (Melamed et al., 2008), thalamic disfacilitation (Contreras et al., 1996b), activation of Ca^{2+}/Na^{+}/ATP-dependent hyperpolarizing potassium currents (Compte et al., 2003; Sanchez-Vives and McCormick, 2000; Timofeev et al., 2001b; Cunningham et al., 2006) and extracellular potassium (Fröhlich et al., 2006) or calcium dynamics (Massimini and Amzica, 2001). The precise contributions of intrinsic versus synaptic factors have not been disentangled so far.

The noise floor necessary to trigger transitions from silent to active as well as active to silent states could be provided by a combination of miniature postsynaptic potentials (mPSPs) or asynchronously firing, persistently active, pacemaker-like neurons (Le Bon-Jego and Yuste, 2007). In fact, pyramidal neurons are submitted to an intense spontaneous, spike-independent synaptic bombardment (Paré et al., 1997). Furthermore, a distinct subgroup of intrinsically bursting layer V pyramidal neurons was found to influence the rhythmicity of active and silent state alterations in mouse brain slices in vitro (Lőrincz et al., 2015).

Role of extracortical inputs.   Input from subcortical structures can profoundly alter the expression of the slow oscillation (Sheroziya and Timofeev, 2014; Lemieux et al., 2014). The block of thalamic output to the neocortex significantly decreases the frequency of slow waves (Rigas and Castro-Alamancos, 2007; Hirata and Castro-Alamancos, 2010; David et al., 2013). External stimuli may affect cortical dynamics during deep sleep, however, the information content is masked by the stereotyped bursts of the relaying TC neurons. Paradoxically, it has been reported that cortical dynamics during active states are insensitive to thalamic inputs in thalamocortical slices of mouse somatosensory cortex in vitro (Watson et al., 2008).

Role of astrocytes.   Astrocytes have also been suspected to play a role in shaping slow-wave activity by tuning extracellular glutamate concentrations (Poskanzer and Yuste, 2011, 2016). Extracellular glutamate in turn can have a variety of effects on cortical pyramidal neurons, such as desensitization of glutamate receptors (Featherstone and Shippy, 2008), inhibition of several potassium channels (Anwyl, 1999) and generation of NMDA spikes (Chalifoux and Carter, 2011).

Origin, propagation and local regulation.   Slow oscillations can in principle be initiated everywhere on the cortex, but tend to propagate from medial frontal cortex to the medial temporal lobe and hippocampus (Nir et al., 2011). They were recorded in associative, motor, somatosensory, and visual cortices (Chauvette et al., 2011). Notably, at least one study in humans reports that not all cortical areas participate in the slow oscillation, in particular the cingulate gyrus and other deep midline structures (Wennberg, 2010). At the scalp level, slow oscillations seem to be global events that behave like traveling waves (Massimini et al., 2004; Murphy et al., 2009). However, intracranial recordings in humans and rodents reveal a different, more complex picture (Hangya et al., 2011; Mohajerani et al., 2010). Activity spreads along typical pathways and is determined by the cumulative drive of afferents that have just transitioned to

an active state (Fucke et al., 2011; Nir et al., 2011; Chauvette et al., 2010). Learning and intensive use leads to localized increases of slow-wave activity in human sleep (Huber et al., 2004, 2006).

Furthermore, in humans the origin of slow oscillations is age-dependent, moving from posterior cortical regions in early life to frontal regions during adolescence (Kurth et al., 2010).

Electrophysiological correlates.   In the local field potential, silent states appear as depth-positive and active states as depth-negative wave. However, the polarity reverses towards superficial layers. In the EEG, positive peaks correspond to depth-negative waves and vice versa (Nir et al., 2011; Csercsa et al., 2010; Cash et al., 2009; Wennberg, 2010). Note that this also depends on the location of the reference electrode.

K-complex.   The K-complex (KC) is an isolated sharp negative deflection in the EEG and occurs during light non-REM sleep (N2) at the pace of the intracellular SO (Amzica and Steriade, 1997b). It is often followed by a prominent positive half wave and a spindle oscillation (Mölle et al., 2002). Common variations of this theme are multiple peaks in the negative component or an initial positive bump before the negative-positive sequence. The K-complex has long been viewed as an independent phenomenon, but is now believed to be the EEG expression of an isolated silent state (Steriade and Amzica, 1998; Cash et al., 2009; Wennberg, 2010). The negative peak of the KC marks the transition to the cellular active state (Nir et al., 2011). The components of peripherally evoked KCs were found to have typical latencies, namely the P200, N550 and P900 peaks (Bastien et al., 2002; Laurino et al., 2014). It was suggested that these components are not independent and share a common generation mechanism. Sometimes later components (N1500, P1900) with smaller amplitude are reported too (Colrain, 2005).

1.3. Delta oscillations

Several sources contribute to the delta band ($1-4\,\text{Hz}$) in the EEG. One is of thalamic origin, the other is generated in the cortex. Furthermore, the non-sinusoidal wave form of the K-complex produces higher harmonics that lie in the delta band (Amzica and Steriade, 1997b).

Delta and slow oscillations represent two distinct phenomena. The latter declines in activity from the first to the second non-REM sleep episode, whereas the former does not (Achermann and Borbély, 1997).

Thalamic delta.   Thalamocortical (TC) neurons in the thalamus are able to generate a stereotyped, clock-like delta rhythm in isolation via an interplay between their low-threshold Ca^{2+} current, I_T, and the hyperpolarization-activated cation current, I_h (Steriade et al., 1993a). It was also shown that at a certain level of leak current, the "window" component of I_T in TC neurons may create delta oscillations (Williams et al., 1997).

Due to the lack of connectivity between thalamocortical neurons, those oscillations in general do not synchronize on their own (Timofeev and Steriade, 1996). External signals such as K-complexes or slow oscillations, however, do exert a synchronizing influence on thalamocortical neurons. They in turn project to the cortex, where they may lead to switching between active and silent states at the frequency of the delta volley. The thalamus perceives cortical silent states as a cessation of excitatory inputs that causes a hyperpolarization. Simulations suggest, that self-sustained delta oscillations can easily be reset to a new phase by cortical input (Lytton et al., 1996).

Delta oscillations also possess a sleep stage dependence, which might be related to the slowing of K-complexes with deepening of sleep (Amzica and Steriade, 1998; Olbrich and Achermann, 2005). The frequency of the TC delta oscillation is increased at more negative membrane voltage (Dossi et al., 1992).

Delta oscillations are generated at a more negative voltage than spindles (Steriade et al., 1991, 1993a). The prerequisite for the appearance of delta waves in TC neurons is the hyperpolarization to levels between -65 and -90 mV, so that I_T is deinactivated sufficiently (McCormick and Pape, 1990; Leresche et al., 1991; Soltesz et al., 1991; Dossi et al., 1992). On average it starts at -71 mV. Beyond -90 mV no delta oscillation is observed (Steriade, 2003; Dossi et al., 1992). Moreover, delta oscillations and spindles oscillations were postulated to be mutually exclusive (Nunez et al., 1992).

Cortical delta. Another delta oscillation is presumably generated within the cortex, because it can be recorded even after extensive thalamectomy (Ball et al., 1977; Villablanca, 1972). Combined EEG/PET and EEG/fMRI studies found strong association of EEG delta activity with activity in ventromedial prefrontal regions. (Dang-Vu et al., 2005, 2008). A recent in vitro study in cortical slices of the rat also demonstrated the ability of isolated cortical tissue to generate a delta rhythm (Carracedo et al., 2013). There is evidence that cortical delta is driven by a population of intrinsically bursting neurons, which discharges at 3-4 Hz upon depolarization (Amzica and Steriade, 1998). An interesting observation comes from Steriade (2003), who noted that depth-positive delta waves are associated with a diminished discharge rate or even firing suppression that is generated by summation of long-lasting afterhyperpolarizations (AHPs) produced by a variety of K^+ currents in deeply lying pyramidal neurons (Schwindt et al., 1988a,b).

1.4. Spindle oscillations

Spindle oscillations are field potentials in the EEG with a frequency of 9-15 Hz and a bell shaped amplitude envelope, similar to Gabor wavelets (Figure 1.2). They last 0.5-3 s, recur every 4-15 s and are typically observed during the light stages of non-REM sleep (N2), often during the active phases of slow oscillations (Achermann and Borbély, 1997; Olbrich and Achermann, 2008; Panas et al., 2013). In vivo, in vitro, and modeling studies suggest that the minimal substrate contributing to the generation of spindle oscillations is the thalamus (Steriade and Deschenes, 1984; Steriade et al., 1985, 1987; Steriade and Llinás, 1988; Von Krosigk et al., 1993). Spindles are also visible in the hippocampus (Sullivan et al., 2014; Andrillon et al., 2011).

Generation of spindle oscillations. The ”classic“ theory of sleep spindle generation is by the reciprocal interaction of inhibitory reticular thalamic (RE) and excitatory thalamocortical (TC) neurons (Timofeev and Bazhenov, 2005). A spontaneous burst in the RE population causes hyperpolarization in the TC population, which deinactivates its T-type calcium current. Upon release from inhibition a rebound of activity occurs that in turn drives the RE population to produce another burst. Oscillations at spindle frequency may be sustained in an isolated network of RE neurons (Steriade et al., 1987; Destexhe et al., 1994; Golomb et al., 1994), but see Ulrich and Huguenard (1997) for a study that argues against this possibility. Underlying the ability of TC and RE cells to produce rhythmic burst activity is the presence of a T-type Ca^{2+} current, which deinactivates upon hyperpolarization (Huguenard, 1996; Astori et al., 2011).

Subsequent excitation causes the transient activation of this current, which leads to a slow depolarization called the low-threshold spike (LTS) (Llinás and Jahnsen, 1982). The LTS is often crowned by 2-5 fast Na$^+$ spikes, at a rate of ≈ 300 Hz (Nunez et al., 1992). The hyperpolarizing drive to keep this machinery going is provided by a potassium leak current, whose conductance is increased due to lowered acetylcholine levels during non-REM sleep (Steriade et al., 1990). Besides the T-type current, Ca^{2+}-dependent small-conductance (SK)-type K$^+$ channels and sarco/endoplasmic reticulum Ca^{2+}-ATPases have also been shown to significantly impact the burst behavior of RE cells (Cueni et al., 2008). Interestingly, a study in knock-out mice lacking T-type Ca^{2+} channels in TC nerons reported normal spindle activity despite the absence of LTS (Lee et al., 2013).

Termination of spindle sequences. Several mechanisms have been suggested for the termination of a spindle sequence. Intrinsic slow activity-dependent positive feedback in either TC (Destexhe et al., 1996a; Bal and McCormick, 1996; Lüthi and McCormick, 1998, 1999) or RE cells (Kim and Mccormick, 1998) during spindle oscillations increasingly counteracts their ability to produce a LTS and determine the inter-spindle lull (Contreras et al., 1997; Destexhe and Sejnowski, 2003; Timofeev and Bazhenov, 2005). In TC cells, this is mediated by a hyperpolarization-activated cation current, I_{h}. However, up-regulation of I_h alone was insufficient to terminate spindling (Steriade, 2003).

Another important source of spindle desynchronization is thought to be the corticothalamic input, which progressively increases during a spindle. In cats anesthetized with ketamine-xylazine, the length of spindles is less than 400 ms, while after decortication spindles last more than 1 second (Timofeev et al., 2001a; Bonjean et al., 2011).

In contrast, a recent study during natural sleep in vivo indicates that termination of spindles is controlled by inhibition from the reticular nucleus, which in turn depends on network state (Barthó et al., 2014). The precise mechanism remained unclear. A possible explanation comes from a theoretical investigation by Langdon et al. (2012). There it was shown that the reticular nucleus is multistable and can switch between a homogenous oscillatory state, mutli-cluster oscillations and silence. Furthermore, the inhibition involved may not be synaptic, but extra-synaptic (Rovó et al., 2014).

Interaction with slow oscillation. Similar to slow oscillations, the full expression of spindle rhythms depends on the interplay of the thalamus and neocortex (Bonjean et al., 2011; David et al., 2013; Sheroziya and Timofeev, 2014). Cortical input synchronizes spindles locally (Contreras et al., 1996a; Contreras and Steriade, 1996; Contreras et al., 1997) and is effective in initiating spindles in the RE nucleus (Steriade et al., 1993a).

Spindle types. Despite the synchronizing influence of slow oscillations, spindle oscillations often occur independently and localized in different brain regions (Nir et al., 2011; Andrillon et al., 2011; Frauscher et al., 2015; Peter-Derex et al., 2012), which might in part be due to the existence of several distinct thalamic nuclei (Jones, 2001, 2002; Groh et al., 2014; Sherman, 2005; Slezia et al., 2011; Sheroziya and Timofeev, 2014). Topographically specific sleep spindles have also been found in mice (Kim et al., 2015).

At least two major types of spindles can be distinguished, which differ in frequency, topography and possibly function: slow spindles (9-12 Hz), that are found at frontal cortical sites, and fast spindles (12-15 Hz) with centro-parietal prevalence (Jobert et al., 1992; Żygierewicz et al., 1999; Anderer et al., 2001).

The mechanisms of these two types of spindles appear to be different. The fast spindles are usually triggered at a transition from silent to active states of the SO (Mölle et al., 2002), but slow spindles are usually either independent of the SO or their onset is at a transition from active to silent states (Mölle et al., 2011). Whether there is a temporal relation such that slow spindles precede fast spindles or the other way around is still not resolved. Many studies conclude that fast spindles occur before slow spindles (Andrillon et al., 2011; Mölle et al., 2011), but at least in auditory evoked responses, slow spindles precede fast spindles (Weigenand et al., 2016). Optogenetic excitation of reticular thalamic nucleus neurons in mice triggered spindle activities in the somatosensory cortex without any spindle oscillation in the corresponding thalamic nuclei (Halassa et al., 2011). Systemic administration of the T-type Ca^{2+}-current antagonist flunarizine reduced only fast spindles suggesting the classic mechanism of generation was disturbed. In contrast, administration of the voltage-dependent Na^+ channels antagonist carbamazepine increased only slow spindles (Ayoub et al., 2013). Therefore, only properties of fast spindles correspond to the classic mechanism. The mechanisms of generation of slow spindles remain to be investigated.

Sleep stage dependence.   The frequency of fast spindles exhibits a sleep stage dependence, with lower frequencies at deeper sleep stages, which leads to a U-shape in the spectrogram when going from light non-REM to deep non-REM and back to a lighter sleep stage (Himanen et al., 2002; Olbrich and Achermann, 2005). Their density is maximal in sleep stage N2 and increases during the course of the night (Dijk et al., 1993; Knoblauch et al., 2003; Olbrich and Achermann, 2008; Nir et al., 2011).

1.5. Models of the cortical slow oscillation

From experiments it is clear that bistability or transient switching to active or silent states is not an intrinsic property of single neurons, but mediated by some kind of network effect. Firing during the active state of slow oscillations must be asynchronous and firing rates must be in a reasonably low range (1-50 Hz). Furthermore, transitions to the active state should occur (quasi) synchronously across the whole network, not restricted to localized parts of it.

Sustained firing has been proposed to be a result of recurrent activity and is the expression of network attractors. Models of slow oscillations can be classified by how these attractors are initiated, maintained and terminated in cortical circuits. In general, self-sustained oscillations involve a positive and a negative feedback loop at different time scales. The negative feedback loop is either mediated by activity-dependent hyperpolarizing currents (additive), synaptic (multiplicative) adaptation or feedforward inhibition via an inhibitory neuron population. A negative feedback loop is not required if transitions between states are noise driven (Figure 1.3).

Different model types can be used to answer different questions. While biologically realistic network models allow to relate to intracellular data, investigate the time course of membrane potentials, timing of synaptic inputs, synchrony, correlations etc. they are hard to analyze and tend to obscure the mechanisms that determine their dynamics. Rate models and their relatives, neural mass models and mean-field models, on the other side often allow exact and comprehensive statements about the dynamic repertoir of a model and the stability of states via bifurcation analysis. They have shown great success in elucidating the generation of brain rhythms and evoked responses of the awake brain (Wilson and Cowan, 1973; Lopes da Silva et al., 1974; Jansen et al., 1993; Kerr et al., 2007). They describe the dynamics of a large number of cells

Relaxation oscillations
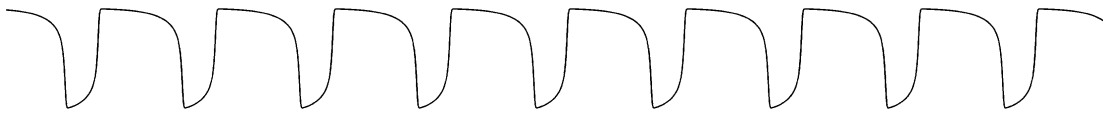
Hopf oscillations

Bistable system with noise driven transitions
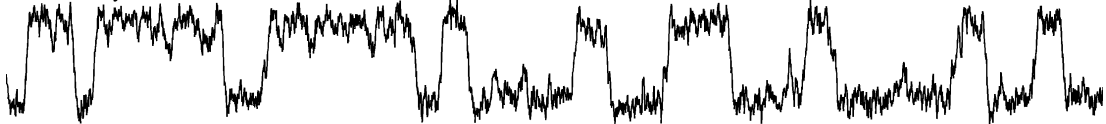
Figure 1.3.: Illustration of oscillation types. Relaxation oscillations: typically nonsinusoidal oscillations, where slow drifts (relaxation) alternate with quick transitions between states. Hopf oscillation: a more sinusoidal oscillation compare to relaxation oscillations. Noise driven transitions: although not a true oscillation, frequent noise driven transitions between stable states may appear oscillatory.

by the evolution of a single population average and provide an output which directly relates to EEG signals (Coombes, 2005; Deco et al., 2008).

Spike-dependent adaptation. Activity-dependent feedback via slow potassium channels has been suggested as a mechanism for the generation of SOs and KCs because of their sensitivity to the sleep related neuromodulator acetylcholine and their implication in the slow afterhyperpolarization (Steriade et al., 1993b; Hasselmo and Giocomo, 2006).

Timofeev et al. (2000) developed a cortical model of the slow oscillation comprising pyramidal and interneurons, AMPA and $GABA_A$ synapses with short-term depression (STD) (Tsodyks et al., 1998). It is based on observations from isolated cortical slabs in cats. The transition to the active state was achieved by spontaneously (stochastically) occuring miniature PSPs (excitatory and inhibitory) (Bekkers and Stevens, 1995), which can increase the membrane potential so much that a persistent sodium current, $I_{Na(p)}$, (Kay et al., 1998; Alzheimer et al., 1993) is activated, which in turn drives spiking. Termination of active states was proposed to be mediated by slow adaptation currents, such as a Ca^{2+}-dependent K^+ current, and synaptic depression.

The model of Bazhenov et al. (2002) builds on the same mechanisms as (Timofeev et al., 2000) and extends it to a thalamocortical network model, with additional slow NMDA and $GABA_B$ conductances. The thalamus model consists of RE and TC neurons, which contained I_T and I_h currents for the "classic" spindle generation mechanism.

Bonjean et al. (2012) extended the model of Bazhenov et al. (2002) to have 3 cortical layers (layer II/III/IV, layer V, layer VI) and distinguished between thalamic core and matrix subpopulations, which project to different cortical layers. A version with only two cortical layers was subsequently used by Chen et al. (2012) to highlight the role of the inhibitory population in active state termination. Both, increased feedforward inhibition and increased excitability of interneurons lead to higher synchrony of active to silent transitions.

Wei et al. (2016) added spike-timing-dependent plasticity (STDP) to the model of Bonjean et al. (2012) in order to explain the influence of hippocampal replay on the formation of spike

patterns and, thus, memory consolidation.

The model of Compte et al. (2003) is very similar to Bazhenov et al. (2002), but restricted to the cortex and based on in vitro data from ferret visual cortex slices (Sanchez-Vives and Mc-Cormick, 2000). It does not include mPSPs and no short-term depression. Activity in the network is initiated by neurons, which spontaneously fire due to higher intrinsic excitability (pacemaker neurons). Among others channels, the model additionally includes a Na^+-dependent K^+ current as slow activity-dependent adaptation mechanism. Although it was not explicitly implemented, the model exhibits rhythmicity in the beta and gamma range during active states (Compte et al., 2008). Isolated model neurons were only weakly correlated with the global rhythm, as it was in measurements. Furthermore, it successfully captures modulation of active states by changes in synaptic inhibition (Sanchez-Vives et al., 2010) and propagation speed (Sanchez-Vives et al., 2008).

A version with simplified synapses (instantaneous rise, exponential decay) was used to reproduce the effects of weak electric fields on the slow oscillation in vitro (Fröhlich and Mc-Cormick, 2010).

Short-term depression was added to the version of Compte et al. (2003) by Benita et al. (2012) to study the different expression of short-term depression between active and silent states observed by Reig and Sanchez-Vives (2007). Interestingly, an increase of short-term depression lead to a stabilization of active states and abolished silent states. Decreasing synaptic depression resulted in higher firing rates of both excitatory and inhibitory neurons, which shortened active states due to larger slow acitivity-dependent potassium conductances.

An elaborate thalamocortical model comprising two visual cortical areas with three layers and associated thalmocortical and thalamic reticular nuclei is presented in Hill and Tononi (2005). A change in leak conductance counteracts excitation and brings the system into a state where transitions to silent states are possible. As in (Compte et al., 2003) and Bazhenov et al. (2002) depolarization/activity-dependent currents build up during the active state and lead to its termination, together with short-term synaptic depression. A persistent sodium current helps to maintain the active state, but is primarily needed for its initiation, together with a hyperpolarization activated current. Sources of noise are mPSPs as well as external Poisson input.

The model was subsequently used by Esser et al. (2007) to model the impact of decreased synaptic strength on the properties of slow oscillations and its EEG correlates. In Olcese et al. (2010) this effect was achieved using STDP in the same model.

Activity-dependent adaptation.   The main criticism regarding a spike-dependent adaptation mechanism is that firing rates during active states are usually low so that adaptation would not be sufficient to cause transitions to the silent state. However, activity-dependent mechanisms can also simply be based on depolarization, not requiring spiking.

Ghorbani et al. (2012) developed a rate model encompassing an excitatory and an inhibitory population that is capable of slow oscillatory activity. Instead of deploying synaptic or somatic adaptation they postulate a mechanism that mimics dendritic spike-frequency adaptation and only affects excitatory-excitatory synapses. Nevertheless, this approach is analogous to the synaptic depression mechanism deployed in Holcman and Tsodyks (2006). Only the functional form differs slightly, by an additional sigmoidal nonlinearity. The noise free model performs chaotic relaxation oscillations (Figure 1.3) - a property inherited by the multiplicative adaptation mechanism (Cortes et al., 2013). The active state is close to a Hopf bifurcation, which may induce prominent afteroscillations in the gamma range upon transition to the active state.

A slow activity-dependent ionic mechanism has also been incorporated in the mean-field model introduced by Molaee-Ardekani (2007), where it modulates the shape of the sigmoidal firing rate function.

Curto et al. (2009) used the Fitzhugh-Nagumo model to investigate dynamics of multiunit activity in auditory cortex of urethane-anesthetized rats, as phenomenological approach motivated by heuristic arguments. Basically, the model provides a rich set of dynamics, e.g., bistability, and fits the data surprisingly well. In hindsight the model could be interpreted as one dimensional rate model with slow negative feedback, as in (Compte et al., 2003) and Bazhenov et al. (2002).

Mattia and Sanchez-Vives (2011) use network simulations and a simple rate model to emphasize the necessity of some activity-dependent mechanism, synaptic or somatic, in addition to bistability to achieve temporal correlations in the durations of active and silent states and to produce regimes akin to relaxation oscillations. This way an anti-correlation between active and silent state durations can be produced, as has been observed for the very regular slow oscillation activity in ferret brain slices in vitro.

Short-term depression.   (Holcman and Tsodyks, 2006) use a noise driven rate model with one equation describing the mean activity of an excitatory population and a second equation for the mean rate of synaptic depression, based on a phenomenological model for short-term plasticity Markram et al. (1997); Tsodyks et al. (1998). Among other regimes, the model can have two stable fixed points, separated by an unstable limit cylce around the active state. This limit cycle may lead to large population spikes when the silent state gets sufficiently perturbed. During a spike, noise may push the system into the basin of attraction of the active state, which generates a typical overshoot on the transition from silent to active states. The presence of the limit cycle also leads to noise driven oscillations when in the active state. Transitions between states are purely noise driven. They report that adding an inhibitory population does not change their results qualitatively. Notably, network models with similar mechanisms are used to explain working memory (Barak and Tsodyks, 2007; Mongillo et al., 2008).

Deploying a synaptic short-term depression mechanism Millman et al. (2010) demonstrate in a noise driven network of excitatory leaky integrate-and-fire neurons that active states exhibit self-organized criticality and neural avalanches. In their model active state durations are also exponentially distributed.

Mejias et al. (2010) analyze a bistable rate model model conceptually equivalent to that of Holcman and Tsodyks (2006), but contains an additional noise term in the equation for synaptic depression. They show that in this model active state dynamics can be described by an Ornstein-Uhlenbeck process and derive analytical solutions for the distribution of active state durations - a power law with exponent $-3/2$. Without noisy synapses the distribution would be exponential. A regime with well defined active state duration can also be found.

Short-term facilitation and feedforward inhibition.   Holcman and Tsodyks (2006) also investigated the emergence of bistability in a noise-free, wilson-cowan type firing rate model with facilitating excitatory synapses onto interneurons (Melamed et al., 2008), which have been observed in animal studies (Silberberg and Markram, 2007; Reyes et al., 1998; Thomson et al., 1993; Markram et al., 1998). The same model of short-term plasticity was used as in Holcman and Tsodyks (2006); Tsodyks et al. (1998). They show that such feedforward inhibition shapes the frequency of slow oscillations and determines the profile of active and silent states. The transition from silent to active states occurs via increased excitability and

low inhibition in the network, similar to the model by Compte et al. (2003). Up states terminate due to increased feedforward inhibition, as in (Parga and Abbott, 2007; Chen et al., 2012; Krishnamurthy et al., 2012). As there is no noise input to the model it oscillates regularly between active and silent states, as in relaxation oscillations. The authors point out that inhibitory conductance increases throughout the active state, which is in contrast with experimental observations (Contreras et al., 1996b; Shu et al., 2003; Neske et al., 2015).

Interestingly, feedforward inhibition involving NMDA receptors and intrinsically bursting interneurons has been reported to be responsible for the generation of cortical delta oscillations in vitro Carracedo et al. (2013).

Krishnamurthy et al. (2012) build on the same mechanism as Melamed et al. (2008), but use a neural network with two interneuron populations, one connected via depressing, the other by facilitating synapses. They show that the population receiving depressing excitatory synapses has a high firing rate at the beginning of the active state, while the population receiving facilitating synapses fires later in the slow oscillation cycle and tends to terminate the active state.

Increasing the time constant of inhibitory synaptic connections is the mechanism that is used to induce slow oscillatory activity in some neural mass models of anesthesia (Steyn-Ross et al., 2013, 1999; Wilson et al., 2005). The increased time constant spreads inhibition in time and allows recurrent excitation to build up. The delayed impact of inhibition causes the destabilization of the active state.

Intrinsic nonlinearity.　Parga and Abbott (2007) examine a network of excitatory and inhibitory integrate-and-fire neurons endowed with a cubic nonlinearity and static synapses. The cubic nonlinearity leads to bistability in connection with synaptic currents induced by population activity. There is no bistability in isolated neurons. Noise drives the transitions between active and silent states and the network is truly bistable, i.e., no oscillatory regime or canard explosions were reported. As in other models (Compte et al., 2003; Hill and Tononi, 2005; Kang et al., 2004) some neurons are persistently active due to randomness in the parameters and lead the whole network into the active state.

Importantly, only inhibition seems to be able to induce a switch from the active to the silent state, which is at odds with experimental observations (Shu et al., 2003). There remains the possibility that this is only due to the specific choices of parameters and short stimuli used. The model contains spike-frequency adaptation, which should be able to shift the excitation/inhibition balance upon an extended excitatory stimulus. However, spike-frequency adaptation is actually not the critical component of the proposed mechanism.

Deco et al. (2009) use a data driven approach to capture the slow oscillation dynamics underlying intracellular recordings of slow oscillations. They assume a one dimensional stochastic rate model with piecewise quadratic nonlinearity, that efficiently parameterizes doublewell-like energy functions. Hence, the system allows the presence of several fixed points, but no other bifurcations/oscillations are present. Transitions between attractor states are purely driven by noise. The fitted model accurately captures the distribution of durations of active and silent states for light ketamine-xylacine anesthesia in rats, but deviates for deep anesthesia.

A large set of mechanisms leading to slow oscillations has been investigated. However, little work has been done in trying to find unique signatures that can unambiguously distinguish between them. In the neural mass framework somatic (additive) and synaptic (multiplicative) adaptation mechanisms have been discussed by Loxley and Robinson (2007). An attempt to distinguish the contributions of additive and multiplicative adaptation in slow oscillation generation has been presented by Tabak et al. (2011).

2. Model I: The cortical slow oscillation as phase oscillator

Parts of this chapter have been published in Weigenand et al. (2012). Networks of neurons can be approximated as one large oscillator, if they exhibit collective oscillations (Grannan et al., 1993). Indeed, the cortical slow oscillation can be very regular in brain slices and under deep anesthesia, with pronounced peaks in the distribution of durations of up and down states (Deco et al., 2009; Steriade, 2006). In this chapter we regard the neural substrate underlying slow oscillations as phase oscillator and obtain, based on computational models, predictions for the phase response curve (PRC) of mammalian cortex during deep sleep or deep anesthesia for a wide range of stimulus strengths.

The PRC is a map that describes how an oscillating system reacts in response to single pulses (Granada et al., 2009). Phase oscillator models have a long tradition and were successfully applied to study the interaction between systems (Acebrón et al., 2005; Smeal et al., 2010). Knowing the PRC one has a valuable tool to analyze the influence of external stimulation, e.g., electric, magnetic or sensory stimulation, on cortical sleep rhythms and also to investigate the interaction of the sleeping cortex with other brain structures, like hippocampus and thalamus. These interactions are assumed to be of substantial relevance for memory consolidation and transfer of memories between brain regions (Peyrache et al., 2009). However, only few analytical results exist for the PRCs of ensembles of oscillators (Levnajić and Pikovsky, 2010; Ko and Ermentrout, 2009; Kori et al., 2009). Here, we numerically study the case where the collective rhythm is a network effect and is not present in the isolated elements of the network.

The basic dynamics of slow oscillations can be modeled by a discrete-time integrate-and-fire model having intrinsic inhibitory currents but lacking inhibitory connections (Ngo et al., 2010). It would be desirable to validate and transfer this result to a biophysically more detailed model: Cortical tissue ubiquitously is made of excitatory and inhibitory neural subpopulations connected recurrently in a spatially distributed network. In addition, modeling of spike shapes or the effects of neuromodulators requires incorporation of the respective ion channels. Moreover, in many situations a certain degree of biological realism is required to be able to relate to an experiment. Therefore, the established conductance-based cortex model by Compte et al. (2003) was used and the double pulse stimulation protocol described by Shu et al. (2003) was applied to this network.

Using ferret brain slices, Shu et al. (2003) characterized the response of slow-oscillation-like recurrent activity to a variety of current pulses. Their main finding was that up states can not only be triggered by applying a depolarizing current pulse, but can likewise be terminated this way. The up state duration is a function of time between two pulses and their intensity (Figure 2.2). Increasing the intensity decreased the duration of the up state. Delivery of the second pulse during recurrent activity terminated it with a delay that depended on the time since the onset of activity.

This chapter is organized as follows. In section 2.2, we demonstrate that in the biophysically plausible network model by Compte et al. (2003) it is possible to switch up states on and off with current pulses and reproduce qualitatively the experiment by Shu et al. (2003). Second, we build on this result and argue that this model is a suitable candidate for a phase reduction

that can then be used to study interactions of thalamus and hippocampus with the neocortex during deep sleep. The phase response and phase transition curves for Type 1 (weak) and Type 0 (strong) resetting as well as for intermediate stimulus intensities are presented, that serve as predictions for experiments. Third, we semi-analytically obtain the infinitesimal PRC from the mean-field model for up-down state dynamics by Ngo et al. (2010). The network model and the mean-field model yield qualitatively similar results. Finally, we discuss how the results can be used in stimulation studies in vivo and to further investigate interactions of cerebral structures within the phase oscillator framework.

2.1. Model description

The network network model originally introduced by Compte et al. (2003) is conductance-based and exhibits up-down state dynamics as were observed in ferret brain slices in vitro (Sanchez-Vives and McCormick, 2000). The model proved its usefulness in several studies (Sanchez-Vives et al., 2008; Fröhlich and McCormick, 2010; Sanchez-Vives et al., 2010). We provide the full equations of (Compte et al., 2003) in the appendix A. In the following we state some of its main features. The system contains 80% regular spiking pyramidal neurons and 20% fast spiking interneurons. The pyramidal neurons possess two compartments and show spike-frequency adaptation when seeing a constant injected current. Pyramidal neurons are all excitatory and connect via AMPA and NMDA type synapses. Inhibitory connections are only formed via GABA_A synapses. The transition from the down to the up state is caused by spontaneously firing pyramidal neurons and recurrent excitation. Importantly, the model does not require noise to switch between up and down states and exhibits self sustained activity without external drive. The mechanism for the termination of up states is the activity dependent build up of inhibitory currents during the up state. This occurs via a sodium dependent potassium channel whose activation increases with each spike. The original model uses 1280 neurons in total. However, one can reduce the size of the system without changing the overall dynamics, if one also scales down the range of the synaptic connections accordingly. We compared the behavior of the system for different sizes and found no significant differences. We therefore chose to work with a system size of only 320 neurons because of the large number of simulations necessary for the results presented in this chapter.

2.2. Network model reproduces characteristic delay of up-down transition upon stimulation

In this section we show that the network model introduced by Compte et al. (2003) is capable of qualitatively reproducing the experiment of Shu et al. (2003). Shu and colleagues showed that cortical activity can be switched on and off externally with excitatory stimuli. In their experiment two short current pulses of same polarity where applied to ferret brain slices exhibiting spontaneous slow oscillations.

The second pulse was applied during the evoked up state and would lead to a termination of the up state after a certain delay. That delay was consistent across trials and depended strongly on the stimulus amplitude and the actual interstimulus interval.

The network is stimulated two times with depolarizing current pulses of same polarity, intensity and duration. The pulses are applied to all neurons in the network at the same time. The pulse duration is 10 ms. The first stimulus is applied during the hyperpolarization phase inbetween two otherwise self–generated up states. We implicitly assume that the external stimulation with
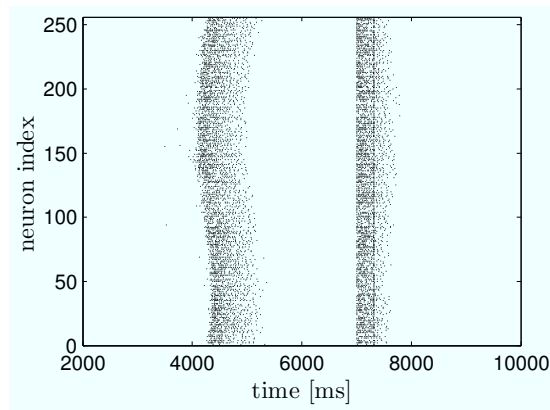
Figure 2.1.: Response of neural network to two consecutive strong stimuli as in (Shu et al., 2003). The first stimulus causes an immediate transition from the down to the up state . The following second stimulus (straight line within second up state) determines the remaining time the system spends in the up state (ISI $= 310$ms, $I_s = 1\mu$A). It causes a massive influx of calcium which in turn activates the inhibiting I_{KCa} (not shown) that then leads to the termination of the up state. Only pyramidal neurons are shown. The stimuli are applied to each neuron in the network.

electric shocks translates into atransmembrane current that equally effects pyramidal neurons and interneurons. We also point out that stimulating all neurons is in contrast to the experiment, where the stimulation was applied locally. The protocol is illustrated in the raster plot (model data) in Figure 2.1. We applied the above stimulation protocol to the network model and yield a similar dependence of up state duration on stimulus amplitude and interstimulus interval. This is depicted in Figure 2.2. For comparison see Shu et al. (2003).

The protocol for obtaining a PRC is very similar to paired pulse stimulation. Hence, if a model reproduces the response to a paired stimulus protocol it is likely that one can obtain the biologically realistic PRC from it. The simulations show that the experimental results obtained by Shu et al. (2003) are in the strong resetting regime.

2.3. The slow oscillation's phase response curve in a network model and a mean-field model

We now present PRCs of the network model introduced above for weak resetting (infinitesimal PRC, Figure 2.5), intermediate stimulus intensities (Figure 2.6) and strong resetting (Figure 2.7) . The infinitesimal PRC of the network model is compared with the infinitesimal PRC of the mean-field model introduced by Ngo et al. (2010). As in the network model the mechanism for terminating up states is the activity dependent build up of an inhibiting current. This is in contrast to rate models of the slow oscillation that are based on fluctuation-driven transitions between two stable fixed points (Deco et al., 2009; Mejias et al., 2010). Although the models are of a different class and complexity they lead to PRC's with similar features.

2.3.1. Phase reduction of network model

The phase θ can assume values between 0 and 1. The beginning of the down state corresponds to $\theta = 0$ and the end of an up state corresponds to $\theta = 1$, respectively. Determining the beginning and end of up states from the voltage trace of single neurons of the network was done with the MAUDS algorithm (Seamari et al., 2007). The phase definition is illustrated in Figure 2.4.
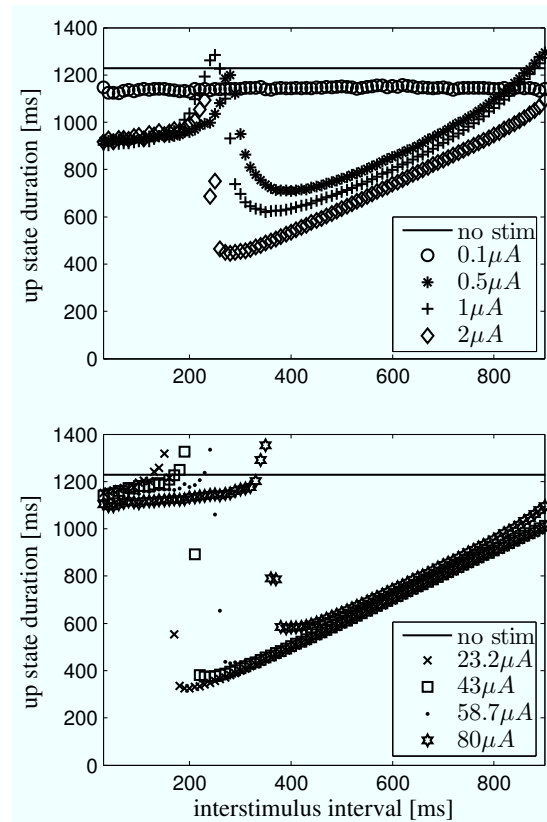
Figure 2.2.: Qualitative reproduction of the experimental results reported by Shu et al. (2003) with the network model. Data points are the average of 5 trials. Two depolarizing stimuli, separated by the interstimulus interval, where applied (see Figure 2.1). The peaks just before the transition to shorter up state durations, that are visible in every curve, are an artifact stemming from a heterogenous network response like the one shown in Figure 2.3. (top) Weak stimuli, e.g., $I_\mathrm{s} = 0.1\mu A$, that already cause strong resetting only reduce the up state duration by a certain amount, independent of the phase they are applied at. Increasing the stimulus strength reduces the up state more the more the two stimuli are apart, until the second stimulus directly terminates an up state. For certain stimulus strengths the second stimulus ends an up state immediately for almost all interstimulus intervals. (bottom) In the simulations it was possible to evoke up state like network behavior also with very high stimulus strengths. This was different from mere after spiking. The higher the stimulus strength was the larger the interstimulus interval had to be in order to reduce up state durations. This reversed tendency is not covered by (Shu et al., 2003) and remains to be tested experimentally.
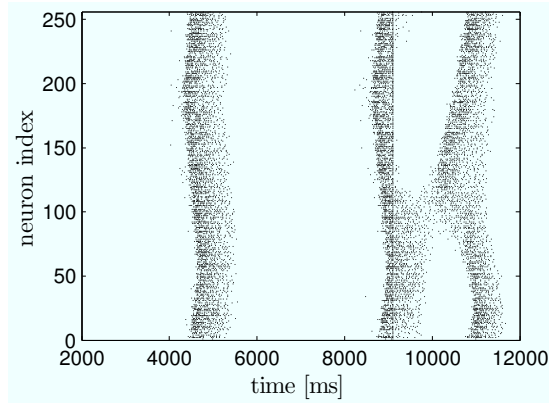
Figure 2.3.: Disrupting effect of a strong stimulus applied at phases with rapidly changing slope of the PRC for strong resetting, depicted in Figure 2.7. Stimulus: ($I_{\mathrm{s}} = 6.7\mu A$, $\theta \approx 0.85$). As individual neurons never have identical phases when being in a collective up state it is possible to terminate the up state in one part of the network while at the same time extending it in another part, thus resulting in an effective desynchronization of the 1D system.
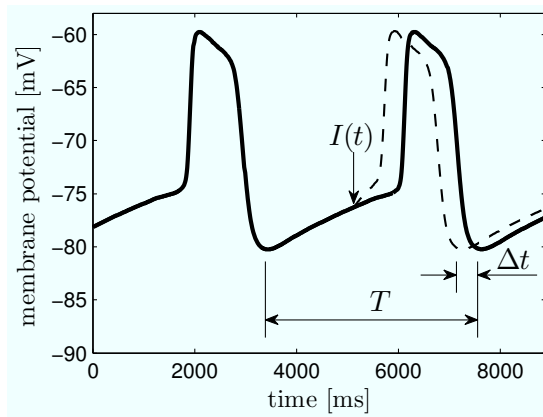
Figure 2.4.: Definition of phase resetting in network model and mean-field model. The solid line is the membrane potential trace produced by the network model averaged over all pyramidal neurons and smoothed subsequently. The arrow indicates the time when the square pulse of $10\mathrm{ms}$ duration is applied to the whole network. The pulse $I(t)$ causes a phase reset that can delay or advance the oscillation (dashed line). We defined phases 0 and 1 to be the beginning of a down state/end of an up state. The phase reset is $\Delta\theta = \frac{\Delta t}{T}$.
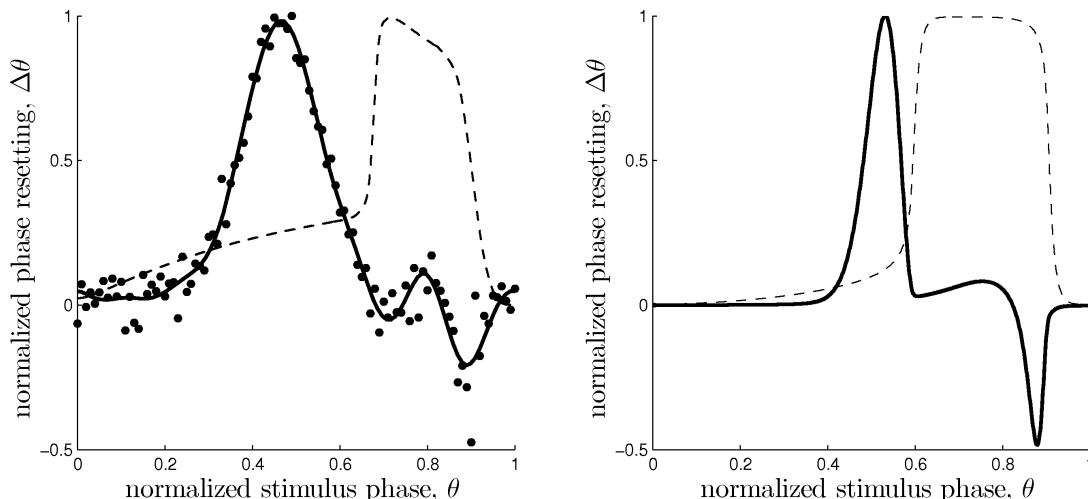
Figure 2.5.: Comparison of the two estimates of the slow oscillation's infinitesimal PRC. The dashed curves show the phase of the unperturbed oscillation in both plots and are in arbitrary units. Left: PRC of the network model for $I = 19$nA. Black dots are from direct perturbation of the network at the respective phase θ. The solid curve is a Fourier approximation of the data points of order 7. The voltage trace was obtained by averaging one oscillation period over all pyramidal neurons and subsequent smoothing. Right: PRC of mean field model with $d_f = 0.17$, $d_b = 0.98$, $C = 0.6$, $\sigma = 0.05$, $\lambda_\nu = 0.96$, $\lambda_\mu = 0.9$, $g = 0.1$, $h = 0.2$. The parameters where chosen to closely match the PRC of the network model. The model has a similar qualitative behavior over a wide range of parameters. In both models stimulation is ineffective right after an up state. It has the largest impact at the end of the down state right before the transition to the up state. Within the up state, stimulation initially leads to a phase advance, i.e., a reduced up state duration. During the following up-to-down transition a phase delay is possible resulting in a prolonged up state.

The phase reset $\Delta\theta$ is defined as the phase difference between the perturbed and unperturbed system as

$$\Delta\theta = \overline{\theta} - \theta = \frac{\Delta t}{T}, \qquad (2.1)$$

where $\overline{\theta}$ is the new phase of the system immediately after the perturbation and θ is the phase in the unperturbed system at which the stimulus was applied. Δt and T are as in Figure 2.4. The new phase is calculated from the simulation data via

$$\overline{\theta} = 1 - \frac{t_{\rm d} - t_{\rm s}}{T} \qquad (2.2)$$

with T being the oscillation period, $t_{\rm d}$ the beginning of the down state following the perturbation and $t_{\rm s}$ the time when the perturbation is applied. The old phase θ is $(t_{\rm s} - t_2)/T$, where t_2 is the beginning of the down state before the perturbing stimulus. The PRC simply is $\mathrm{PRC}(\theta) = \Delta\theta(\theta)$, i.e., it describes the phase resetting at all phases θ of an oscillation. Quantifying the effect of external electric stimulation on a neuron is not trivial and a field of active research (Reato et al., 2010; Radman et al., 2007). However, for determining the PRC in the weak coupling regime this is not an issue because of the infinitesimal nature of the perturbation. The PRC can be defined with respect to conductance changes or with respect to current perturbations. We chose the latter option as this is more general and reflects only the intrinsic properties of a neuron. It has been shown that both approaches are equivalent (Achuthan et al., 2010). First, we calculated θ and $\overline{\theta}$ for 50 different stimulus times, seperately for each neuron in the network. The perturbation is applied to all neurons at the same time but of course they are all in a slightly different phase of their oscillation. Because of that, we then used nearest neighbor interpolation to transform the data points $(\theta, \overline{\theta})$ to an equidistant grid. Finally, the

ensemble phase is determined using the order parameter

$$Z = \frac{1}{N} \sum_{k=1}^{N} \mathrm{e}^{i2\pi\bar{\theta}_k} = R\mathrm{e}^{i2\pi\Theta} \tag{2.3}$$

with N being the number of pyramidal neurons. The ensemble phase Θ is then $\Theta = \arg Z$. The infinitesimal PRC of the network model is depicted in Figure 2.5 (left). For stimulus amplitudes up to about 19nA it scales linearly with stimulus amplitude. Figure 2.6 shows the PRC's dependence on intermediate stimulus intensities. Between 19nA and ca 400nA the PRC is still
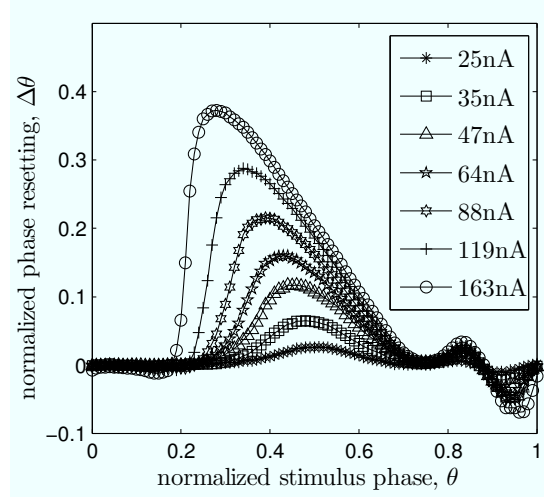
Figure 2.6.: Dependence of the network model's PRC on stimulus strength I_s. The PRC tilts to the left as the stimulus strength increases. Note that the phase resetting is only normalized to the oscillation period and not to I_s.

topologically equivalent to the infinitesimal PRC but does not scale linearly with stimulus intensities anymore.

2.3.2. Phase reduction of mean-field model

Ngo et al. (2010) recently introduced a minimal model for the generation of cortical up and down states The original model of Ngo et al. (2010) is a time-discrete map. The full model, reformulated as system of differential equations, is

$$\frac{\mathrm{d}x}{\mathrm{d}t} = \left(1 + \mathrm{e}^{-\beta(Cx - d_f - \vartheta)}\right)^{-1} - x \tag{2.4a}$$

$$\frac{\mathrm{d}\mu}{\mathrm{d}t} = \lambda_\mu \mu + gx - \mu \tag{2.4b}$$

$$\frac{\mathrm{d}\vartheta}{\mathrm{d}t} = \lambda_\vartheta \vartheta + h \left(1 + \mathrm{e}^{-\beta(\mu - d_b)}\right)^{-1} - \vartheta. \tag{2.4c}$$

The variable x ranges between 0 and 1 and describes to what extent the population is active. μ is an activity dependent variable that increases when x is active and could be interpreted as calcium current. ϑ has an inhibiting effect on x and is triggered by μ. It could be interpreted as calcium dependent potassium current. β describes the noise level of the population, C stands for the coupling strength, d_f is a constant firing threshold and λ_μ and λ_ϑ are recovery rates of μ and ϑ respectively.

XPP was then used to numerically obtain the PRC. The result is shown in Figure 2.5 (right). The parameters of the mean-field model were chosen to closely match phases of up and down
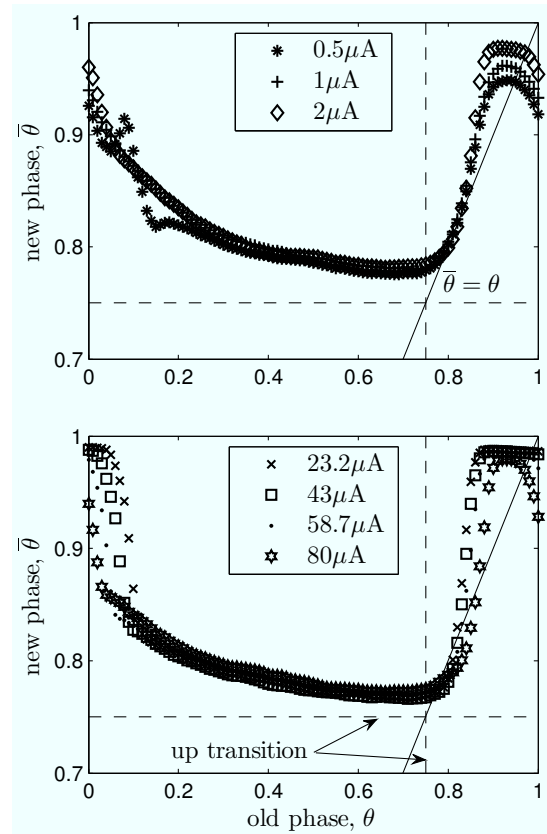
Figure 2.7.: Phase transition curves (PTCs) of the network model for Type 0 (strong) resetting.
The solid line marks the condition $\overline{\theta} = \theta$, e.g., slope 1. The shortening of an up state that results from
a stimulation at $\theta = [0.1 \ldots 0.75]$ is almost independent of the stimulus intensity, as indicated by the
overlapping curves in that range. Significant differences are apparent at the transition from up to down
state and down to up state, respectively. (top) The PTCs mostly stay above $\overline{\theta} = \theta$, indicating that in
this intensity range up state durations can only be decreased. (bottom) The model predicts that there is
a refractory period only for mediumly strong stimuli ($I_s = [23.2, 43, 58.7] \cdot \mu A$), as the phase transition
curve is close to $\overline{\theta} = 1$. Also, the slopes near the state transitions are steeper for strong stimuli. Hence,
it is more likely for very strong stimuli to have the desynchronizing effect shown in Figure 2.3.

states and PRC of the network model. According to this model perturbations have the largest
influence in a relatively short time window right before the transition to the up state and lead to a
phase advance, i.e., a shortening of the down state. At the beginning of an up state perturbations
also lead to a phase advance and a shortening of the up state, however only to a comparatively
small extent. Perturbations toward the end of an up state have a larger impact, leading to a
phase delay and hence can prolong the up state.

Figure 2.8 illustrates the formation of traveling waves and their entrainment by external stim-
ulation in a 2D network of weakly coupled phase oscillators, endowed with the PRC of the
mean-field model.
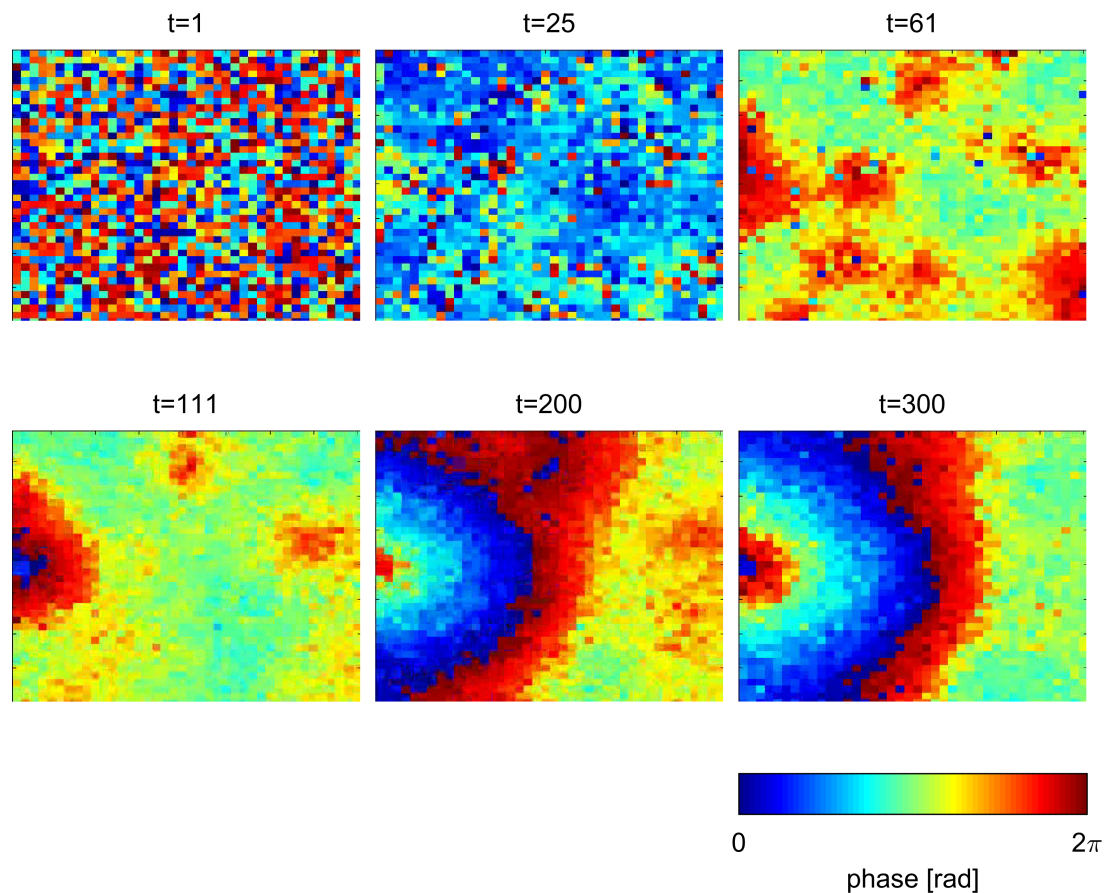
Figure 2.8.: Wave propagation in a network of phase oscillators. The images depict snapshots of the phases of an array of 200x200 weakly coupled phase oscillators at different points in time. The units are arranged as two-dimensional grid and each unit is coupled locally to its four nearest neighbors. The phase response curve of the oscillators is the one derived from the mean-field model (Figure 2.5, right). The frequency of unit (0,100), middle left in images, is fixed, i.e., an external forcing is applied. ($t = 1$)Random initial state. ($t = 25$) Increasing homogeneity of phases. ($t = 61$) Appearance of several local wave generators (red blobs). ($t = 111$) Reduced number of local wave generators. Periodically forced unit (0,100) begins to dominate wave pattern. ($t = 200$) Wave fronts regularly originate from unit (0,100). Only minor irregularities in propagation pattern remain. ($t = 300$) Regular wave propation pattern originating from externally driven phase oscillator (0,100) is established.

2.4. Discussion

We obtained a testable prediction for the PRC of the neocortex during deep sleep and for slices of cortex tissue exhibiting up and down states. In the weak resetting regime we found type II PRCs with similar features for two different models that reproduce many aspects of up and down states in slices. The obtained PRCs show maximal responsiveness to be close to the transition to the up state. This is in agreement with evoked potential studies (Massimini, 2002). In the strong resetting regime both models also conform to the experimental results by Shu et al. (2003). The results strictly apply only to ferret brain slices, as both investigated models build on observations from those preparations. However, considering the universality of sleep and related phenomena like spindles and hippocampal ripples across mammals the results should, at least qualitatively, translate to other species as well.

Treating a neural population as phase oscillator is a strong simplification that is not justified in general. However, slow oscillations during deep sleep and deep anesthesia present a rare

case where this approximation can be valid, because they exhibit a high degree of regularity. Theoretical investigations predict a power law distribution (Mejias et al., 2010) of the residence times in up and down states but also showed that a purely fluctuation driven transition between up and down states is not sufficient to account for the statistics of residence times (Deco et al., 2009). Rather, the probability density function obtained from experimental data is unimodal and centered on a preferred frequency not close to zero (Deco et al., 2009), which is in contrast to the theoretically derived power law distribution (Mejias et al., 2010).

The population activity of network and mean-field model is reminiscent of relaxation oscillations and phase model theory can be used to predict the synchronization behavior (Izhikevich, 2000; Varkonyi and Holmes, 2008). In particular, phase equations of a relaxation oscillator are appropriate to describe its synchronization behavior if coupling is weak and the oscillator is not close to the limiting case of discontinuous jumps.

Phase response theory allows for accurate prediction of phase locking between oscillators and can be useful to analyze interactions between brain regions (Levnajić and Pikovsky, 2010; Ko and Ermentrout, 2009; Kori et al., 2009; Perez Velazquez et al., 2007). During mammalian deep sleep hippocampal sharp wave ripple complexes and thalamic spindles tend to be phase-locked to the neocortical slow oscillation (Mölle et al., 2002; Clemens et al., 2007; Mayer et al., 2007) and parahippocampal activity seems to be phase-locked to the troughs of parietal and parahippocampal spindles. A characterization of these rhythms in terms of PRCs might shed light on the nature of this observation.

Furthermore, knowing the PRC of a system enables one to estimate cortical inputs based on the drift velocity of spiral waves (Biktasheva et al., 2010).

3. Excursus: Fitting models to time series of stochastic processes

This section describes a batch method for the estimation of parameters in nonlinear stochastic dynamical models. It is based on the global optimization of a cost function that is evaluated on the complete data set. State of the art methods usually fall into the category of recursive Bayesian filters and smoothers (Särkkä, 2013; Daunizeau et al., 2009), e.g., unscented Kalman filters (Wan and Van Der Merwe, 2000), which can perform simultaneous parameter and state inference. However, they are somewhat hard to implement and can be computationally very demanding, especially for long time series.

3.1. Cost function

We utilize the result from Kazakov and Lavrov (1994) that the two-dimensional density $w(x_1, t_1; x_2, t_2)$ of a stochastic process, s, notably even a non-Gaussian and non-Markov process, is completely defined by two univariate functions, namely the the amplitude distribution, $f(x_1) = \int w(x_1, x_2) dx_2$, and the correlation function, $R(\tau)$. Specifically, they show that w can be represented by the expansion

$$w(x_1, t_1; x_2, t_2) = f(x_1) f(x_2) \sum_{k=0}^{\infty} R(\tau)^{\gamma_k} Q_k(x_1) Q_k(x_2) \tag{3.1}$$

with $\tau = t_1 - t_2$, γ_k related to f and the Q_k being orthogonal polynomials of degree k, satisfying the orthonormalization condition

$$\int Q_i(x) Q_j(x) f(x) dx = \begin{cases} 1, i = j, \\ 0, i \neq j. \end{cases} \tag{3.2}$$

With this in mind we use the probability density function (pdf) f and correlation function R to define a distance function between stochastic processes s_1 and s_2 as

$$D(s_1, s_2) := D_1(f_{s_1}, f_{s_2}) + D_2(R_{s_1}, R_{s_2}) + D_1(f_{S_1}, f_{S_2}). \tag{3.3}$$

Regarding D_1, a common choice for the "distance" between probability density functions would be the Kullback-Leibler (KL) divergence. However, we chose to use the Mallows distance, because it is easy to compute, statistically efficient and assumes non-trivial values even when the distributions have disjoint support. Consider two distinct probability density functions f_1 and f_2, with $f_i(x) > 0 \, \forall \, x \in [a, b]$ and $\int_a^b f_i(x) dx = 1$. Further, let F_1 and F_2 be the corresponding distribution functions and F_1^{-1} and F_2^{-1} the inverse distribution functions. The Mallows distance for the one-dimensional case is

$$D_M(f_1, f_2) = \left(\int_0^1 |F_1^{-1}(t) - F_2^{-1}(t)|^r dt \right)^{1/r}. \tag{3.4}$$

3. Excursus: Fitting models to time series of stochastic processes

If sample vectors x and y are given, each drawn from densities f_1, f_2, and having equal length, then the Mallows distance can be calculated directly from these vectors via

$$D_M^*(f_1, f_2) = \left(\frac{1}{n} \sum_{i=1}^{n} |x_{(i)}^* - y_{(i)}^*|^r \right)^{1/r}, \tag{3.5}$$

where x^* and y^* are the sorted versions of x and y.

Regarding D_2, the Wiener-Kinchin theorem states that for a stationary stochastic process the Fourier transform of its autocorrelation function is equivalent to the power spectral density of the process (given the Fourier transform exists). Hence, the problem of calculating the distance between two correlation functions can be transformed to calculating the distance between power spectral densities. For this problem several Riemannian metrics and geodesic distances have been proposed that take into account the differential-geometric structure of spectral densities (Li and Wong, 2013; Georgiou, 2007). Here, we use three of them and compare their performance in the parameter estimation problem.

Moakher (2005) defined

$$D_{LS}(f_1, f_2) = \sqrt{\int_{-\pi}^{\pi} \log^2 \left(\frac{f_1(\theta)}{f_2(\theta)} \right) \frac{d\theta}{2\pi}}, \tag{3.6}$$

which is sometimes called log spectral distance (Georgiou et al., 2009).

Li and Wong (2013) suggested

$$D_H(f_1, f_2) = \sqrt{1 - \int_{-\pi}^{\pi} \sqrt{f_1(\theta) f_2(\theta)} \frac{d\theta}{2\pi}}, \tag{3.7}$$

which is equivalent to the Hellinger distance.

Georgiou (2007) proposed the "geodesic prediction distance"

$$D_G(f_1, f_2) = \sqrt{\int_{-\pi}^{\pi} \left(\log \frac{f_1(\theta)}{f_2(\theta)} \right)^2 \frac{d\theta}{2\pi} - \left(\int_{-\pi}^{\pi} \log \frac{f_1(\theta)}{f_2(\theta)} \frac{d\theta}{2\pi} \right)^2}. \tag{3.8}$$

The term $D_1(f_{S_1}, f_{S_2})$ uses higher order statistics of the time series that are necessary to capture temporal asymmetry. A simple a way of doing this is to look at the pdf f_S of the set $S = \{ s_t - s_{t-1} \}$.

The cost function $D(s_1, s_2)$ can be optimized by standard methods, e.g., a stochastic global optimizer. Here, the MEIGO package was used (Egea et al., 2014), which is based on scatter search.

3.2. Evaluation

It is an obvious requirement that the cost function should allow an assessment of the quality of a solution. For parameter estimation this means that the cost function should reflect the deviation from the ground truth, i.e., the true parameters. This will be checked by reporting the average relative error $e = \frac{1}{N} \sum_i^N |p_i^{\text{estim}} - p_i^{\text{true}}| / p_i^{\text{true}}$, given an ensemble of candidate solutions from a stochastic optimization scheme.

Table 3.1.: Stochastic differential equations of test models.

Double well	$\mathrm{d}x = (-a_1 x + a_2 x^3)\mathrm{d}t + a_3\mathrm{d}W$
Fitzhugh-Nagumo	$\mathrm{d}V = (V(a_1 - V)(V - 1) - w)\mathrm{d}t + a_5\mathrm{d}W$
	$\mathrm{d}w = (-a_2 w + V - a_3)/a_4)\mathrm{d}t$
Wilson-Cowan	$\mathrm{d}E = (-E + f(a_1 E - a_2 I + a_3))/a_4\mathrm{d}t + a_{11}\mathrm{d}W$
	$\mathrm{d}I = (-I + f(a_5 E - a_6 I + a_7))/a_8\mathrm{d}t$
	$\mathrm{d}c = (-a_9 c + E)/a_{10}\mathrm{d}t$
	$f = 1/(1 + \exp[-x])$

Table 3.2.: Parameters of test models.

Double well	$a_1 = -1$, $a_2 = 0.1$, $a_3 = 2$
Fitzhugh-Nagumo	$a_1 = -1.33$, $a_2 = 20.7$, $a_3 = 9.5$, $a_4 = 5.7$, $a_5 = 0.04$
Wilson-Cowan	$a_1 = 16$, $a_2 = 11$, $a_3 = 2$, $a_4 = 2$, $a_5 = 12$, $a_6 = 18$, $a_7 = -3$
	$a_8 = 1$, $a_9 = 0.2$, $a_{10} = 100$, $a_{11} = 0.02$

Table 3.3.: Fitting results. The error e is measured as relative deviation from true parameter values, $|(p_{estim} - p_{true})/p_{true}|$. e_{best} is the best result in all runs and $\bar{e}$ denotes the median error across all runs. [parameters, function evaluations, samples, runs, step size]: [1] [5,5000,3000,20,0.1], [2][3,5000,3000,20,0.1], [3][11,10000,3000,20,1]. All SDEs were solved using the Euler-Maruyama scheme and global optimization was done with MEIGO (Egea et al., 2014).

D_2 Method	Fitzhugh-Nagumo[1]		Double well[2]		Wilson-Cowan[3]	
	e_{best} [%]	$\bar{e}$	e_{best} [%]	$\bar{e}$	e_{best} [%]	$\bar{e}$
KL	2.8	30.6	9.1	49.5	55.2	374
Log-spectral	2.5	31.1	2.4	46.3	65.1	509
Hellinger	2.2	26.1	3.1	37.2	72.0	214
Georgiou	5.7	29.8	9.7	49.7	45.8	240
Mallows	5.2	23.4	9.5	44.3	27.6	232

The algorithm is tested on three low-dimensional nonlinear stochastic systems, which can generate patterns that resemble slow oscillations: a double well potential, the Fitzhugh-Nagumo model, and a Wilson-Cowan type two population model with adaptation. The equations are given in Table 3.1, the parameters in Table 3.2. Simulations were performed using the Euler-Maruyama scheme. Due to the different complexity of the models a different number of function evaluations was used for each model. The number was chosen so that convergence could be achieved reliably. Each run was repeated 20 times. The results are summarized in Table 3.3. No method performs consistently best on all test problems. The log-spectral distance achieved the highest accuracy for the small problems, whereas the Mallows distance performed best in the Wilson-Cowen model with many parameters. The generally large median errors across all runs indicate that the stochastic solver sometimes fails to converge. A high variance in the estimate of a parameter might also indicate that the model is almost invariant with respect to this parameter.

3.3. Discussion

The proposed method for parameter estimation in nonlinear stochastic differential equations is simple, easy to implement and fast. The treatment of an observation function has not explicitly been described, as it is trivial to implement. In the given setting it belongs to the model equations and parameters are inferred along with the model parameters. The evaluation showed that it is possible to obtain small errors ($<3\%$) in some test problems and the estimation error becomes larger as the number of parameters increases.

It should be noted that the method will not perform well for deterministic problems, that depend strongly on the initial conditions. It amounts to a single shooting approach in this limit and multiple shooting methods are known to be superior in this setting (Voss et al., 2004). Furthermore, it has been shown that simultaneous estimation of the system trajectory is necessary to yield correct parameter estimates in the presence of measurement noise (Voss et al., 2004).

Kleinhans et al. (2005) proposed a related method based on minimization of the Kullback-Leibler distance between the two-point distribution of the model and that of the data. The problem with this approach is that it requires the evaluation of two-dimensional probability density functions, which is error prone. This could be circumvented by using direct esimators of multi-dimensional Kullback-Leibler distance based on nearest neighbors. However, these estimators tend not to scale well with sample size (Wang et al., 2009).

Alternative ways of approaching the problem of parameter inference are Bayesian filters and smoothers, e.g., the unscented Kalman filter or particle filters. These algorithms are recursive and have the additional advantage of performing simultaneous state and parameter inference. Moreover, gradient based optimzation methods can be used for inference, making them potentially more accurate than algorithms relying on stochastic solvers. An excellent introduction to recursive state and parameter estimation is (Särkkä, 2013). The reason to nevertheless resort to a batch algorithm and a stochastic solver is that gradient based solvers in general only find local minima. This suggests to use a batch algorithm and global optimization to find good initial guesses and to refine the solution with a recursive technique.

4. Model II: A thalamocortical neural mass model of non-REM sleep

Parts of this chapter have been published in Weigenand et al. (2014) and Costa et al. (2016). It is generally accepted that most parts of the neocortex (auditory cortex is a counterexample (Hromadka et al., 2013)) are in an asynchronous active state during wakefulness, maintained by a balance of excitatory and inhibitory inputs (Taub et al., 2013; Okun and Lampl, 2008; Shu et al., 2003; Haider et al., 2006), and that a K-complex reflects an isolated silent state (Cash et al., 2009). Hence, when transitioning from wakefulness to sleep a K-complex is necessarily an excursion from the active state to the silent state and back to the active state.

Surprisingly, this obvious observation has been ignored in modeling studies so far, most likely because they often relate to animal data from slice preparations or deep anesthesia, where down states are dominant. KCs were described as excursions from a stable silent state to an unstable active state and SOs as relaxation oscillations or purely noise driven transitions between stable active and silent states (Mattia and Sanchez-Vives, 2011; Wilson et al., 2006; Curto et al., 2009; Steyn-Ross, 2005; Ghorbani et al., 2012), which is not consistent with the observation above. Furthermore, while for certain forms of anesthesia it seems plausible that the cortex undergoes a phase transition, it is not clear whether this holds for natural sleep (Molaee-Ardekani, 2007; Wilson et al., 2010). Therefore, a characterization of KCs in natural sleep is missing.

Addressing these issues a thalamocortical neural mass model is developed in the following sections, which generates K-complexes, slow-wave activity (<4 Hz) and fast spindles (12-15 Hz). Neural mass models, pioneered by the work of Knight (1972), Wilson and Cowan (1973) and Lopes da Silva et al. (1974), are an ideal tool to better understand the changes in neuronal dynamics between the different sleep stages in vivo, because they relate directly to the large-scale dynamics measured by a non-invasive EEG. They successfully described many phenomena of the human EEG, e.g., alpha and gamma rhythms, evoked responses and epilepsy (Jansen et al., 1993; Wendling et al., 2002; David and Friston, 2003).

We incorporated a slow firing rate adaptation into a cortical neural mass and mechanisms for rebound bursts into a thalamic neural mass to account for sleep specific dynamics. Activity-dependent feedback via slow potassium channels has been suggested as a mechanism for the generation of SOs and KCs because of their sensitivity to the sleep related neuromodulator acetylcholine (McCormick, 1992; Hasselmo and Giocomo, 2006) and their implication in the slow afterhyperpolarization (Steriade et al., 1993b; Timofeev et al., 2001b). Multiple studies also point out that potassium leak channels can be activated by several anesthetics (Patel et al., 1999; Nicoll et al., 1990; Talley and Bayliss, 2002). This approach links the neural mass model to modeling studies on SO generation based on single neurons as well as to experimental studies (Compte et al., 2003; Benita et al., 2012).

The model allows the investigation of responses to auditory stimulation during wake and non-REM sleep. Its output resembles EEG time series of sleep stages N2 and N3 to a high degree and shows key features of spontaneous and evoked KCs. In particular, it reproduces EEG data from phase-independent and closed-loop auditory stimulation of recent sleep studies in humans (Ngo et al., 2013).

First, we introduce the concept of neural mass models. Next, the cortex model is motivated and described. Building upon a bifurcation analysis, we go on to characterize the dynamic repertoire of the cortex model. The analysis and identification of parameters from EEG data with the method described in chapter 3 indicates that cortical SOs and KCs are related but different phenomena. This suggests a route for the transition from wake to deep sleep and highlights differences between natural sleep and anesthesia.

In section 4.3, we show that the isolated thalamic neural mass is able to generate different oscillatory behavior found in vivo. In section 4.4, the model is extended to the thalamocortical model. The extension serves two purposes. First, for sensory inputs the thalamus is the gateway to the neocortex and, hence, indispensable. Second, it provides a proof of concept that the postulated cortical K-complex dynamics indeed lead to reasonable thalamocortical dynamics, in particular the experimentally observed grouping of spindles by the slow oscillation and the specific phase relation (Mölle et al., 2002).

4.1. Neural mass framework

The class of conductance-based neural mass model employed here has been derived from (Robinson et al., 1997; Liley et al., 1999, 2002; Wilson et al., 2006). Instead of considering the evolution of high-dimensional states in a large ensemble of single neurons, the population activity can be approximated by the evolution of the mean membrane voltage of that population.

Firing rate function   The complex spiking dynamics is replaced by an empirical firing rate function

$$Q_k = \frac{Q_k^{\max}}{1 + \exp(-(V_k - \theta)/\sigma_k)}, \tag{4.1}$$

with maximal firing rate $Q_k^{\max}$, firing threshold θ and neural gain σ_k. It converts the average membrane voltage V_k of the population k to an output spike rate. Here, $k \in \{p, i, t, r\}$ stands for cortical pyramidal, cortical interneuron, thalamic relay and thalamic reticular populations, respectively. The firing rate function often has a sigmoidal shape and can be interpreted as stemming from the fluctuations of neuronal states or a distribution of thresholds in the population (Marreiros et al., 2008).

Postsynaptic response   The spike rate $Q_{k'}$ of the presynaptic population k' then elicits a postsynaptic response s_{mk} within the receiving population k. The strength of this response can be calculated by the temporal convolution

$$s_{mk} = \sum_{k'} \alpha_m * (N_{kk'} Q_{k'}), \tag{4.2}$$

of the incoming spike rate $Q_{k'}$, scaled with the averaged connectivity constant $N_{kk'}$ between the presynaptic population k' and the postsynaptic population k and an alpha function

$$\alpha_m = \gamma_m^2 t \exp(-\gamma_m t), \tag{4.3}$$

representing the average synaptic response to a single spike. Here, γ_m depicts the rate constant of the synaptic response, whereas $m \in \{e, g, r\}$ denotes the type of synapse with e standing for excitatory AMPA and g, r for inhibitory GABA synapses in the cortex and thalamus, respectively.

The convolution can be written as second order differential equation

$$\ddot{s}_{mk} = \gamma_m^2 \left(N_{mk} Q_m(V_m) + \phi_n - s_{mk} \right) - 2\gamma_m \dot{s}_{mk}, \tag{4.4}$$

External inputs Background noise, ϕ_n, coming from unspecified brain structures and spontaneous miniature postsynaptic potentials within the population is assumed to be uncorrelated Gaussian white noise with zero mean. To model external stimulation the mean of the background noise is elevated by ϕ_s, representing increased incoming spike rates.

Population membrane voltage An important assumption of most neural mass models is the existence of an equilibrium state V_0 the system is always close to (Wilson and Cowan, 1973). However, this is not fulfilled for the large amplitude KCs and SOs and the scaling of synaptic currents with the driving force $(V_k - E_{rev})$ becomes important Liley et al. (1999). The evolution of the population membrane voltage, V_k, then obeys

$$\begin{aligned}
\tau_k \dot{V}_k = & -g_{\mathrm{L}}(V_k - E_{\mathrm{L}}^k) - g_{\mathrm{AMPA}} s_{ek}(V_k - E_{\mathrm{AMPA}}) - g_{\mathrm{GABA}} s_{gk}(V_k - E_{\mathrm{GABA}}), \\
= & -I_{\mathrm{L}} - I_{\mathrm{AMPA}}(s_{ek}) - I_{\mathrm{GABA}}(s_{gk}),
\end{aligned} \tag{4.5}$$

where g denotes the weights that relate the respective quantities to a change in mean population voltage and E the corresponding Nernst potential. While we use the naming convention of Hodgkin-Huxley models to highlight the structural similarity, please note that the above quantities I and g have different units. The membrane potential is then again turned into an updated firing rate according to Eq. 4.1.

Intrinsic currents may additionally be included in the equation of the mean membrane voltage, given their time constant is large compared to the time constant of neuronal spiking (Marreiros et al., 2008; Zandt and Visser, 2013). The signal measured in the EEG stems mainly from the activity of pyramidal neurons (Buzsáki et al., 2012). we use the pyramidal membrane voltage as model output, which is similar to other studies (Steyn-Ross et al., 2001; Sotero and Trujillo-Barreto, 2008). Populations comprising multiple clusters have been considered in (Langdon et al., 2012) and lead to interesting effects. In order to keep the complexity of the model low we consider a single point source. Therefore, filtering effects by the skull/scalp can be approximated by a linear scaling and do not affect the interaction between thalamus and cortex.

EEG signal The potential fluctuations measured in an EEG are mainly generated by pyramidal neurons (Buzsáki et al., 2012). Therefore, we use the membrane voltage of the excitatory population as output variable. Similarly, multiple studies (Jansen et al., 1993; Liley et al., 1999; Steyn-Ross et al., 2001; Suffczynski et al., 2004; Sotero and Trujillo-Barreto, 2008) used either the deviation of the membrane voltage from the resting state, $V_e - V_{\mathrm{rest}}$, or the membrane voltage itself. As the system has no spatial extension and we only assume ohmic effects of skull and scalp, the EEG signal can be approximated by a linear scaling of the excitatory membrane voltage. When comparing experimental data and model output both time series are z-scored, because this linear transformation normalizes mean and standard deviation but preserves the other statistical properties of a signal. As we are only interested in qualitative properties of the model, e.g., the ratio between medium amplitude background oscillations and large amplitude deflections during N2, the different sleep stages are z-scored independently. For quantitative statements the same transformations must be used.

4.2. Cortex model

4.2.1. Model description

The cortical neural mass model consists of an excitatory and an inhibitory neural mass, representing populations of pyramidal neurons (p) and interneurons (i), respectively. The connectivity structure (all to all) of the model is given in Figure 4.1. The membrane potentials evolve according to

$$\tau_p \dot{V}_p = -I_L^p - I_{\text{AMPA}}(s_{ep}) - I_{\text{GABA}}(s_{gp}) - C_m^{-1}\tau_p I_{\text{KNa}},$$
$$\tau_i \dot{V}_i = -I_L^i - I_{\text{AMPA}}(s_{ei}) - I_{\text{GABA}}(s_{gi}).$$

(4.6)

and are linked by the AMPA and GABAergic synaptic inputs. The pyramidal population contains a slow, additive and activity-dependent firing rate adaptation in the form of a sodium dependent potassium current (Schwindt et al., 1989; Bischoff et al., 1998),

$$\tau_{\text{Na}}[\dot{\text{Na}}] = \alpha_{\text{Na}}Q_p(V_p) - \text{Na}_{\text{pump}}([\text{Na}]),$$
$$I_{\text{KNa}} = \bar{g}_{\text{KNa}}\frac{0.37}{1 + \left(\frac{38.7}{[\text{Na}]}\right)^{3.5}}(V_p - E_K),$$

(4.7)

which is believed to be the main driver for the transition to the silent (down) state (Timofeev et al., 2001b; Sanchez-Vives and McCormick, 2000; Benita et al., 2012). The current is connected to the excitatory membrane voltage by a membrane capacity $C_m = 1\mu\text{F/cm}$. Sodium influx responsible for I_{KNa} activation results from spiking or I_{NaP} activation, for which a depolarization above -60 mV is sufficient. We do not explicitly model these mechanisms but combine their effects via the V_e-determined spike rate Q_e and regard α_{Na} as average sodium influx per spike. Sodium extrusion is due to an active pump (Wang, 2003; Bischoff et al., 1998). For simplicity, we neglect synaptic depression and other candidate mechanisms for additive feedback, like calcium dependent potassium currents.

This approach is qualitatively different to changes in the firing rate function, as utilized by Molaee-Ardekani (2007). Gradually switching between two firing rates alters the overall shape of the sigmoid function in a multiplicative, activity-dependent manner, whereas we employ an additive threshold modulation.

4.2.2. Bifurcation analysis

In order to characterize the dynamic repertoire of the cortical model we conducted a numerical bifurcation analysis of the noise-free system. The qualitative behavior of the model was most sensitive to changes in the inverse gain, σ_e, of the pyramidal population and the strength of the adaption, g_{KNa}.
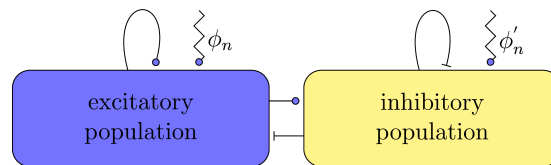
Figure 4.1.: Connectivity of the cortex model. The two populations are all to all coupled. In addition to intrinsic activity both populations receive background noise from unspecified brain structures. Circles indicate excitatory synapses, butts inhibitory synapses.
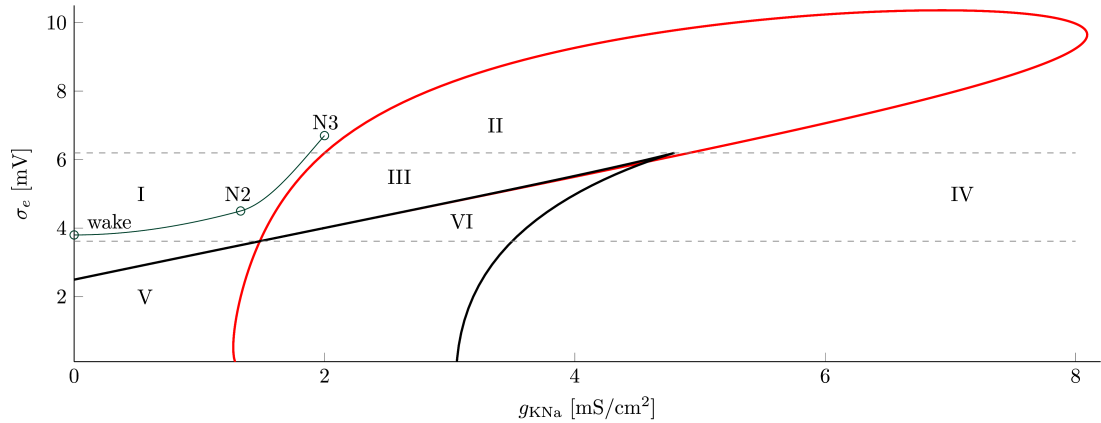
Figure 4.2.: Bifurcation diagram of the cortex with respect to g_{KNa} and σ_e. Overview over the models dynamic regimes, obtained via numerical bifurcation analysis of the cortex with respect to σ_e and g_{KNa}. Hopf bifurcations are drawn in red, while the black line depicts saddle-node bifurcations. The bottom gray line marks the intersection of Hopf and saddle curves, the top gray line the cusp bifurcation. The green line depicts the proposed route for the transition from wake to sleep stage N3. The region around "wake" corresponds to parameter settings commonly used for wake EEG. N2 and N3 are settings used within this study for the respective sleep stages, as given in Table 2 and 3. Regions I-VI are described in the text and Table 4.2 (Parameters as in Table 4.1).
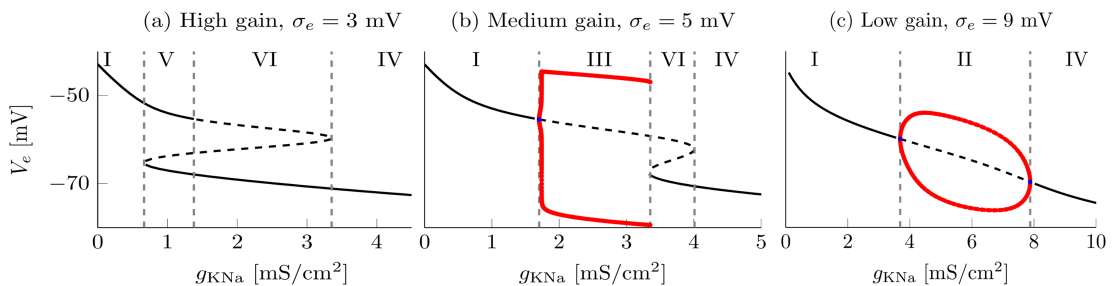
Figure 4.3.: One-dimensional bifurcation diagrams for different gain levels σ_e. Low gain corresponds to high values of σ_e. Thick black lines depict stable fixed points, dashed lines unstable fixed points and red lines stable periodic solutions. The gray dashed lines mark bifurcations and separate the different regimes. (a) Two saddle-node bifurcations lead to excitability in region VI and bistability in region V. (b) A Hopf bifurcation appears (between I and III) in addition to the two saddle-nodes. The initial small amplitude limit cycle transitions into a high-amplitude relaxation cycle via a canard explosion. The high-amplitude periodic solutions vanish at the left saddle-node via a homoclinic bifurcation. The period of the relaxation oscillations goes to infinity as one approaches the homoclinic bifurcation.(c) Only the Hopf bifurcation remains, after the saddle nodes disappeared via a cusp bifurcation. Within region II there is no canard anymore.

4. Model II: A thalamocortical neural mass model of non-REM sleep

Table 4.1.: Parameters of stage N2 and N3.

Symbol	N2	N3	Description
σ_e	4.6 mV	6.7 mV	inverse gain
g_{KNa}	1.33 mS/cm^2	2 mS/cm^2	conductivity

Table 4.2.: Dynamic regimes of the cortical module.

Region	dynamical properties
I	active cortex
II	limit cycles
III	limit cycles and relaxation cycles
IV	silent cortex
V	bistable
VI	excitable

Additionally, both parameters are known to be susceptible to changes in the neuromodulatory milieu, and the concentration of many major neuromodulators is known to change throughout the sleep-wake cycle. Cortical acetylcholine levels are lowest during slow-wave sleep and highest during wake and REM sleep, whereas serotonin and norepinephrine levels are highest during wake, intermediate during SWS and lowest during REM sleep (Léna et al., 2005).

Tonic application of acetylcholine blocks leak and activity-dependent potassium currents I_{Kleak}, I_m, I_{KNa}, I_{KCa} (reviewed in (McCormick, 1992)), as well as I_{NaP} (Mittmann and Alzheimer, 1998). Furthermore, many studies show that σ_e can be altered by norepinephrine, serotonin, acetylcholine as well as dopamine (Soma et al., 2012; Disney et al., 2007; Polack et al., 2013; Timmons et al., 2004; Thurley et al., 2008; Zhang and Arsenault, 2005) (Mehaffey, 2005; Gulledge et al., 2009; Hasselmo and Giocomo, 2006). Consequently, σ_e and g_{KNa} were chosen as bifurcation parameters. The adaptation currents are primarily found in excitatory pyramidal cells and less so in inhibitory interneurons, which justifies the restriction of the parameter changes to the excitatory population.

As can be seen in Figure 4.2 the dynamics of the system is shaped by two bifurcations. The first one is a fold created by two saddle node bifurcations (black), that vanishes in a cusp. Between the two saddle nodes there are three equilibrium states, leading to bistability or excitability, see Figure 4.3a or Figure 4.3b. This is in good agreement with (Steyn-Ross et al., 2005) and (Robinson, 2011), as in the case of a fixed sodium concentration I_{KNa} is constant, and an increase in g_{KNa} acts as a decrease in resting potential.

The second bifurcation is a Hopf arising at the upper stable branch (red). Importantly there is a canard explosion, where the small amplitude limit cycle of the Hopf bifurcation transitions into a high-amplitude relaxation cycle. This phenomenon was first described by Benoit et al. (1981) and is typical for systems where fast and slow subsystems interact. The relaxation cycle vanishes at the left saddle-node via a homoclinic bifurcation. At the cusp both saddle nodes coalesce and the homoclinic bifurcation turns into a second Hopf point.

Based on those bifurcations we define multiple dynamical regimes, see Table 4.2 for a short overview. Within region I a single stable state exists at depolarized membrane voltages where the cortex shows relatively high activity (see Figure 4.3). Especially for small values of g_{KNa}

even large excitatory and inhibitory inputs only cause a passive response. A switch to the lower branch of the S-shaped curve in Figure 4.3 (region IV, silent state) is not possible. Because of these properties we assume the waking brain to operate within this regime.

When crossing the curve of saddles to region V two new fixed points appear (see also Figure 4.3a). The system becomes bistable, with a stable active and silent state. Positive and negative inputs can cause a switching between the two stable branches.

A further increase in g_{KNa} turns the upper branch (active state) unstable. However, within region VI there are still multiple equilibria leaving the system excitable. Here a stimulus can produce a large positive response, which was previously thought to be responsible for the generation of KCs as well as SOs (Wilson et al., 2005).

Only after the second saddle node is crossed the upper two equilibria vanish and a single stable state remains. This state is characterized by hyperpolarized membrane voltages leading to a quiescent cortex.

Region III is characterized by periodic limit cycles or relaxation oscillations and, hence, high rhythmicity. The initial Hopf bifurcation is accompanied by a canard explosion: due to an exponentially small variation of the bifurcation parameter an abrupt transition from a medium-amplitude limit cycle to a high-amplitude relaxation cycle can take place.

This phenomenon was first described in (Benoit et al., 1981) and is typical for systems where fast and slow subsystems interact. The corresponding one-dimensional bifurcation diagram is shown in Figure 4.3b. The periodic solutions vanish at the left saddle-node via a homoclinic bifurcation, and the period of the relaxation oscillations goes to infinity as one approaches the homoclinic bifurcation.

Additionally, with increasing σ_e the amplitude of the limit cycle increases and approaches the form of relaxation oscillations. This explains the similarity between the limit cycles and relaxation oscillations. Both are shaped by the same homoclinic orbit.

At the cusp the two saddle nodes vanish and the homoclinic bifurcation turns into a second Hopf point. Without the homoclinic bifurcation there is no canard anymore. Therefore, in region II above the cusp bifurcation only limit cycles remain, illustrated in Figure 4.3c, leading to high-amplitude oscillations.

4.2.3. Response to perturbations

While the bifurcation analysis provides the basic repertoire of the unperturbed model, its responsiveness with respect to perturbations, e.g., external stimuli or background noise, is crucial for its behavior. As mentioned before, within region I the cortex shows only a passive response. However, this changes for larger values of g_{KNa}, i.e., closer to the curve of Hopf points (red line in Figure 4.2, separating region I from II and III).

There, positive as well as negative inputs may cause a reverse spike resembling a KC. Additionally, close to the curve of Hopf points the stable active state turns into a stable focus, i.e., the system behaves like a damped oscillator upon perturbation. In Figure 4.4a we show the response to artificial stimuli ϕ_{stim} of varying strength, when the cortex is set close to the Hopf bifurcation between region I and III.

Stimuli of low strength lead to damped oscillations whose amplitudes are considerably larger than during the wake state but smaller than KCs or SOs. However, as the strength of the stimuli increases the system is pushed into the canard explosion and the amplitude of the response increases rapidly. While in Figure 4.4a there seems to be a threshold separating the two types
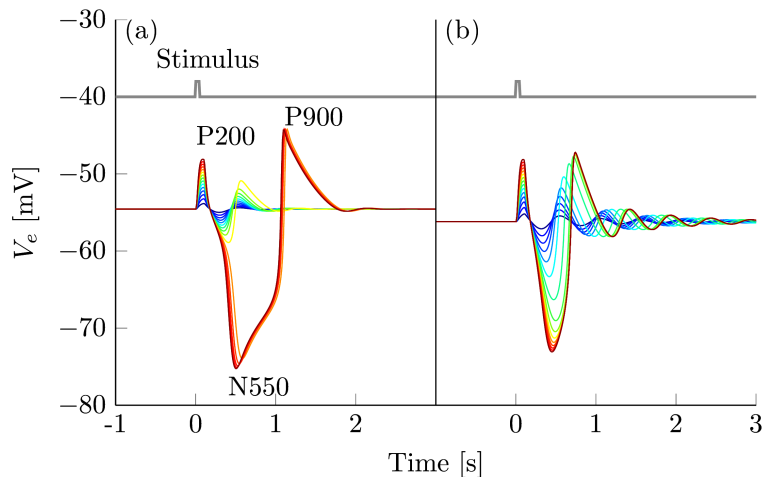
Figure 4.4.: Response of the noise-free cortex to artificial stimuli. Excitatory bursts of 50 ms duration were applied to both populations. The spike rate of the stimuli ϕ_{stim} varies uniformly from 5 Hz (dark blue) to 100 Hz (dark red). The stimulus is shown in grey. (a) Bifurcation parameters are set to the mark "N2" close to region III (see Table 2). There, a canard explosion leads to large amplitude responses that qualitatively resemble a typical evoked KC with its P200, N550 and P900 components. (b) Parameters are set to mark "N3", so that the cortex is beyond the cusp close to region II (see Table 3). The canard vanished, leading to an even increase in the amplitude of the response.

of responses, it is actually a smooth transition given sufficiently small increases in stimulation strength.

The induced relaxation cycles show a good qualitative match with KCs seen during sleep. In the noise driven simulation the majority of inputs would lead to medium-amplitude oscillations, whereas only the rare outliers would trigger a KC like response. This is in good agreement with the dynamics seen in sleep stage N2, where medium-amplitude background oscillations are interrupted by large amplitude KCs.

We assume this mechanism to be responsible for the generation of KCs during sleep stage N2. Furthermore, this requires the cortex to be in the *active* state close to the Hopf bifurcation to region III, rather than being in the silent down state. This is in good agreement with multiple studies who report that during SWS of naturally sleeping animals more time is spent in up states than in down states (Steriade et al., 2001; Destexhe et al., 1999; Timofeev et al., 2001b; Chauvette et al., 2011; Ji and Wilson, 2007; Vyazovskiy et al., 2009).

Close to the Hopf, an increase of the inverse gain, σ_e, leads to an *increase* in the amplitude of the background oscillations and they approach the shape of a relaxation cycle. Beyond the cusp the canard vanishes and isolated events in the sense of KCs are not possible anymore (see Figure 4.4b).

This behavior is well reflected in what is seen during sleep stage N3, where SOs appear as large amplitude oscillations, that are *not* separated from the ongoing background activity. Furthermore, it explains the high similarity between KCs and SOs, as they are both shaped by the same homoclinic orbit. We hypothesize that during sleep stage N3 the cortex is in region I close to the Hopf bifurcation to region II.

Together these findings give rise to a new interpretation of the sleep/wake transition. At the transition to sleep stage N2, the cortex approaches the Hopf bifurcation close to region III, which shifts the EEG trace to higher amplitudes and lower frequencies compared to wake activity. By virtue of a canard explosion this background activity is then interrupted by single, isolated relaxation cycles. As sleep deepens further, the cortex follows the route depicted in Figure 4.2,

while the amplitude of the background oscillations increases and ultimately approaches the form of a KC.

However, this is in contrast with the view that the cortex undergoes a phase transition when entering non-REM sleep. Interestingly, a similar model was utilized to describe characteristics of anesthesia (Molaee-Ardekani, 2007). We can reproduce similar behavior, e.g., burst suppression in region VI (See Supplementary Figure 1).

4.2.4. Reproduction of sleep stages N2 and N3

To verify the ability of the model to reproduce sleep stage N2 we set the model to parameter configuration "N2" from Figure 4.2 (See Table 4.1). The chosen parameter set is within region I close to the border of region III, an example time series is shown in Figure 4.5.
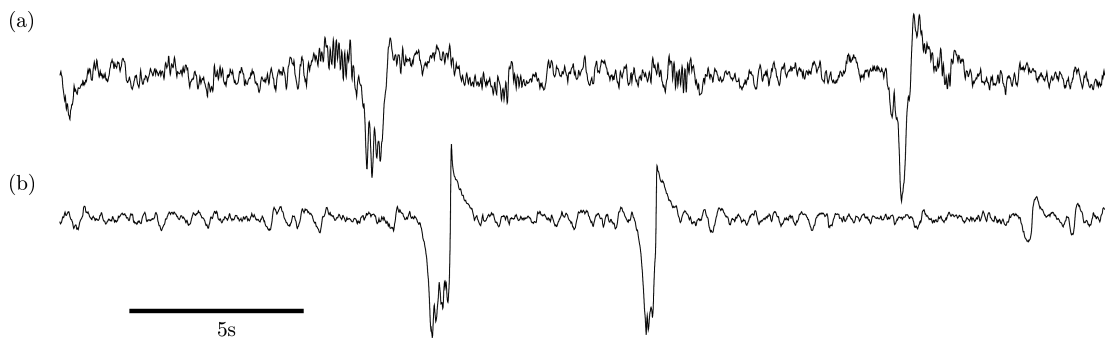
Figure 4.5.: Comparison of human EEG with model output in regime N2. Qualitative comparison of (a) human EEG data of sleep stage N2 from electrode Cz with (b) the isolated cortical module in regime N2 (region IV in the bifurcation diagram in Figure 4.2). The traces illustrate the medium-amplitude background oscillations and the stereotypical shape of spontaneous KCs at the EEG level. It may or may not have an initial bump followed by a large negative peak and a pronounced positive overshoot. The model-KC is noise induced and represents a single relaxation cycle. An evoked KC in the noise-free case is shown in Figure 4.4a. Model output is excitatory membrane voltage V_e, and both time series are z-scored (Parameters as in Table 4.1).
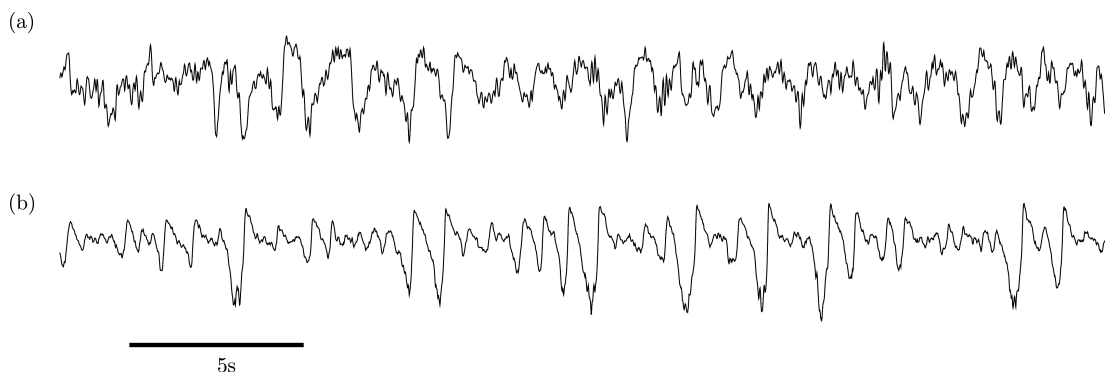
Figure 4.6.: Comparison of human EEG with model output in regime N3. Qualitative comparison of (a) human EEG data of sleep stage N3 from electrode Cz with (b) the isolated cortical module in regime N3 (region I in the bifurcation diagram in Figure 4.2). As the system is close to the Hopf bifurcation noise leads to quasiperiodic oscillations around the stable focus (up state). Large amplitude oscillations resemble KCs as both are shaped by the same homoclinic orbit. The model output is excitatory membrane voltage V_e, and both time series are z-scored (Parameters as in Table 4.1).

In a region close to the chosen parameters the cortex is in the up state and shows the expected noise driven medium-amplitude oscillations. In addition, background noise may push the model into high-amplitude deflections that closely resemble KCs seen in human EEG. Similar to the

data the KCs can show a single pronounced peak or a prolonged down state, which depends on the noise.

Following the proposed route for the sleep/wake transition in Figure 4.2 we then moved along the Hopf bifurcation to a setting beyond the cusp and close to region II, labeled as "N3". In Figure 4.6 a representative time series is shown with the parameters given in Table 4.1. There the cortex shows high amplitude oscillations around 0.8 Hz. In contrast to the N2 stage, the cortex does not produce KCs in the sense of isolated events that differ from the background oscillations. Rather, the response increases until it approaches the form of a KC, depending on the strength of the perturbation.

4.3. Thalamus model

In the previous section, we have shown that the cortical neural mass model equipped with an additive activity-dependent feedback current can generate a time series that closely resembles the EEG signal of sleep stages N2 and N3, without spindles. Here, we extend the cortical model by adding a thalamic module to incorporate spindle activity and investigate the underlying dynamics of the coupled system. We test the evocability of SOs and spindles by auditory stimulation during non-REM sleep and validate the results with scalp EEG data from a recent sleep study in humans (Ngo et al., 2013). This demonstrates the possible application in predicting the outcome of external stimulation on EEG rhythms. This adds further support to the dynamic mechanisms proposed in the previous section.

The model employed for spindle generation follows the "classical" mechanism and is very similar to the neural mass model of Żygierewicz et al. (2001). We first show that the isolated thalamic submodule is able to generate different oscillatory behavior found in vivo.

4.3.1. Model description

Similarly to the cortex model, the thalamic module comprises an excitatory and an inhibitory neural mass, representing a thalamocortical (t) and the reticular (r) nucleus. They are coupled via AMPA and GABA synapses but have different synaptic time constants and only the RE population possesses a self-connection (Figure 4.7).

Both populations are equipped with additional currents. The inclusion of those currents within the thalamic submodule is necessary because spindle oscillations require rebound bursts. In classical neural mass models, this kind of bursting is not possible due to the monotonic firing rate function and demands the inclusion of additional mechanisms. The same argument was used in a previous neural mass model of spindle activity (Żygierewicz et al., 2001) and a thalamocortical neural mass model of epileptic activity (Suffczynski et al., 2004). Finally, in
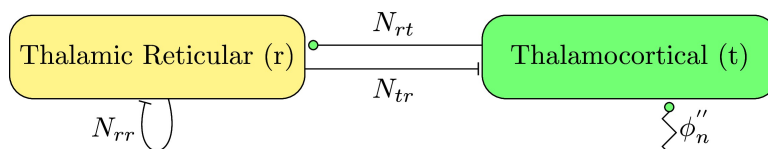
Figure 4.7.: Connectivity of the thalamus model. The TC and RE populations are interconnected. The reticular nucleus is recurrently connected, while thalamocortical neurons do not connect to each other. The TC population receives background noise from unspecified brain structures and external input. Circles indicate excitatory synapses, butts inhibitory synapses.

(Langdon et al., 2012) the authors arrive at a HH-type extension of their population model of thalamic burst activity, which has been derived from integrate-and-fire-or-burst neurons. The potassium leak current is given by

$$I_{\mathrm{LK}} = \bar{g}_{\mathrm{LK}}(V_k - E_{\mathrm{K}}), \tag{4.8}$$

as well as T-type calcium currents

$$I_{\mathrm{T}} = \bar{g}_{\mathrm{T}} m_{\infty}^2 h (V_k - E_{\mathrm{Ca}}), \tag{4.9}$$

which deinactivate upon hyperpolarization. They are essential for the generation of low-threshold spikes (LTSs) and rebound bursts. We use the description of I_{T} given in (Destexhe et al., 1996a) for the RE and the one in (Destexhe et al., 1998) for the TC population.

The TC population further includes the anomalous rectifier current

$$I_{\mathrm{h}} = \bar{g}_{\mathrm{h}} (m_{\mathrm{h1}} + g_{inc} m_{\mathrm{h2}})(V_t - E_{\mathrm{h}}), \tag{4.10}$$

responsible for the waxing and waning structure of spindle oscillations in the isolated thalamus (Destexhe et al., 1996a). Other currents, such as the calcium-dependent potassium currents I_{KCa} and I_{CAN}, are also known to play a role in spindle oscillations, but are omitted for simplicity. The thalamic module is summarized by

$$\begin{aligned}
\tau_t \dot{V}_t &= -I_{\mathrm{L}}^t - I_{\mathrm{AMPA}}(s_{et}) - I_{\mathrm{GABA}}(s_{rt}) - C_m^{-1} \tau_t (I_{\mathrm{LK}}^t - I_{\mathrm{T}}^t - I_{\mathrm{h}}), \\
\tau_r \dot{V}_r &= -I_{\mathrm{L}}^r - I_{\mathrm{AMPA}}(s_{er}) - I_{\mathrm{GABA}}(s_{rr}) - C_m^{-1} \tau_r (I_{\mathrm{LK}}^r - I_{\mathrm{T}}^r).
\end{aligned} \tag{4.11}$$

Parameter settings for the currents are identical to (Chen et al., 2012), with the exception of the deactivation function h_{∞}^t of the thalamic relay population, which is shifted towards more depolarized membrane voltages. The complete equations and all parameters are in Appendix C.

4.3.2. Thalamic spindle oscillations

In the isolated thalamic module, incorporation of the intrinsic currents may lead to oscillations in the spindle band (Figure 4.8). We follow closely the mechanisms established in the models by Destexhe et al. (1996a); Bazhenov et al. (2002); Destexhe and Sejnowski (2003). Physiologically, these oscillations are generated, through reciprocal interaction of the RE and TC populations. A LTS in the RE population causes hyperpolarization in the TC population, that deinactivates its T-type calcium current. Upon release from inhibition a rebound of activity occurs, that in turn drives the RE module to produce another LTS. Additionally, the deinactivation of the T-type calcium currents requires a strong tonic hyperpolarization by a potassium leak current (Destexhe et al., 1996b; Bazhenov et al., 2002).

4.3.3. Bifurcation analysis

As previously shown in (Destexhe et al., 1996a; Lüthi and McCormick, 1999; Destexhe and Sejnowski, 2003; Timofeev and Bazhenov, 2005), the rhythmicity of spindle occurrence and the waxing and waning of the spindle amplitude is caused by an anomalous rectifier channel I_{h}. A sequence of LTS leads to the build-up of calcium, which increases the effective conductivity $\bar{g}_h = \bar{g}_h(m_{\mathrm{h1}} + g_{inc} m_{\mathrm{h2}})$ of I_{h}. The ensuing depolarization of the TC population increasingly counteracts its ability to produce a LTS and terminates the spindle oscillation (Lüthi and McCormick, 1998; Contreras et al., 1997). Therefore, we chose $\bar{g}_h$ and $\bar{g}_{\mathrm{LK}}$ as bifurcation parameters. A two-dimensional bifurcation analysis of the thalamic module reveals the existence of a Hopf bifurcation, as depicted in Figure 4.9, which generates continuous oscillations
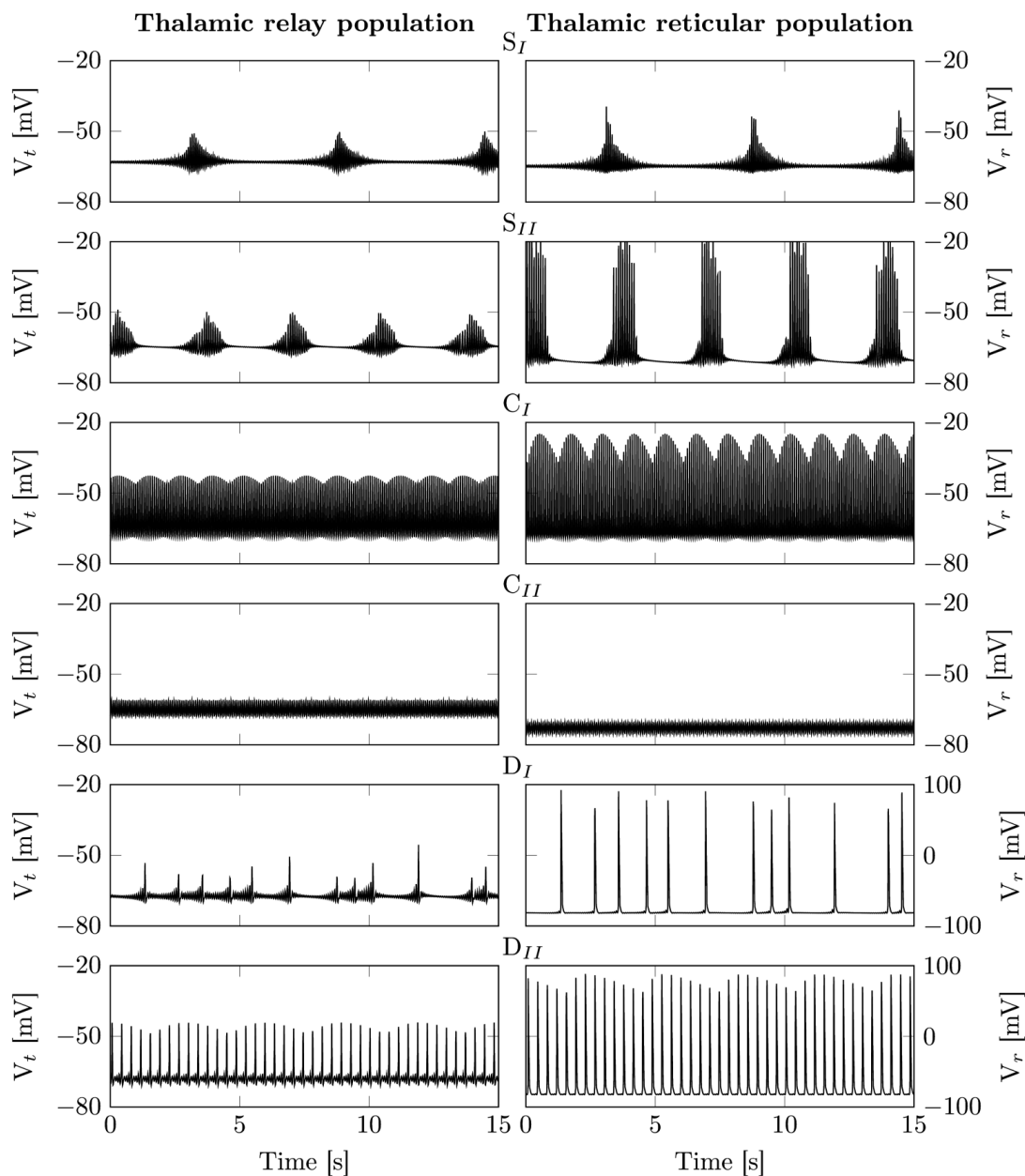
Figure 4.8.: Dynamic modes of the isolated thalamic module. Here, we illustrate the different dynamic modes the isolated thalamic module exhibits. The left panels depict the thalamic relay membrane voltage, whereas the right panels illustrate that of the thalamic reticular population. The parameter values are depicted in Figure 4.9 and given in Table 4.3. S_I and S_{II}: The isolated thalamus generates rhythmic spindle oscillations via a balanced interplay between I_T and I_h. The length and the average time between spindles is governed by $\bar{g}_h$. C_I and C_{II}: Outside of the spindle regime fast oscillations generated by the T-type calcium currents dominate and I_h is unable to sufficiently depolarize the thalamic relay population to cease them. D_I and D_{II}: For strong hyperpolarization through I_{LK} the thalamic module switches into low frequency delta oscillations.
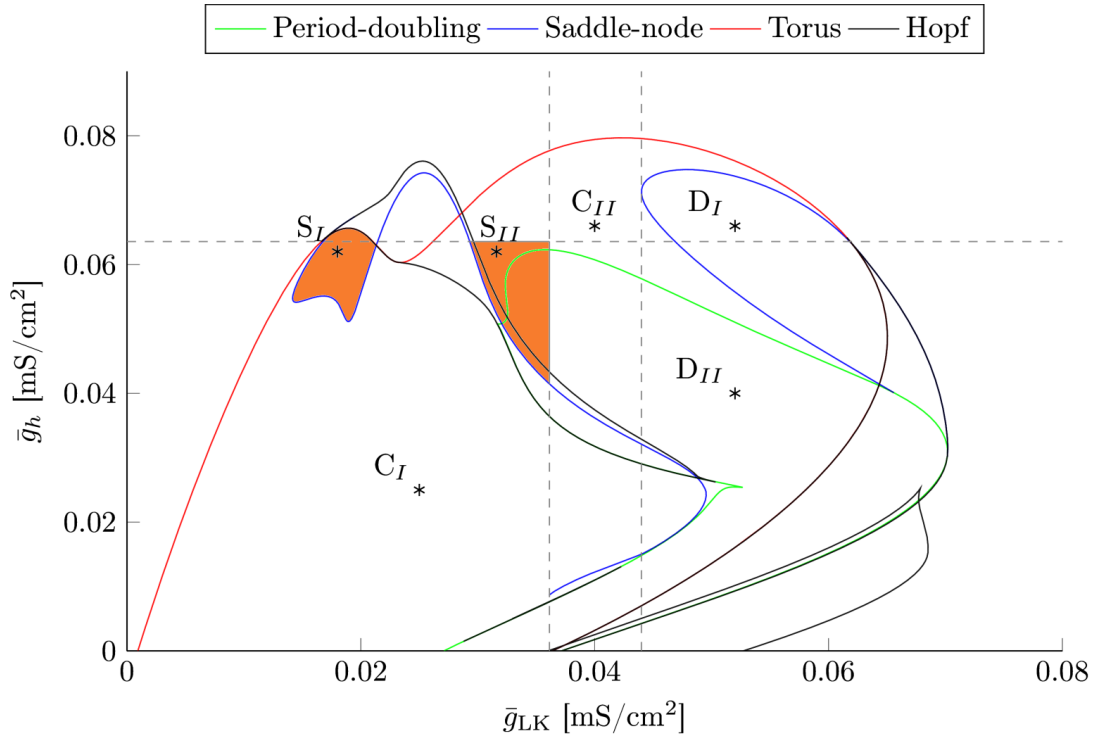
Figure 4.9.: Two-dimensional bifurcation analysis. Here, we illustrate the bifurcation diagram of the isolated thalamus with respect to the two key parameters $\bar{g}_h$ and $\bar{g}_{LK}$. The interaction between the currents incorporated into the thalamic module results in the emergence of two torus bifurcations via a blue sky catastrophe. They lead to spindle oscillations in the orange shaded regions. The left spindle regime (S_I) is encased by a Hopf and a torus bifurcation, whereas the right spindle regime (S_{II}) is constrained by two global bifurcations that are indicated by the dashed gray lines. The vertical line marks the emergence of the torus bifurcation, whereas the horizontal gray line marks the cusp bifurcation where the two saddle-nodes that accompany the left torus bifurcation vanish. The torus bifurcation on the right marks the transition from spindle oscillations to delta oscillations. The labeled points mark the parameter settings utilized in Figure 4.8, which are given in Table 4.3.

in the spindle band due to hyperpolarization induced rebound bursts, see Figure 4.8-C_I and Figure 4.8-C_{II} for representative time series.

The torus bifurcations emerge from a blue sky catastrophe that is generated by the slow-fast interaction between the fast T-type channels and their slow modulation via I_h, which is similar to other models that exhibit switching between tonic spiking and structured bursting activity (Shilnikov and Cymbalyuk, 2005; Mayer et al., 2006).

Table 4.3.: Parameter settings of the isolated thalamus. This table lists the parameter values for the different dynamic regimes of the isolated thalamic module, that are utilized in Figure 4.8.

Symbol	S_I	S_{II}	D_I	D_{II}	C_I	C_{II}	Unit
$\bar{g}_{LK}$	0.018	0.032	0.052	0.052	0.025	0.04	mS/cm^2
$\bar{g}_h$	0.062	0.062	0.066	0.04	0.025	0.066	mS/cm^2

As depicted in Figure 4.8-S_I and Figure 4.8-S_{II} this leads to spindle like oscillations in the orange shaded regions in Figure 4.9. The spindles exhibit an oscillation frequency of around 13 Hz. The spindle frequency depends on the strength of the T-type calcium current $\bar{g}_T$. Importantly, spindle oscillations are initiated intrinsically. The thalamic module does *not* require modulatory input from external sources to initiate/terminate them.

Activation of I_h is responsible for a refractory period that follows a spindle. As long as I_h activation persists, LTS generation is impeded and stronger perturbations are necessary to trigger spindle oscillations. Consequently, an increase in $\bar{g}_h$ results in a larger inter-spindle interval. The left spindle regime (S_I) is encased by the Hopf and the torus bifurcation, whereas the right spindle regime (S_{II}) is constrained by two global bifurcations that are indicated by the dashed gray lines. The vertical line marks the emergence of the torus bifurcation, whereas the horizontal gray line marks the cusp bifurcation where the two saddle-nodes that accompany the left torus bifurcation vanish.

Furthermore, for larger values of $\bar{g}_{LK}$ the model transitions from high frequency spindle oscillations to low frequency delta oscillations, e.g., Figure 4.8-D_I and Figure 4.8-D_{II}.

4.4. Thalamocortical model

4.4.1. Model description
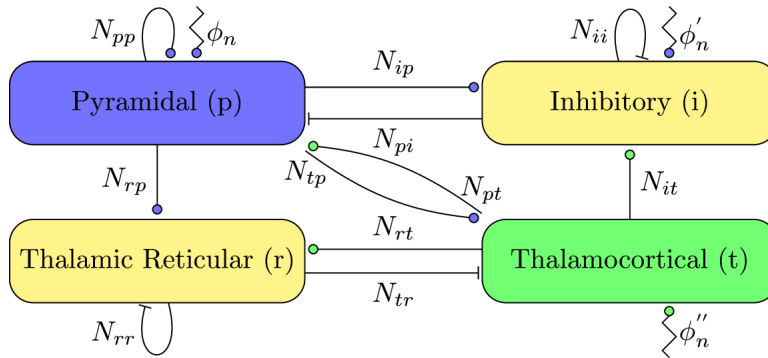
Figure 4.10.: Connectivity of the thalamocortical model. Excitatory synapses are depicted by filled circles, inhibitory synapses by bars. Independent background noise entering the different populations is denoted by ϕ_n, ϕ_n' and ϕ_n'', respectively. Stimulation is applied as an elevation in the mean of the background noise ϕ_n'' of the thalamic relay population.

The model consists of one thalamic and one cortical module. We assume the long range afferents from the cortical pyramidal population project to both populations of the thalamic nuclei, and the long range afferents of the thalamic relay population project to both populations of the cortex, as depicted in Figure 4.10. The delays introduced by these long range afferents might play a crucial role in cortical dynamics (Jirsa, 2009; Nakagawa et al., 2014). However, as the axonal conduction delay between thalamus and cortex is rather small (Agmon and Connors, 1992; Salami et al., 2003; Gentet and Ulrich, 2004; Traub et al., 2005), we approximate it by a convolution with an alpha function (Biggio et al., 2013), which can be written as

$$\ddot{\phi}_k = \nu^2 \left(Q_k(V_k) - \phi_k \right) - 2\nu \dot{\phi}_k, \tag{4.12}$$

where ϕ_k is the resulting delayed firing rate and ν depicts the average delay introduced by that connection. In the case of short range connections ϕ_k can be replaced with Q_k. The full equations and parameter values of the thalamocortical model are given in Appendix C.

Auditory stimulation   We model an auditory stimulus as an elevation in background noise ϕ_n'' (square pulse) being gated through the thalamus. For all stimuli, we use a duration of 80 ms and 70 spikes per second.

Event triggered averages KCs and SOs were detected similar to (Mölle et al., 2011). The model output was bandpass filtered between 0.25 and 4 Hz. Zero-crossings were detected to extract the negative half-waves. Negative half-waves with peaks below -70 mV were considered to be KCs/SOs.

Experimental data Experimental data has been described in (Ngo et al., 2013). 11 Subjects were measured during two experimental nights in balanced order in a stimulation and control condition. For averages of the endogenous activity data was taken from the control condition.

In the following section we perform a bifurcation analysis and demonstrate the ability of the thalamic module to generate spindle oscillations and reproduce different experimental observations. Afterwards, we investigate the interplay between thalamus and cortex to reproduce the characteristics of different sleep stages. Finally, we examine the effect of auditory stimulation in the model and compare different stimulation protocols with experimental findings.

4.4.2. Approximation of long range connection delay

As discussed in the methods section (Eq. 4.12), long range connections are modeled by a convolution with an alpha function representing the average axonal conduction delay. This is an approximation of the delay differential equations that describe the axonal conduction delay, which we justify briefly.

First, the alpha function acts as a lowpass filter with magnitude response function $|H(\omega)| = \nu^2/(\nu^2 + \omega^2)$ and cutoff frequency $f_c = \nu/(2\pi)$. Hence, with $\nu = 120 \cdot 10^{-3} \ \text{ms}^{-1}$ the input is attenuated by 3dB at ≈ 19 Hz. This is not problematic as long as the model does not generate sharp discontinuities or high frequency oscillations, which is the case for our model (see Figure 4.11).

Second, physiological measurements suggest that the transmission delay between the thalamus and the cortex is in the range of a few milliseconds Agmon and Connors (1992); Swadlow (2000); Salami et al. (2003); Gentet and Ulrich (2004), in particular for neurons receiving sensory inputs. Recent investigations in humans find a one-way conduction delay in the range of 12.5-19.8 ms Roux et al. (2013). We find that for those cases the effective delay is well approximated by the median of the alpha function $\Delta t = -1 - W_{-1}(-\frac{1}{2e}) = 1.67835/\nu$, where W_{-1} is the bottom branch of the Lambert W function (see Figure 4.12). Please note that the effective delay is considerably larger than the time to peak of the alpha function. This is due to the asymmetric shape of the alpha function, which has a heavy tail.

4.4.3. K-complexes and spindles during sleep stage N2

In the coupled system, the cortex provides excitatory drive to the thalamic module, since it is predominantly in the active state. In order for the thalamic module to exhibit rhythmically occurring spindle oscillations we had to adjust $\bar{g}_h$ and $\bar{g}_{LK}$ (see Table 4.4).

As can be seen in Figure 4.13 spindles may be triggered by KCs in the full model, but may also occur independent of KCs. During a KC the sudden drop of excitatory drive hyperpolarizes the RE and TC population, leading to deinactivation of I_T. The ensuing depolarization upon the transition back to the active state triggers a LTS and a spindle sequence in turn. The spindle then projects back into the depolarizing phase of the KC. This is in good agreement with the grouping of spindles and KCs observed experimentally (Contreras and Steriade, 1995; Mölle et al., 2002).
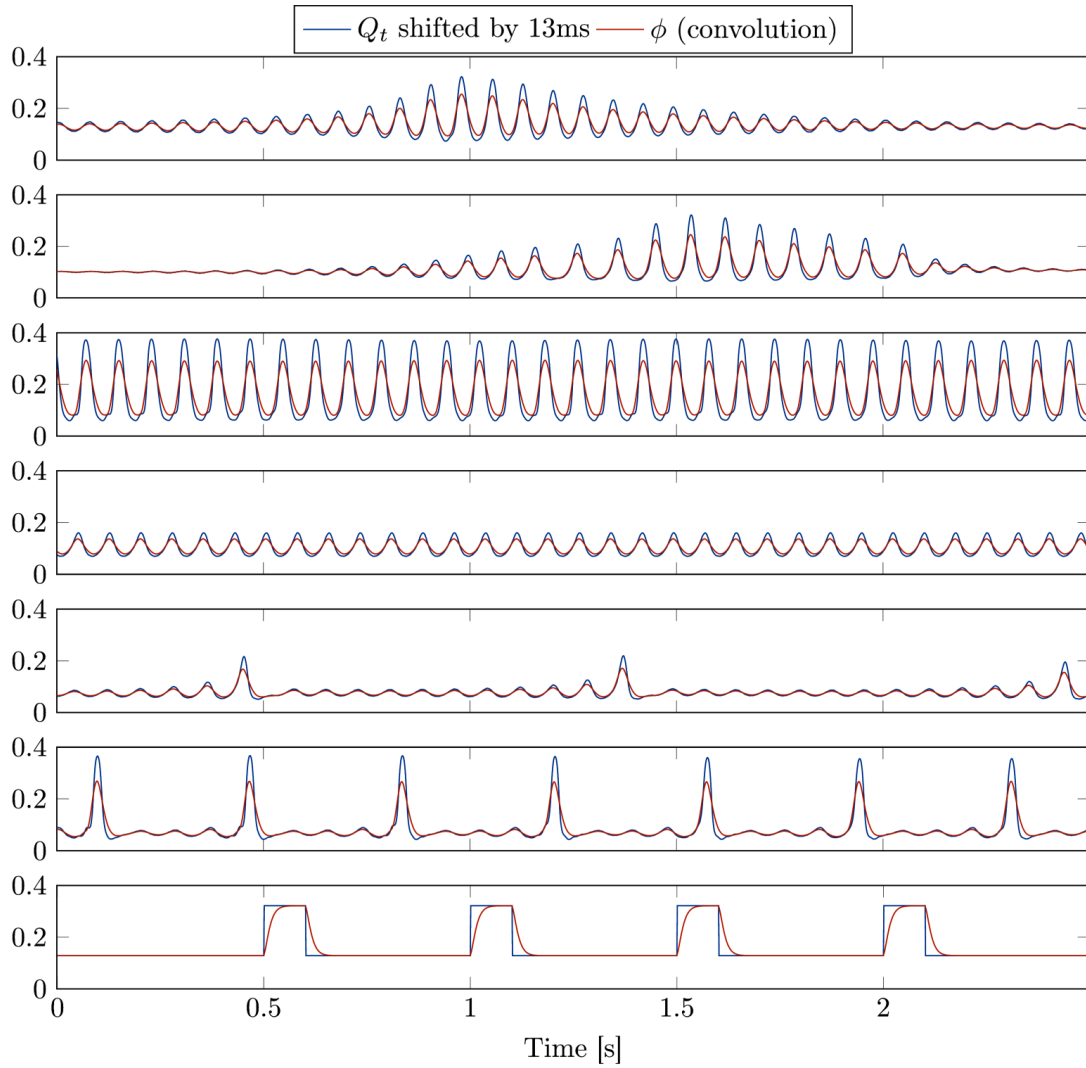
Figure 4.11.: Comparison of convolved and time shifted signals. The panels depict a comparison of the thalamic firing rate time shifted by 13 ms and the axonal flux ϕ. The upper 6 panels represent excerpts from the time series shown in Figure 4.8, with a focus on the sharpest features. The bottom panel additionally compares both signals for a delta pulse.
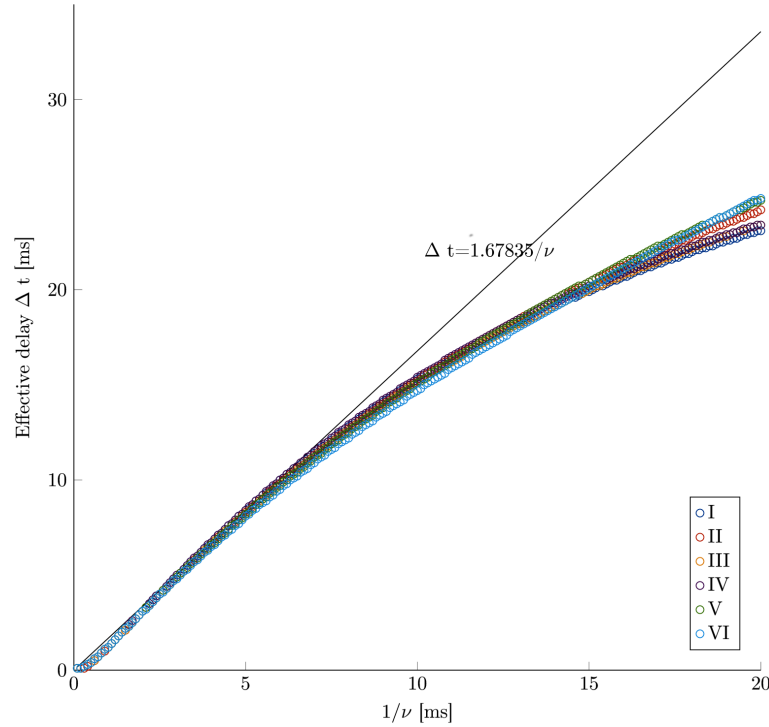
Figure 4.12.: Effective delay for different rate constants. Here the effective delay determined by crosscorrelation of the different time series from Figure 4.8 is depicted for a range of axonal rate constants ν. For comparison the median of the respective alpha function is depicted in black.

Although less likely the model can also give rise to KCs triggered by a spindle. This can be achieved by increasing the connection strength from the thalamic to the cortical module (model output not shown). During N2, KCs occur at a low rate. Hence, spindle initiation and termination are closely linked to the time course of I_h (Figure 4.8A), similar to the isolated thalamic module. The parameters for the output in Figure 4.13 are given in Table 4.4.

Table 4.4.: TC parameter settings. This table shows the different parameter settings of the full model used throughout this study. Columns N2 and N3 give the parameters for the respective sleep stages.

Symbol	N2	N3	Unit	Description
σ_p	4.7	6	mV	Neuronal gain
$\bar{g}_{\mathrm{KNa}}$	1.33	1.88	mS/cm^2	Adaption strength
$\bar{g}_{\mathrm{LK}}$	0.034	0.034	mS/cm^2	Potassium leak conductance
$\bar{g}_{\mathrm{h}}$	0.052	0.062	mS/cm^2	h-current conductance

Given the parameter setting in Table 4.4, the cortical module is within a stable focus, close to a Hopf bifurcation accompanied by a canard explosion. This leads to noise driven medium amplitude background oscillations around the stable focus, that are interrupted by large amplitude deflections (KCs). In good agreement with experimental findings, KCs also appear within the isolated cortex, although they may be initiated through thalamic input.

4.4.4. Slow oscillations and spindles during sleep stage N3

On the transition to sleep stage N3 the canard phenomenon vanishes in a cusp bifurcation and only a high amplitude limit cycle remains. SOs are noise driven oscillations around a stable
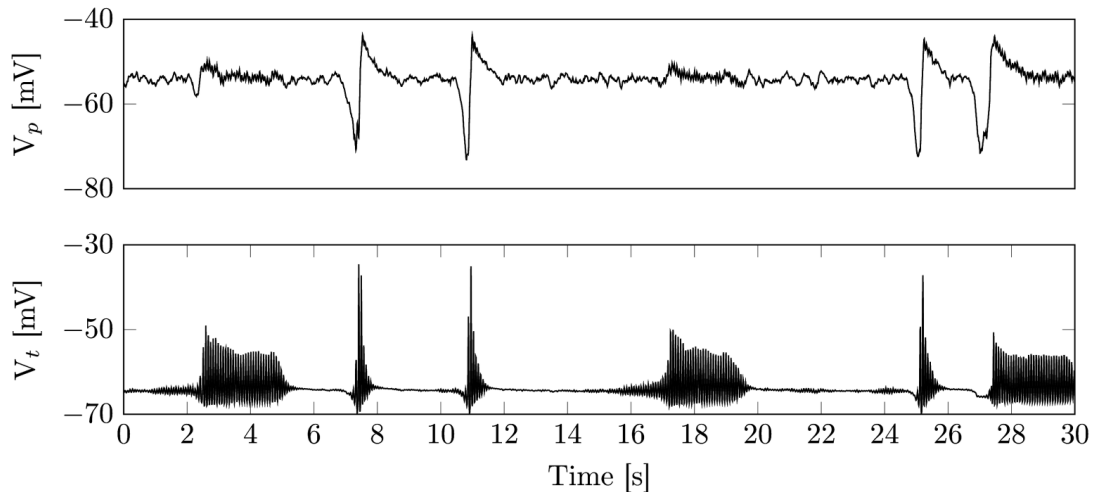
Figure 4.13.: Example time series of sleep stage N2. Shown are membrane voltages of the cortical pyramidal (top) and the thalamic relay population (bottom). The spindle oscillations induced within the thalamic module project into the cortical module. While the spindle oscillations are generally induced by fluctuations in background noise, there is also a grouping between cortical KCs and thalamic spindles (see 7s-9s and 19s-21s). The grouping stems from the lack of depolarizing input during a cortical KC. Parameters are as in Table 4.4.

focus, close to a Hopf bifurcation (Weigenand et al., 2014).

In contrast to sleep stage N2 spindle initiation and termination are now dominated by the modulatory input from the cortical module, that overrules the I_h rhythm. Rather than occurring rhythmically spindles are time-locked to the depolarized phase of a SO. In Figure 4.14 an example time series is shown. Importantly, not every SO is able to trigger a spindle, as can be seen in Figure 4.14 (1-3 s, 11-13 s, 25-28 s). We observed that in a sequence of SOs the first triggers a spindle, which leads to an activation of I_h. This reduces spindle amplitude or even inhibits spindle initiation by the following SO.
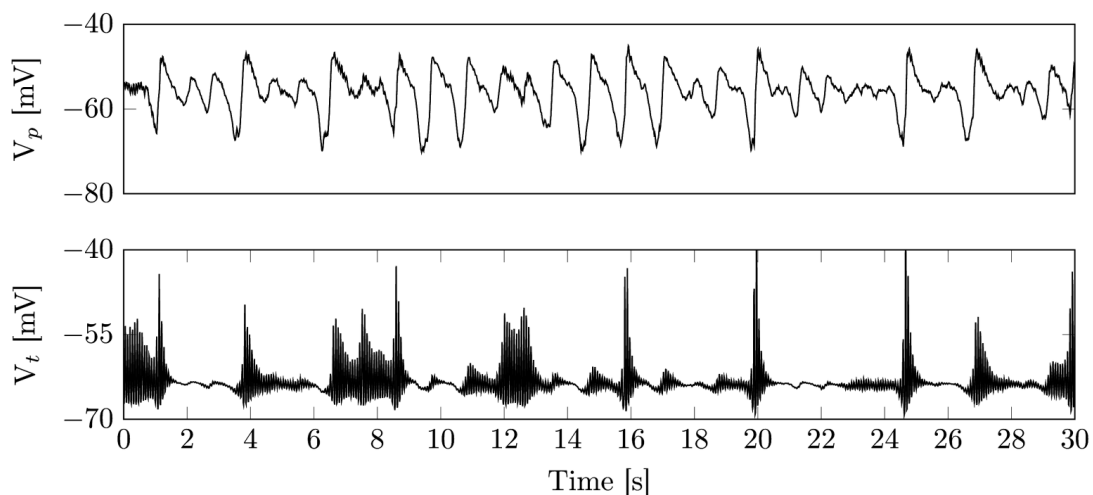
Figure 4.14.: Example time series of sleep stage N3. Shown are membrane voltages of the cortical pyramidal (top) and the thalamic relay population (bottom). During N3 the model shows ongoing slow oscillatory activity. In contrast to sleep stage N2, SOs cannot be identified as isolated events. Furthermore, there are no isolated spindle oscillations and spindle activity is time-locked to SOs. Parameters are given in Table 4.4.

4.4.5. Endogenous event triggered averages

To further validate the model, we determined averages of the generated EEG signal and fast spindle power time-locked to the negative peak of the endogenous KCs/SOs during N2 and N3. This method is often used to illustrate the grouping of spindles by SOs and morphological features of SOs, e.g., in (Ngo et al., 2013, 2015; Mölle et al., 2002). Model output and data for N2 and N3 is depicted in Figure 4.15.
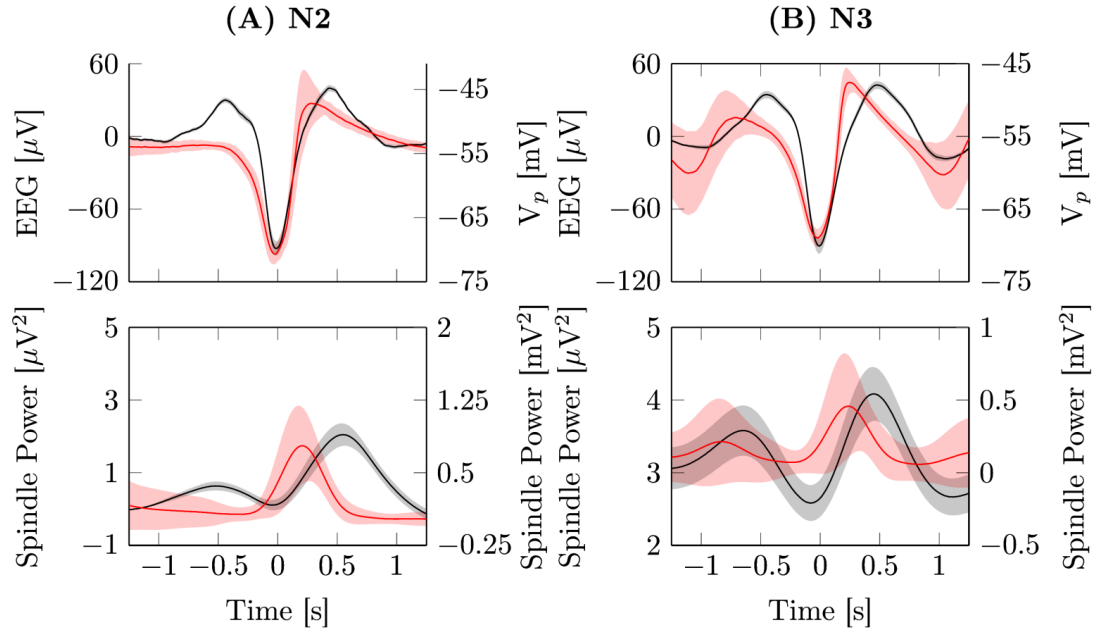
Figure 4.15.: Event triggered average potentials. Averaged EEG signal (top) and fast spindle band power (bottom) time-locked to the negative peaks ($t = 0$ s) of all detected events from electrode *Cz* (black, left axis) and model output (red, right axis). (A) Detected KCs from data scored as sleep stage N2 (Experiment: $227, 45 \pm 19, 22$, Model: 180 events). (B) SO average from data scored as sleep stage N3 (Experiment: $983, 64 \pm 106, 1$, Model: 530 events). Each simulation was run for 3600 s with parameters set according to Table 4.4.

As can be seen in Figure 4.15, the grouping of spindles by SOs is present in the model. Spindle power is highest during the positive half-wave following the negative peak. However, there are some notable differences. Compared to the experimental data the initial depolarization preceding the transition to the down state is less prominent, leading to a shallower slope of the transition to the down state. In the thalamocortical model the transition to the depolarized up state occurs considerably earlier with a time to peak of 300 ms, compared to 440 ms in the data. This stems from strong depolarizing input by thalamic spindle bursts, which start directly after the negative peak of a KC/SO and push the cortex further into the depolarized state. However, this is still in line with other experimental studies, that find different timings of spindles for the supplementary motor area of the cortex (Andrillon et al., 2011).

4.4.6. Closed-loop and open-loop auditory stimulation

In the following we show the ability of the model to reproduce data from a recent experiment in humans performing auditory closed-loop stimulation during non-REM sleep (Ngo et al., 2013). The stimulation protocol is as follows: After the negative peak of a SO was detected, two auditory stimuli were applied phase-locked to the following positive peak of the depolarized up phase of the detected and the subsequent SO.

4. Model II: A thalamocortical neural mass model of non-REM sleep

In the experimental study the delay time between the negative peak and the ensuing positive half-wave peak was determined for every subject independently. The second stimulus followed after a fixed interval of 1075 ms. Detection was then paused for 2.5 s. We accordingly determined the delay time from the model output, resulting in a delay of 450 ms for the N3 parameter setting. The second stimulus was chosen to occur 1075 ms after the first one and we also paused detection for 2.5 s. Stimuli are given as elevations in mean background noise of the thalamic relay population for a duration of 80 ms.

Figure 4.16.: Closed-loop stimulation. The upper panel depicts in black the mean ($\pm$ SEM) evoked potentials of human EEG data from electrode *Cz* during closed-loop stimulation, time locked to the first stimulus (11 subjects, 245.6 ± 38.1 stimuli). In red the reproduction of the stimulation protocol with the model is shown (mean $\pm$ SD, 88 stimuli). The dashed line marks the stimulus onset. The lower panel shows the corresponding fast spindle power. Parameters used for model simulation are given in Table 4.4.

Figure 4.16 shows the averaged EEG signal and model output time-locked to the first stimulus ($t = 0$). There is a good agreement between model output and the experimental data. Especially the large amplitude, late components of the ERP are very close to the original waveform. The early component of the evoked potential, the P200, can be seen in the experimental data after each stimulus, but it is more pronounced in the model output.

In addition, the evoked spindle responses of model and data also have similar time courses. In both cases spindle power is systematically increased during the depolarized up phases induced by the stimuli. However, the strong increase in spindle power seen in the data after the first stimulus is not visible in the model. We hypothesize this to stem from a recruitment effect, where the stimulus activates a larger fraction of the thalamus than the endogenous slow oscillation would. As the thalamic module is a point model without any spatial extent, these effects are excluded by construction.

Interestingly, in the experimental data there is a drop in spindle power after the second stimulus is applied. This seems to be a refractoriness of the thalamus after the second slow oscillation, which has also been observed in (Ngo et al., 2015). Despite the model showing such a refractory period in the isolated thalamus (Figure 4.8A), as well as during trains of endogenous SOs in the full model (Figure 4.17A), it lacks it upon stimulation (Figure 4.17B).

This happens because stimulation disturbs the I_h mediated spindle termination mechanism. As the stimulation depolarizes the TC population, the calcium concentration drops, because
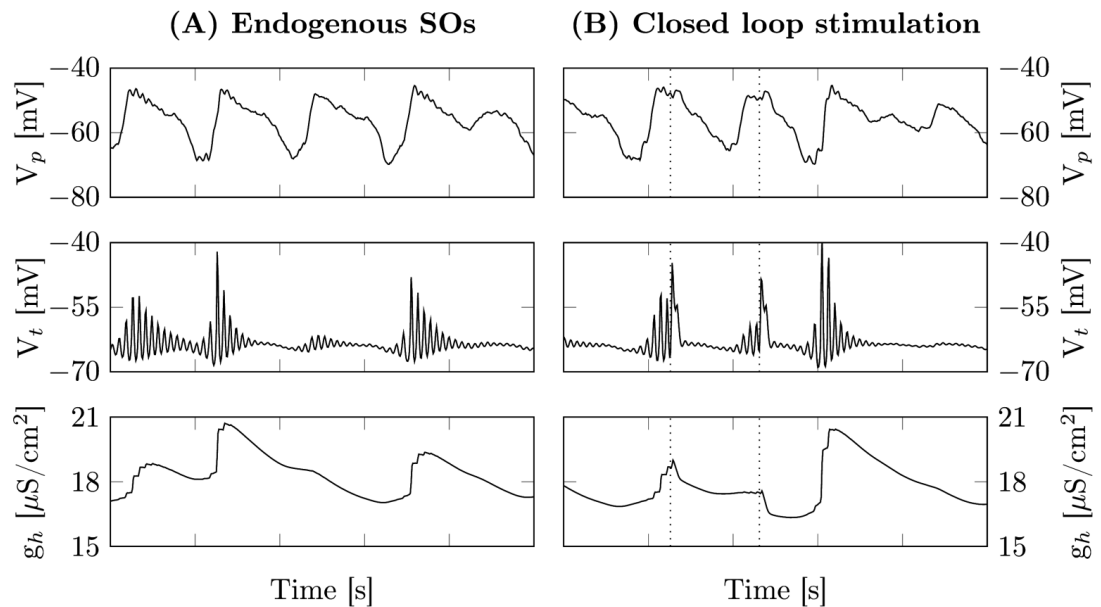
Figure 4.17.: Stimulation disturbs refractoriness. The upper two panels depict the membrane voltages of the pyramidal and thalamic relay populations, respectively. In the third panel the conductivity of the I_h current is shown. (A) Example time series of an unperturbed train of SOs during sleep stage N3. The first SO leads to an activation of I_h, that slowly declines back to baseline levels. As I_h activation is still well above baseline, the second and third SOs are unable to trigger a spindle response. During the fourth SO I_h activation is sufficiently low so that a spindle occurs. (B) Shown is an example of closed-loop stimulation during sleep stage N3, with the dashed lines indicating stimulus onset. In contrast to the endogenous case, the depolarization of the thalamic relay population induced by the stimulation leads to a rapid decrease in I_h activation, so that the following SO triggers a spindle. Parameters as in Table 4.4.

calcium influx through the I_T current stops and calcium leaks out with a time constant of 10ms. Without the elevated calcium concentration, I_h deactivates back to baseline levels and immediately allows for a new full fledged spindle.

We also reproduced the EEG response of the open-loop stimulation used in the experiment presented in detail in chapter 6 (Figure 4.18). The model parameters and stimuli where the same as for the closed-loop stimulation, except for the timing of the stimuli. Stimuli consisted of sequences of 3 clicks, where the first and second click were separated by 975 ms and the second and third click by 1075 ms. Sequences were separated randomly by 5-9 s.

Similar to the closed-loop paradigm cortical model responses match the experimental observation quite well, in particular the afteroscillation around $t = 3.7$ s and the P200 bumps following each stimulus. A notable difference is again in the spindle response, which is comparable in magnitude across all three stimuli, whereas it is maximal for the first stimulus and markedly lower upon second and third stimuli in the experimental data.

4.5. Discussion

Characterization of KCs and SOs We explored an extended neural mass model of the cortex and related its multiple dynamical regimes to different sleep stages.

A bifurcation analysis revealed the existence of a fold as well as a Hopf bifurcation accompanied by a canard phenomenon. We argue that deflections generated by the canard explosion are identical to KCs seen in the EEG during natural sleep, leading to the spike-like nature of the
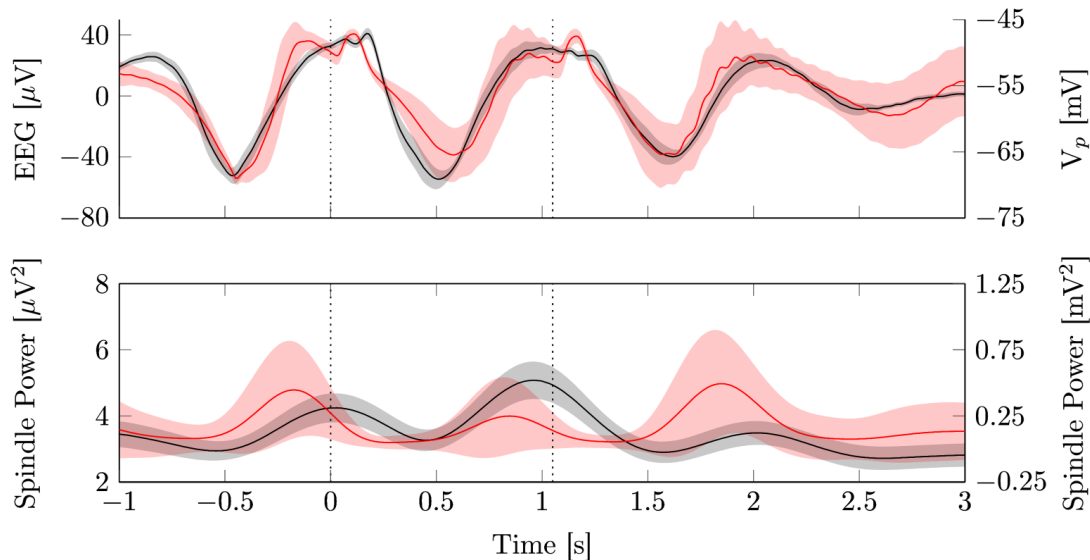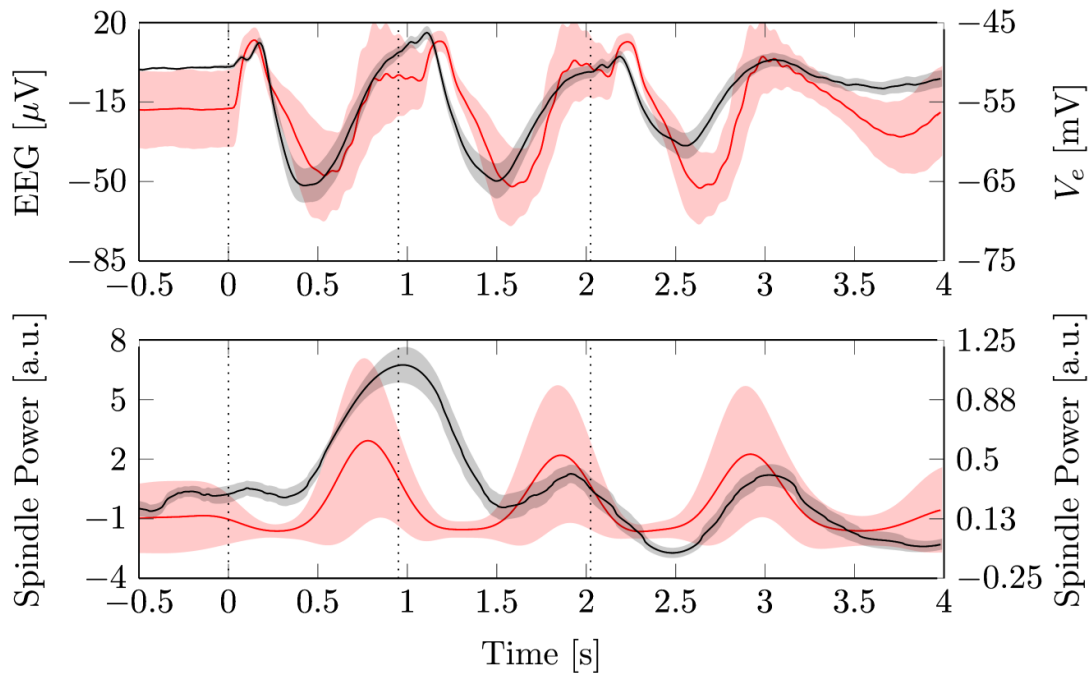
Figure 4.18.: Open-loop stimulation. The upper panel depicts in black the mean ($\pm$ SEM) evoked potentials of human EEG data from electrode *Cz* during open-loop stimulation, time locked to the first stimulus (21 subjects, 295 ± 119 stimuli). In red the reproduction of the stimulation protocol with the model is shown (mean $\pm$ SD, 88 stimuli). The dashed line marks the stimulus onset. The lower panel shows the corresponding fast spindle power. Parameters used for model simulation are given in Table 4.4.

KCs. Increasing the bifurcation parameter σ_e the canard vanishes, explaining the damped oscillatory behavior of SOs. Our analysis provides a clear theoretical distinction between KCs and SOs. However, as both the limit and the relaxation cycle are shaped by the same underlying homoclinic orbit, the actual transition is rather smooth even in the noise-free deterministic system (see Figure 4.4). Therefore, it might be challenging to find this distinction within experimental data.

Based on the bifurcation analysis we identified parameter regimes that show characteristics of sleep stage N2 and N3 and showed that the model is able to reproduce the EEG of both sleep stages to a high degree. Building upon these findings we propose an alternative scenario for the sleep wake transition. Rather than entering a bistable regime the cortex stays primarily within the active state. As sleep deepens, the cortex approaches the Hopf bifurcation, leading to an increase in amplitude and slowing of noise driven background oscillations, as well as large amplitude deflections, i.e., KCs. At the transition to sleep stage N3 the canard phenomenon vanishes due to the cusp bifurcation. The remaining Hopf bifurcation is responsible for the generation of noise driven SOs. Isolated events as in sleep stage N2 are not possible within that regime.

Parameter settings within region II or III lead to highly regular relaxation oscillations or limit cycles, that do *not* resemble human EEG. It is crucial that the cortex must be within region I *close* to region II or III to reproduce the data. In a study on resting state networks (Deco and Jirsa, 2012) found the awake brain to be in a state of criticality, which leads to an increased responsiveness. In this study, we also find the sleeping cortex close to a phase transition and suggest that the concept of criticality is not restricted to wakefulness, but carries over to sleep. However, the phase transition and computational goal are different.

Due to the presence of noise bifurcations do not lead to clear-cut qualitative changes of the dynamics (Curto et al., 2009). Noise can shift critical points or induce behavior that is not seen in the deterministic case, such as noise-induced transitions.

Relation to intracellular recordings   Our work deals primarily with the characteristics of EEG signals during non-REM sleep. However, the presented bifurcation analysis is useful in a broader context. Similar activity is found e.g., during non-REM sleep, anesthesia, coma and in isolated cortical preparations. It becomes increasingly clear that there exists a continuum of slow oscillatory states, which are mainly characterized by the fraction of time spent in up or down states, the temporal regularity with which state transitions occur and the response to external stimuli.

The phenomenon of up and down states in intracellular recordings is commonly associated with the notion of bistability or relaxation oscillations. However, it is important to note that most results on SOs were obtained in deeply anesthetized animals or slice preparations. Under these conditions, the system is down state dominated, i.e., down states last longer than up states, the occurrence of up states is often highly rhythmic (Deco et al., 2009; Chauvette et al., 2011) or up states are infrequent and transient (Poskanzer and Yuste, 2011). In the model these classical regimes are also present, namely in regions III, V and VI.

Generally, SOs produced by anesthesia are much more regular than during natural sleep (Chauvette et al., 2011; Amzica and Steriade, 1998). Under ketamine-xylazine anesthesia neurons spend twice the time in silent states compared to natural SWS (Chauvette et al., 2011), and in the auditory cortex of awake rats prolonged up states are not even observed at all (Hromadka et al., 2013). Furthermore, SO properties differ from one anesthetic to the other (Amzica and Steriade, 1997a). Ketamine-xylazine anesthesia produces a uniform and continuous SO state (Ruiz-Mejias et al., 2011), whereas with urethane epochs of stable SOs are short-lived and desynchronized periods may occur spontaneously (Clement et al., 2008). This is similar to SWS where one finds waxing and waning of slow-wave complexes interleaved with periods reminiscent of active states (Destexhe et al., 1999).

In contrast, (Cash et al., 2009) pointed out that a KC during light sleep is not always embedded in an ongoing SO, but is mostly an isolated event. Clearly, in N2 the active state dominates. Similarly, many studies report that during SWS of naturally sleeping animals more time is spent in up states than in down states (Destexhe et al., 1999; Steriade et al., 2001) (Timofeev et al., 2001b; Ji and Wilson, 2007; Vyazovskiy et al., 2009; Chauvette et al., 2011) Furthermore, it has been reported that SWS contains many episodes of low-amplitude fast oscillations, lasting several seconds and resembling the active state (Destexhe and Sejnowski, 2003). This evidence points to natural sleep being up state dominated.

Furthermore, bistability is inferred via bimodality in the distribution of individual cells membrane potential. In local field potentials, one can observe a markedly conserved waveform of individual SO events (Crunelli and Hughes, 2010), but bimodality is already less visible. It is known that collective dynamics can exhibit, e.g., limit-cycle regimes, but at the same time emerge from irregular and high-dimensional neuronal activity, which is only apparent at small-scales (Boustani and Destexhe, 2009).

The spectrum of SO phenomena cannot be fully captured by the concepts of bimodality or relaxation oscillations. Our analysis corroborates that the KC can be identified with a single, isolated relaxation cycle and slow-wave activity, including prolonged episodes of low-amplitude fast oscillations, stems from noise driven oscillations around a stable focus. Down states occur frequently in the up state dominated cortex, but they are transient.

Predictions   The assumption that a substantial gain change accompanies the change of sleep stages is reasonable, but still has to be clearly demonstrated experimentally for natural sleep. The only publication we are aware of that touches this issue is (Steriade et al., 2001). Our model indicates that an increase in gain can induce a bistable state when awake, moving from region I to region V. Likewise, looking at comatose states (region IV) a decrease in gain should induce limit cycle oscillations.

Additionally, constant neural activation, i.e., arousal, causes relaxation oscillations in the model. Indeed, this phenomenon seems to occur in comatose patients, too, where one observes an increase in delta activity after stimulation (Evans, 1976). This is termed paradoxical arousal and should not be confused with the paradoxical excitation/biphasic response during the induction process of anesthesia.

Furthermore, given the suggested role of gain change in the transition between N2 and N3, an altered slope of the f-I-relation of excitatory pyramidal cells could be a key factor in distinguishing wake and REM sleep. Activity-dependent and leak potassium currents (or tonically activated extrasynaptic $GABA_A$ receptors) are both able to promote bistability in a cortical population. However, only activity-dependent mechanisms contribute to rhythmicity. It would be interesting to see their contributions revealed for natural sleep and anesthesia.

A study by Molaee-Ardekani (2007) showed that a similar model of slow firing rate adaptation can reproduce the effects seen under anesthesia. A comparison of my findings with their results suggest that the region of bistability (V) as well as as well as the region of excitability (VI) are actually associated with anesthesia.

Sleep: more than bistability and relaxation oscillations   A main result of this work is that on the macroscopic level the cortex is not necessarily in a bistable regime during natural deep sleep. We argue that properties of KCs and SOs at the EEG level support the view of a monostable active cortex close to a Hopf and a saddle node bifurcation.

We stress that the characterization of KCs and SOs is made on the *population* level. While the switching between up and down states on the cellular level points to relaxation oscillations or bistability with noise driven transitions, relatively regular oscillation at the cellular level may appear less regular at the EEG level, due to varying spatial synchrony (Amzica and Steriade, 1998). Relaxation oscillations in the EEG usually correspond to pathological conditions like epilepsy.

We have not explicitly analyzed other adaptation mechanisms like multiplicative feedback arising due to synaptic depression or depletion of extra-cellular calcium or inhibitory modulation (Sanchez-Vives et al., 2010). However, the additive activity-dependent feedback investigated here is sufficient to account for a multitude of phenomena in healthy and pathological conditions. Furthermore, we expect that the bifurcation structure of the system, i.e., presence of saddle-nodes, Hopf and homoclinic bifurcation, will persist in alternative settings. Thus, the main conclusions do not depend on the particular choice of the feedback mechanism.

We developed a neural mass model of the thalamocortical system that produces realistic time courses of EEG signals during sleep stages N2 and N3 and correctly replicates the timing of KCs and spindles. We validated the model with SO triggered averages of the EEG signal and spindle power. Finally, we used the model to reproduce evoked responses from closed-loop auditory stimulation during human non-REM sleep.

Mechanisms of spindle generation. The model emphasizes the role of I_T and I_h currents in the generation of thalamocortical rhythms as they were sufficient to reproduce the investigated EEG phenomena. It reproduces the grouping of spindles and KCs/SOs, observed in human EEG (Mölle et al., 2002), that is thought to play a crucial role in the consolidation of memory (Mölle et al., 2006; Diekelmann and Born, 2010). Additionally, it exhibits refractoriness of spindle oscillations, i.e., not every SO in a train of endogenous SOs triggers a spindle. Although adding extra currents increases dimensionality and parameter space, the model still preserves the overall simplicity and computational efficacy common to neural mass models.

Spindle timing. Relative to the negative deflection of a KC, spindles consistently start earlier than in the data. Consistently, the depolarizing up phase of endogenous KCs and SOs arrives earlier in the model than in the data. A comparison with the results from the isolated cortical module shows, that this is mostly due to strong depolarizing input from the thalamus. Yet, there is no clear explanation for the difference between model and experiment. It might be due to the simplification of the intrinsic mechanisms, e.g., firing rate adaptation in cortex and spindle dynamics in thalamus. On the other hand it could also be that finer details, e.g., spatial extension or the layered structure of the cortex are important for its temporal dynamics. Also the way conduction delays between cortex and thalamus were implemented, namely via an extra convolution with an alpha function, might play a role.

Auditory stimulation. A recent experimental study suggests that the refractoriness of thalamic spindles is a limiting factor for the impact of auditory stimulation upon memory consolidation (Ngo et al., 2015). They found, that longer trains of stimuli do *not* provide any benefit in memory consolidation compared to the two stimulus protocol. Remarkably, the first stimulus triggers a strong spindle, whereas the following stimuli show a diminished spindle response. This clearly indicates the importance of the grouping of spindles and SOs for the consolidation of memory. In contrast to these experimental findings, auditory stimulation in the model alleviates the refractoriness of the thalamic module, leading to spindle oscillations with similar amplitude following every stimulus. This is because strong depolarization of the thalamic populations by the stimulus interrupts the thalamic I_h rhythm. We see this as a challenge for the understanding of how auditory stimulation is processed during sleep and how it interacts with spindle generation.

Relation to other work. Recently, Cona et al. also developed a neural mass model to describe the sleeping thalamocortical system (Cona et al., 2014). They combined two distinct firing modes via the activation of the T-type calcium current, showing that this multiplicative change in firing rate can lead to periodic spindle-like oscillations. However, in this study we include the currents directly into the equation of the membrane voltage, similar to (Żygierewicz et al., 2001; Weigenand et al., 2014). Our model relates directly to scalp EEG signals during natural sleep and auditory stimulation.

Effect of neuromodulators and sleep regulation. In the model, we induce the transition between the different sleep stages by changes of the three key parameters (g_{KNa} and σ_p in the cortex and $\bar{g}_{LK}$ in the thalamus), that are directly linked to the action of neuromodulators (McCormick, 1992; Hughes et al., 2002; Steriade, 2004; Weigenand et al., 2014). These parameters are known to be affected by neuromodulators, such as noradrenalin, serotonin and acetylcholine (McCormick, 1989; Timmons et al., 2004; Zhang and Arsenault, 2005; Gulledge et al., 2009; Soma et al., 2012), whose concentrations vary over the night. Regulation of neuromodulator concentrations arises through complex interactions within different sleep regulatory

networks (Léna et al., 2005; Lydic and Baghdoyan, 2005). Recently there has been progress in the mathematical description of sleep regulatory networks (Tamakawa, 2005; Diniz Behn and Booth, 2010; Phillips and Robinson, 2007; Rempe et al., 2009; Kumar et al., 2012). However, as we focus on the different dynamical modes the thalamocortical system can exhibit and how thalamus and cortex interact, we do not include sleep regulation in this manuscript.

Are KCs biphasic or triphasic? The waveform of a KC has been described as being biphasic, consisting of a large negative deflection (down state) followed by a pronounced depolarization (up state) - or triphasic, comprising an initial positive bump followed by a down state and an up state. Menicucci et al. (2013) analyzed the shapes of KCs in N2 and N3 and found that on average a triphasic pattern, up-down-up, is present in both sleep stages. Our model does not show this sequence for sleep stage N2. In vivo, sleep stage N2 is rarely stationary and spans varying depths of sleep, as well as transitions to other sleep stages. In contrast, the model depicts idealized N2 at a single point in time, to separate it from wakefulness and N3. Choosing a parameter setting closer to N3 will naturally give rise to a depolarization preceding the down state. We predict that biphasic KCs should be found mostly in early N2 or very late N2, as in the second half of the night after the major SWS episodes.

Is there true bistability during natural sleep? The model is consistent with the observation that during N2 and N3 of natural sleep the cortex is mostly in the active state (Chauvette et al., 2011). We adopt the view of (Weigenand et al., 2014), where KCs were characterized as transient events - reversed spikes - initiated by a canard explosion. Consequently the down state is never stable in the model. This may seem counterintuitive as many intracellular recordings support the notion of bistability. However, neural mass models represent population averages, whereas intracellular recordings only sample individual members of a population, leaving open this alternative interpretation derived from stereotypical graphoelements in the EEG.

5. Model III: The K-complex in the Fitzhugh-Nagumo model

5.1. Model description

The Fitzhugh-Nagumo (FHN) model

$$\dot{V} = aV^3 + bV^2 + cV + d - w + I(t)$$
$$\dot{w} = (-ew + V)/\tau$$

(5.1)

has been used to elucidate many aspects of spiking in neurons and other excitable systems. In the context of neural mass models, the variable V with the cubic nullcline can be regarded as the membrane voltage of an excitatory population and the variable w represents an additive, activity-dependent feedback current. The variable V is the fast system and variable w is slow when τ is sufficiently large. External, time-dependent perturbations enter via $I(t)$. Despite its simplicity, the FHN model can generate a rich set of dynamics. It is known that it contains a canard explosion (Benoit et al., 1981; Eckhaus, 1983), which we found to be the key mechanism underlying K-complex generation in the neural mass model of the previous chapter. Hence, the FHN model might be a suitable approximation of large-scale cortical activity and reveal new predictions and insights into the characteristics of K-complexes.

5.2. Reproduction of sleep stage N2 and delta activity

With the algorithm of chapter 3 we fitted the model to 30s traces of EEG data from sleep stage N2. The output of the simple FHN model shares many features with the original data (Figure 5.1), just like the more complicated conductance-based neural mass model (Figure 4.5). Leaving aside the peaks in the spindle band it fits the experimental power spectrum very well, in particular the low frequencies and the power law decay (Figure 5.2).

Using the linearized system one can compute an analytical approximation of the power spectrum. Given the Jacobian $J = \left.\frac{\partial F(x)}{\partial x}\right|_{x=x^*}$ of a system $\dot{x} = F(x) + I$ at its steady-state x^*, then the power spectrum S can be obtained via

$$S(p) = \|(pE - J)^{-1}\mathcal{F}\{I\}\|_2,$$

(5.2)

where $p = i2\pi f$, E is the identity matrix and $\mathcal{F}\{I\}$ is the Fourier transform of the external input. The steady-state is the solution to $F(x^*) = 0$.

The Jacobian of the FHN model is

$$J = \begin{pmatrix} -3aV^2 + 2bV + c & -1 \\ 1/\tau & -e/\tau \end{pmatrix}.$$

(5.3)

The result is depicted in Figure 5.3. It demonstrates that fitting a model only with spectral information of the linearized system, which unfortunately is common practice (Bojak and Liley,
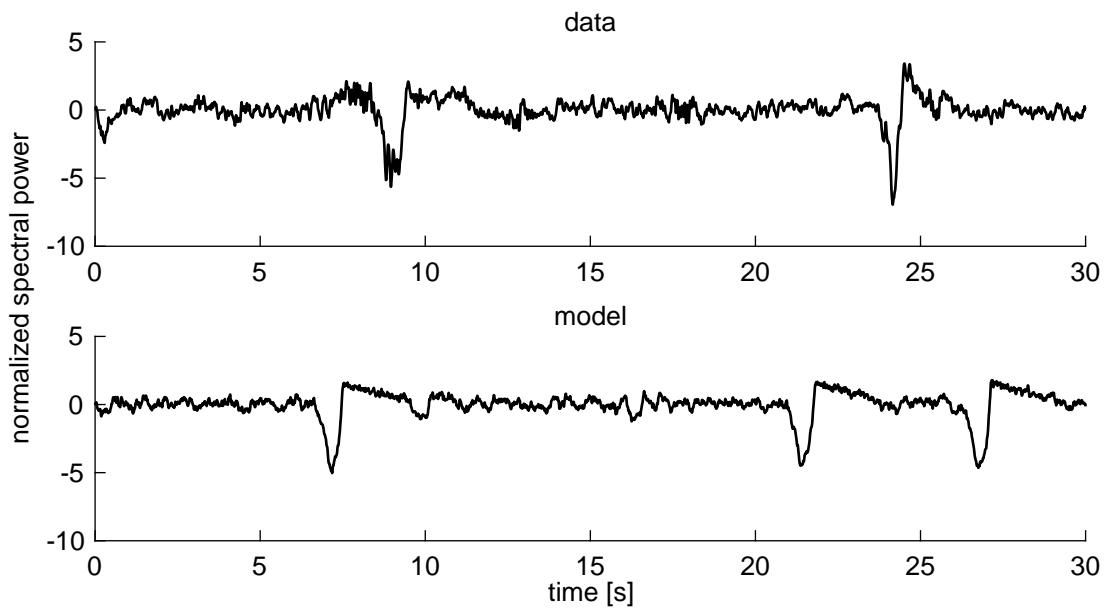
Figure 5.1.: Qualitative comparison of (top) human EEG of sleep stage N2 with (bottom) the behavior of the FHN model. The traces illustrate the medium-amplitude background oscillations and the stereotypical shape of spontaneous KCs at the EEG level. The model's KC is noise induced and represents a single relaxation cycle. Both time series are z-scored. Note that the positive overshoot following the sharp negative deflection in the experimental time series is not a filtering artifact.
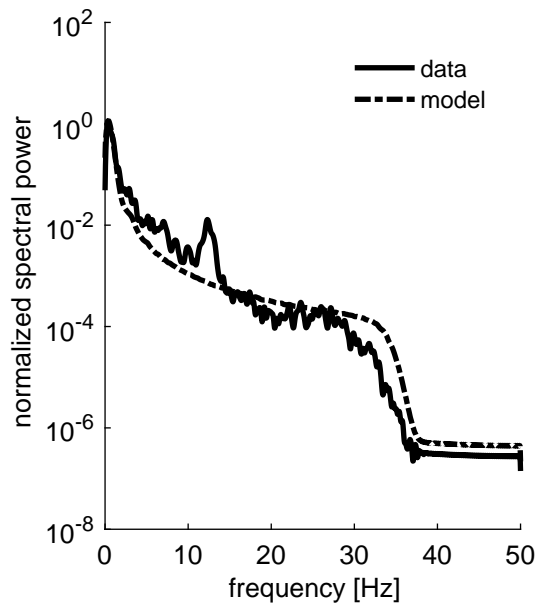
Figure 5.2.: Power spectra of a representative 10min N2 period and a fit of the FHN model ($a = -2.2$, $b = -3.6$, $c = -0.6$, $d = 0.6$, $e = -0.03$, $\tau = 4.9$, $\sigma = 0.11$)**.** The EEG data has been lowpass filtered to remove noise and components that cannot be captured by the model anyway. The same filter was included in the model formulation for the fitting.
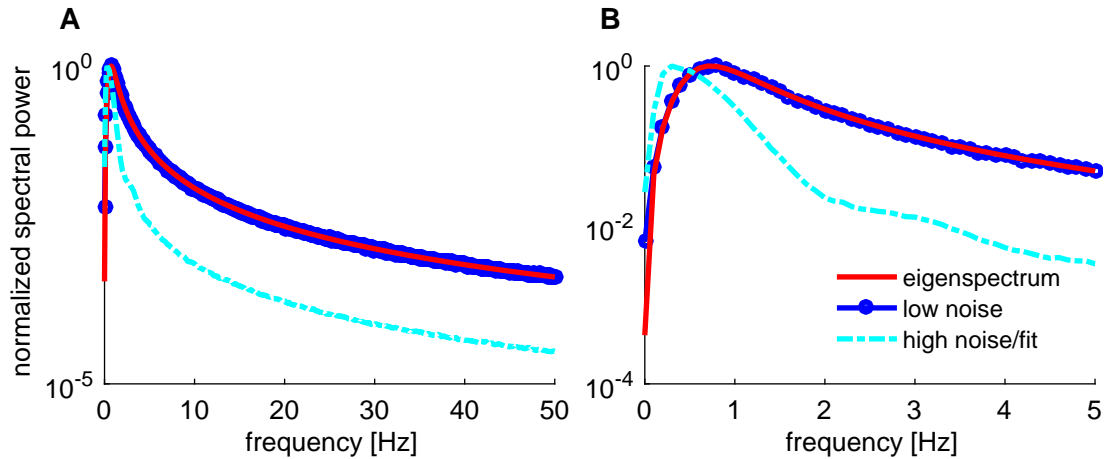
Figure 5.3.: (In)Validity of linear approximation. (A) For *low noise*, with only sub-threshold oscillations, the linear approximation (eigenspectrum, red line) of the nonlinear system by Eq. 5.2 provides a remarkably good fit to the true power spectrum obtained via simulation. For *high* noise, in the presence of K-complexes, the linear approximation is significantly worse. In the true spectrum, signal power is concentrated in lower frequencies. (B) Zoom into low frequency region of (A). Note the bump around 3 Hz. The peak of the model output has moved to lower frequencies. Parameters are the same as in Figure 5.2

2005; Robinson et al., 2002; Foster et al., 2011; Hashemi et al., 2014), will miss important features and bias the estimated parameters. Furthermore, the analysis shows that noise driven "subthreshold" oscillations have a higher frequency than K-complexes. This could be the origin of one type of cortical delta oscillations.

5.3. Phase plane analysis & K-complex mechanism
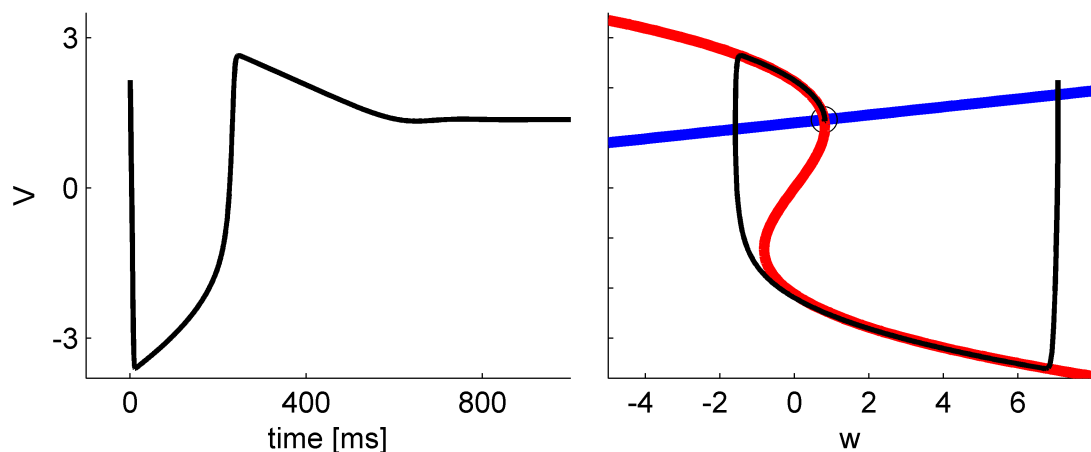
Figure 5.4.: K-complex and canard explosion in the phase plane of the Fitzhugh-Nagumo model. (A) Time course of a canard cycle / K-complex in the noise-free Fitzhugh-Nagumo model. The initial conditions were set away from the equilibrium to initiate the cycle. (B) Shown are the V-nullcline (red) and w-nullcline (blue) of the system 5.1. The black line depicts the trajectory of the canard cycle / K-complex in (A). The circle at the intersection of both nullclines marks the stable fixed point.

Figure 5.4 shows the phase plane of the FHN model and the trajectory of a proposed K-complex. The scenario is the classical canard explosion. The cubic nullcline has two attracting outer branches and a repelling middle branch. For small perturbations the system stays close

to the stable fixed point and exhibits low amplitude oscillations. Large perturbations can move the system beyond the stable manifold. It then moves quickly to the lower branch and follows the upper branch for a significant amount of time, back to the stable fixed point.

The time-constant τ directly controls the width of the K-complex as well as of the slow decay of the afterdepolarization. Furthermore, the shape of the afterdepolarization of the K-complex is determined by the upper branch of the cubic V-nullcline.

At least in this simple model a pure instantaneous increase in voltage, e.g., by very brief strong stimuli, does not cause a K-complex, as the system will stay within the region bordered by the U-shaped stable manifold. In contrast, non-instantaneous stimuli with a certain duration will additionally cause an increase in adaptation current w, which can move the system beyond the basin of attraction of the fixed point. Moreover, excitatory inputs will more likely cause an all or none response, whereas inhibitory inputs allow a more graded response, because the system stays closer to the middle branch. In experiments with humans, such an inhibition could be caused by short muting of a steady background noise or a sudden decrease in illumination.

As one can see from the graph, there is only one fixed point present at the intersection of the two nullclines and the w-nullcline is almost horizontal. Notably, when inputs move the V-nullcline to the left or right, the stability of the fixed point will not change over a wide range. This allows the prediction that, if the slope of the w-nullcline is zero or very shallow, a gradual increase of input and constant offset in the input will have no effect on the K-complex generation. This has implications for e.g., transcranial direct current stimulation (tDCS), namely that it should not affect K-complex dynamics. It also reveals a limitation of this simple model. Its dynamics are almost invariant with respect to the input level. Clearly, an input current cannot grow without bound in a biological system.

The canard phenomenon can also provide an elegant explanation for the consistent experimental observation that the transition to the down state is more synchronous than the one to the up state. The drop to the bottom branch (Figure 5.4 B) occurs almost instantaneously (high synchrony), but repolarization has to follow the bottom branch and takes more time (low synchrony).

Due to its simplicity the FHN model will not exhibit additional rhythms. An extension of the model with another fast subsystem, e.g., an inhibitory population, allows for more complex behavior.

6. Experiment: Open-loop auditory stimulation during non-REM sleep and its effect on memory consolidation

Parts of this chapter have been published in Weigenand et al. (2016).

A recent study in humans showed that two-click auditory stimulation in phase with positive half-waves of endogenous SOs ("closed-loop stimulation") is capable of improving memory performance in a verbal paired-associate learning task (Ngo et al., 2013). This result has been reproduced with more than two clicks, also relying on phase-dependent stimulation (Ngo et al., 2015). Although spindles and SOs seem to be involved, the specific aspect of the closed-loop stimulation paradigm responsible for the improvement remains unclear.

We tested whether a similar effect on learning performance can be achieved with a rhythmic click sequence. The rhythmic sequence also achieves in-phase stimulation, but starts at a random phase of the SO. The stimulation paradigm, termed open-loop stimulation in the following, is based on the observation that a single click has a high probability of evoking a single SO or a K-complex given some time has passed since the last click (Bastien and Campbell, 1994).

We used the first click in a sequence to evoke a SO, thereby resetting the ongoing activity to a known phase. Using a defined interval, a subsequent click can then be delivered during the up state of the evoked SO.

6.1. Materials and Methods

6.1.1. Participants

26 healthy right-handed volunteers participated in this study, of which 21 (11 male, mean age 22.2 years, range 18-28 years) were used for the analysis. Five participants left the study before completion. The experimental protocol was approved by the ethics committee of the University of Lübeck (application 13-172) and all volunteers gave their written consent prior to participation.

The subjects were native German speakers, non-smokers and had no history of neurological, psychiatric or endocrine disorders. Furthermore, all participants were free from medication except the females, who were all taking hormonal contraceptives. Participants slept 7-9 h per night, did not normally take daytime naps and followed a regular sleep schedule as assessed by interview and questionnaire. They reported no major disruptions of the sleep-wake cycle during the 4 weeks before experimentation. Subjects were instructed to abstain from alcohol and caffeine and to get up at 6:00 a.m. on the day of the experiment.
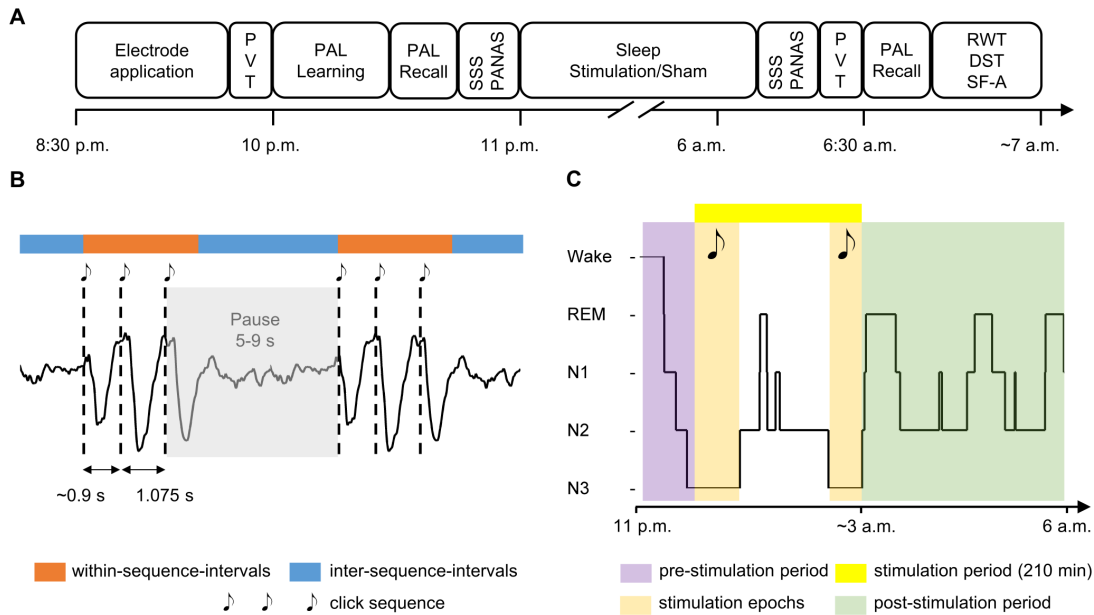
Figure 6.1.: Stimulation protocol. (A) Outline of experimental nights. PVT: psychomotor vigilance test, PAL: paired-associate learning, SSS: Standford Sleepiness Scale, RWT: Regensburg Word Fluency Test, DST: digit span test, SF-A: sleep questionnaire A, PANAS: Positive and Negative Affect Schedule. (B) Sequences of 3 clicks were applied during N3. After a sequence of 3 clicks, there was a 5 to 9 s pause ("inter-sequence-interval") between the last click and the first click of the following sequence. The first and last click of a sequence define the "within-sequence-interval". The interval between the first and second click within a sequence was set to the average SO period of the respective subject, which was determined during the adaptation night from single-click evoked potentials at lead Fz. The interval between the second and third click was fixed to 1.075 s. The first click had a high probability to evoke a SO and, hence, was applied to induce a phase reset. The second and third clicks were then more likely to occur in phase with a SO up state. Essentially, the protocol is a phase-independent modification of the closed-loop auditory stimulation in Ngo et al. (2013). (C) A hypnogram indicating the pre-stimulation period, stimulation period, stimulation epochs and post-stimulation period. Stimulation started after 5 min of stable N3 and only took place during N3 epochs of the 210 min stimulation period. Baseline effects were controlled for in the N2 epochs of the pre-stimulation period. Non-REM sleep epochs of the post-stimulation period were analyzed for after-effects.

6.1.2. Experimental design and procedures

This study followed a single-blind, counterbalanced crossover design. Each subject participated in one adaptation night, and two experimental nights of either a "Stimulation" or a "Sham" session. Experimental nights were separated by at least one week to avoid carry-over effects. Experimental sessions started at 8:30 p.m. with the application of EEG electrodes. Each session consisted of a learning phase followed by an immediate recall phase with feedback and subsequent sleep from 11 p.m.-6 a.m., with either auditory or sham stimulation. A second recall in the morning (6:30 a.m.) served to assess overnight retention. The experimental design is summarized in Figure 6.1A. Please note that feedback at immediate retest does not allow for assessment of a real baseline.

6.1.3. EEG recordings and polysomnography

EEG was recorded throughout the whole night using a BrainAmp DC amplifier (Brain Products) from 21 channels according to the international 10-20 system (Fp1, Fpz, Fp2, F7, F3, Fz, F4, F8, T3, C3, Cz, C4, T4, T5, P3, Pz, P4, T6, O1, Oz, O2), referenced to linked mastoid electrodes. Ag-AgCl electrodes were used and impedances were below 5 kΩ. Signals were low-pass filtered (fcutoff=120 Hz), sampled at 500 Hz and stored for later offline analysis on a PC together with the stimulation triggers. For all subsequent analysis data were downsampled to 100 Hz. Vertical and horizontal eye movements (EOG) as well as electromyogram from the chin (EMG) were obtained for standard polysomnography and artefact detection. For the adaptation night, a reduced set of scalp electrodes was used (Fp1, Fpz, Fp2, F3, Fz, F4, C3, Cz, C4, P3, Pz, P4).

Each night was scored visually for succeeding 30-s epochs according to AASM criteria (Iber et al., 2007) by an experienced sleep scorer blind to the condition. Total sleep time (TST), time spent in different sleep stages (wake; sleep stages N1, N2, N3, REM) and the number of movement arousals were determined for the whole night and separately for the stimulation period and the remaining sleep time. Sleep onset, i.e., the first occurrence of sleep stage N2, was defined with reference to lights off.

6.1.4. Auditory stimulation

The stimulation protocol is outlined in Figure 6.1B. In the Stimulation condition, groups of three click sounds were delivered via in-ear headphones (Philips SHE 8500) during slow-wave sleep (sleep stage N3). A single click consisted of 50ms of pink noise with a 5 ms rise and fall time. The timing of the second and third click relative to the first click was chosen to maximize their probability of coinciding with evoked SO up states, given that the preceding click triggers a SO.

Specifically, the delay between first and second click was chosen individually as the mean delay time between the first click and the maximum peak of the subject's succeeding large positive deflection at electrode Fz. This deflection reflects the presumed depolarizing up state of the evoked K-complex. This delay was assessed in the adaptation night using sixty clicks with interstimulus intervals of 5-9 s (uniformly distributed). The component is known as P900 in the evoked potential literature, since the positive peak occurs ca 900ms after the stimulus (Bastien et al., 2002).

The second and third click were 1.075 s apart, which was adopted from (Ngo et al., 2013) and corresponded to the average duration of a SO. Click sequences were separated by 5-9 s

(uniform scatter). In the Sham condition, subjects wore in-ear headphones but no clicks were generated. The stimulation period always began after 5 minutes of stable N3, which was assessed online by the experimenter and continued for 210 min. When arousals or changes in sleep stage were detected stimulation was paused. It was resumed when stable N3 was detected again. Signals were generated using a CED Power1401 mkII programmed via Spike2 version 7.11 (Cambridge Electronic Design Limited, Cambridge, England). Trigger markers of each tone were recorded in the Stimulation condition. Trigger markers of the Sham condition were generated offline and matched the markers of the Stimulation condition in number, distribution of interstimulus intervals, number of stimulation epochs, and start and end time of the stimulation period.

6.1.5. Paired-associate learning task

The word-pair memory task was adopted from a previous study (Ngo et al., 2013). In brief, subjects had to memorize 120 German word-pairs, which were presented sequentially on a monitor using E-Prime 2.0 (Psychology Software Tools). Each item was displayed for 4 s with an interstimulus interval of 1 s between items. Two different word lists were used for the two experimental sessions and the order of word lists was balanced across subjects and conditions. Furthermore, the lists were matched in difficulty in order to reduce baseline variance. During the immediate recall phase, the subject had to respond by naming the second word upon presentation of the first word of a pair and had unlimited time to recall the appropriate word. The correct answer was revealed on the screen immediately after the response. At testing in the morning after sleep, cued recall was tested in the same manner as after learning, except that no feedback was given after the subject's response. Participants were explicitly advised to visualize word-pairs as learning strategy and to guess instead of giving no answer. Only exact responses were considered correct. Several control tests were performed to assess non-specific contributions of the stimulation to memory performance. Before and after sleep, the subjects' mood and tiredness were assessed with the Positive and Negative Affect Schedule (PANAS) and the Stanford Sleepiness Scale (SSS) (Hoddes et al., 1973; Watson et al., 1988). Sleep quality was assessed by means of questionnaire SF-A (Görtelmeyer, 1981). Additionally, a digit span test (DST) and the Regensburg word fluency test (RWT) were administered in the morning to control for general abilities to retrieve information from long-term memory and for working memory performance (Tewes, 1991; Aschenbrenner et al., 2000). All subjects underwent a psychomotor vigilance test (PVT) to control for general alertness and vigilance. In this task, a counter appears at the center of a computer screen every 2-10 seconds for about 5 minutes and participants have to respond as quickly as possible by pressing a button.

6.1.6. Event related potentials

Data were analyzed using MATLAB R2013a (The MathWorks, Inc., Natick, Massachusetts, United States). Event related potentials of the EEG signal were obtained from the downsampled raw data of which a linear trend was removed ± 6 s around the first click of each sequence. This eliminated the influence of strong dc drifts without distorting the waveform. The number of windows used for averaging in the Stimulation and Sham condition was on average 295 ± 119 and 287 ± 105, respectively.

6.1.7. Offline detection of slow oscillations and K-complexes

The offline detection of SO events is based on (Mölle et al., 2002). A low-pass filter (Chebyshev type II, fstop=4.5 Hz, fpass=3.5 Hz, Astop=60 dB) and a high-pass filter (Butterworth, fstop=0.1 Hz, fpass=0.5 Hz, Astop=20 dB) were applied to the raw signal of the individual channel of interest. Then all zero-crossings were determined and negative and positive half-waves extracted. Segments having a negative half-wave with a width between 150 and 800 ms and exceeding a peak negativity of -65 μV were regarded as SOs and the negative half-wave peaks were used for the identification of the SO events. The validity of detected events was verified visually. Filters were applied in forward and reverse direction to eliminate phase distortion. SOs were considered to be evoked if they occurred within 200 - 900 ms following a click.

6.1.8. Event histogram

In order to examine whether open-loop stimulation actually evoked SO events, delays between the first clicks of presented click sequences and offline detected SO events (all endogenous + evoked), using a bin size of 100 ms were assessed. The resulting histogram was then normalized using the total number of click sequences, yielding the corresponding probability, P. The analysis was limited to the interval [-2,5] s around first clicks (at $t = 0$ s).

6.1.9. Artefact detection

In a first step, epochs with artefacts were marked manually during scoring. Automatic resetting of DC offsets, sudden signal jumps, increased muscle tone (EMG signal) and drifts induced by sweating were regarded as artifacts. In a second step, an automatic algorithm classified epochs as artefactual if the difference between consecutive samples was >100 μV or the standard deviation of the epoch exceeded 150 μV. Epochs with artifacts were removed from the analysis. In the rare case where a single electrode detached or persistently exhibited artifacts, it was replaced by a combination of the remaining intact electrodes determined by linear regression.

6.1.10. Spectral analysis

Power spectra were computed for all artifact-free 30s epochs with Matlab's pwelch method using a Hanning window of 6 s length, 50% segment overlap and zero-padding to a total length of 20 s. The spectra of the epochs of interest, i.e., the N2 epochs of the pre-stimulation period, the stimulation epochs during non-REM sleep of the stimulation period, and the non-REM sleep epochs of the post-stimulation period, were then averaged and subsequently normalized. The mean of the power of all channels between 0.3 - 30 Hz, both conditions and all non-REM sleep epochs of the subject was used for normalization. This procedure maintains the within-subject variance, but reduces between-subject variance by levelling the large baseline differences between subjects common to spectral data. It has the additional benefit of improving gaussianity of the data. Frequencies below 0.3 Hz were discarded for normalization, because they mainly comprise strongly varying DC and drift components. Finally, normalized spectral data were split into the following frequency bands: SO, 0.5-1 Hz, Delta, 1-4 Hz, SWA, 0.5-4 Hz, Theta, 4-8 Hz, slow spindle, 9-12 Hz, fast spindle, 12-15 Hz. Topographic maps are based on normalized spectral data. In order to extract the time-course of slow and fast spindle activity (instantaneous power) the raw signal was band-pass filtered in the respective spindle band (Chebyshev type II, 40 dB stop band attenuation, 2 Hz transition band) and the squared absolute

value of its Hilbert transform was calculated. This procedure was used in the calculation of the event-related power and the measure for phase-amplitude coupling.

6.1.11. Coupling between spindles and slow oscillations

We used two measures for investigating the relation between slow oscillations and spindles in the 210 minute stimulation interval. First, instantaneous spindle power within positive half-wave intervals was summed and normalized by the total duration of positive half-waves. Please note that this is based on all offline detected, not just evoked, slow oscillations.

Second, for the quantification of phase-amplitude coupling between fast spindles and slow oscillations we used the "mean vector length" method described in (Canolty et al., 2006; Tort et al., 2010)

In short, the EEG signal $s(t)$ of a single channel was band-pass filtered from 12 Hz to 15 Hz, Hilbert-transformed, squared and normalized by its standard deviation to obtain the time course of instantaneous power, $A(t)$. The normalization is necessary to facilitate a comparison between conditions by eliminating the dependence on the overall power level. Similarly, $s(t)$ was band-pass filtered from 0.5 Hz to 3.5 Hz, Hilbert-transformed and converted into a phase-signal $\varphi(t)$ by calculating the angle of the resulting complex-valued time series. $\varphi(t)$ assumes values in the interval $(-\pi, \pi]$ radians. The peak of the negative slow oscillation half-wave corresponds to $\varphi = \pi$ and the positive peak of the positive SO half-wave occurs at $\varphi = 0$. The mean vector length, M, is then defined as $M = \|z\|$ and the phase angle of the coupling is $\varphi^* = \Im\{\log(z)\}$, with $z = 1/T \sum_{t=0}^{T} A(t) \exp(i\varphi(t))$. As we compare modulation indices across conditions, no further normalization is needed.

6.1.12. Time-frequency representation

Individual time-frequency representations were computed using EEGLAB's newtimef (Delorme and Makeig, 2004). First, trials of $[-6, 6]$ s around first clicks were extracted and a linear trend removed (same as for event-related potentials). Second, a short-time Fourier transform using the Hanning window and 300 equally spaced, overlapping segments of 1 s length was applied to each trial. Third, the data was squared. Fourth, for each frequency the trial was divided by the average power across trials of the baseline interval $[-2000, 0]$ ms. Fifth, trials were averaged and the logarithm taken. Sixth, P-values were obtained for each pixel using via a paired permutation t-test (Stimulation vs. Sham) with 4999 permutations using EEGLAB s statcond and corrected for multiple comparisons using the false discovery rate method for positively dependent test (Benjamini and Hochberg, 1995).

6.1.13. Statistical analysis

Statistical analysis was performed in Matlab and R (R Development Core Team, 2008). Data is expressed as mean ± SD (or SEM when indicated). Normal distribution of data was assessed by Shapiro-Wilk test. Normalized EEG power was separately analyzed in the six frequency bands using two-way repeated measures analyses of variance (ANOVA) with the factors condition (Stimulation vs. Sham) and lead (Fp1, Fpz, Fp2, F7, F3, Fz, F4, F8, T3, C3, Cz, C4, T4, T5, P3, Pz, P4, T6, O1, Oz, O2). Huynh-Feldt correction of degrees of freedom was applied where appropriate. Running P-values in ERP plots were obtained using two-tailed Student's paired t-tests. P-values were corrected for multiple comparisons using the false discovery rate method for positively dependent tests (Benjamini and Hochberg, 1995).

6.2. Results

Twelve of 21 subjects reported to have noticed auditory stimulation during the night of which 4 perceived it as unpleasant. Eight subjects were clearly sensitive to stimulation, as they had arousals upon the beginning of a stimulation sequence and could only receive stimulation towards the end of the stimulation period. The mean duration of stimulation epochs within the stimulation period was 49 ± 17 min for the Stimulation condition and 47 ± 14 min for the Sham condition. During this time 295 ± 119 (Sham: 287 ± 105) click sequences were applied. The individually determined delay between first and second click (P900) was on average 942 ± 111 ms across subjects. Event-related potentials, power and acute spindle response similar to auditory closed-loop stimulation The EEG (averaged across subjects) time-locked to the first click revealed a series of strong slow oscillatory responses (Figure 6.2A, top). The ability of the click sequences to evoke SO sequences is reflected in the event histogram of the delays (Figure 6.2C). The probability to evoke a SO is similar for each click in a sequence, namely Pclick 1=0.39 ± 0.16, Pclick 2=0.37 ± 0.15, Pclick 3=0.35 ± 0.15. However, the probability of a click sequence to evoke 3 consecutive SOs is relatively low but still significantly higher as compared to Sham (PStimulation(SO3|SO2|SO1) = 0.13 ± 0.09 vs. PSham(SO3|SO2|SO1)=0.05 ± 0.04; P<0.001).

Event-related fast spindle power ($12 - 15$ Hz) is depicted in Figure 6.2A (middle). The first click triggered not only a large positive wave reflecting the depolarized component of the EEG (putative up state) around $t = 1$ s, but also a single strong response in spindle activity. In contrast, responses to the second and third click of a sequence at $t = 2$ s and $t = 3$ s are markedly lower. Furthermore, the baseline level of event-related fast spindle power is lower in the "Stimulation" condition than in the "Sham" condition.

Similarly, the mean level of event related slow spindle power (9-12 Hz) is higher in Sham (Figure 6.2A, bottom). However, in contrast to fast spindle power, an increase in slow spindle power of similar magnitude can be seen after each click. This suggests that refractory processes play less of a role for slow than for fast spindles.

Next, we analyzed the EEG response to clicks separately for the cases where the first click in a sequence successfully evoked a KC and thus the succeeding click could be played into the next up-states as compared to when the click failed to do so ("KC" vs. "no KC"). The event-related responses in Figure 6.3 (top) clearly reflect the presence or absence of KCs. Notably, a significant increase in fast spindle power after the second click was present, regardless of whether the first click evoked a KC or not - the amplitude being larger in the "KC" case (Figure 6.3, middle). Furthermore, the amplitude of the fast spindle response following the second click is lower when the first click successfully evoked a KC. Slow spindles already show an increase upon the first click if it evoked a KC (Figure 6.3, bottom). In order to provide a more comprehensive overview of the frequency content of the EEG response to click sequences we calculated a time-frequency representation of the within-sequence-intervals comparing Stimulation and Sham condition (Figure 6.4).

Next, we investigated how the morphology of slow oscillation events was influenced by the stimulation. For this, we averaged all offline detected slow oscillation events time-locked to the negative peak of their negative half-wave (Figure 6.2B, top). This revealed, that the amplitude of the main negative half-wave of the SO ($t = 0$ s) was unaffected by stimulation ($P_mathrmfdr = 0.17$). Open-loop stimulation, however, increased the amplitudes of positive half-waves (at $t = \pm 0.5$ s, P_{fdr}<0.01) and negative half-waves (at $t = \pm 1$ s, $P_{\text{fdr}} < 0.01$). This may reflect the greater occurrence of SO trains induced by the click sequences, as indicated by the event histogram in Figure 6.2C.
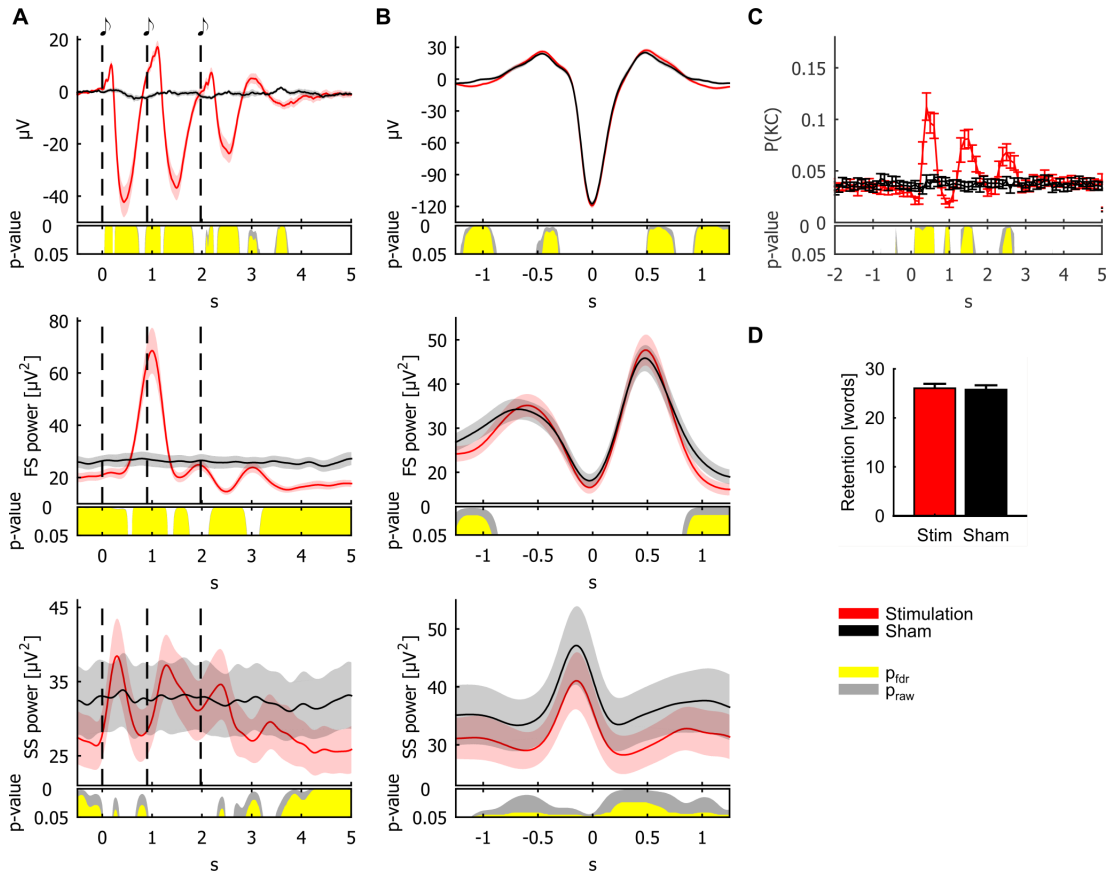
Figure 6.2.: No impact of open-loop auditory stimulation on memory consolidation despite effects on SOs and on spindle power. (A) Mean (±SEM) event-related response at Cz averaged for the wide-band EEG signal, (middle) fast spindle power (FS, $12 - 15$ Hz) and (bottom) slow spindle power (SS, $9 - 12$ Hz), time-locked to the first click of each sequence ($t = 0$ s), for Stimulation (red) and Sham (black) condition. Vertical dashed lines indicate clicks. Time axis is adjusted for individual interstimulus intervals such that the second click occurs at 940 ms. Baseline has not been removed. (B) Mean (±SEM) of EEG signal (top), fast spindle power (middle) and slow spindle power (bottom), time-locked to the negative peak ($t = 0$ s) of all offline detected slow oscillations at Cz, for Stimulation (red) and Sham (black) condition. Baseline correction was not conducted. (C) Mean (±SEM) event histogram of offline detected SO events at Fz during non-REM sleep, time-locked to first click of a click-sequence ($t = 0$ s) and restricted to the window [-2,5] s, for the Stimulation (red) and Sham (black) condition, averaged across subjects. (D) Mean (±SEM) difference between number of successfully recalled word pairs before and after sleep (retention) for the Stimulation and Sham condition, averaged across subjects. (A,B,C) Bottom panels indicate significant differences between conditions (P-values): yellow – corrected using false discovery rate (P_{fdr}); grey – uncorrected (P_{raw}).
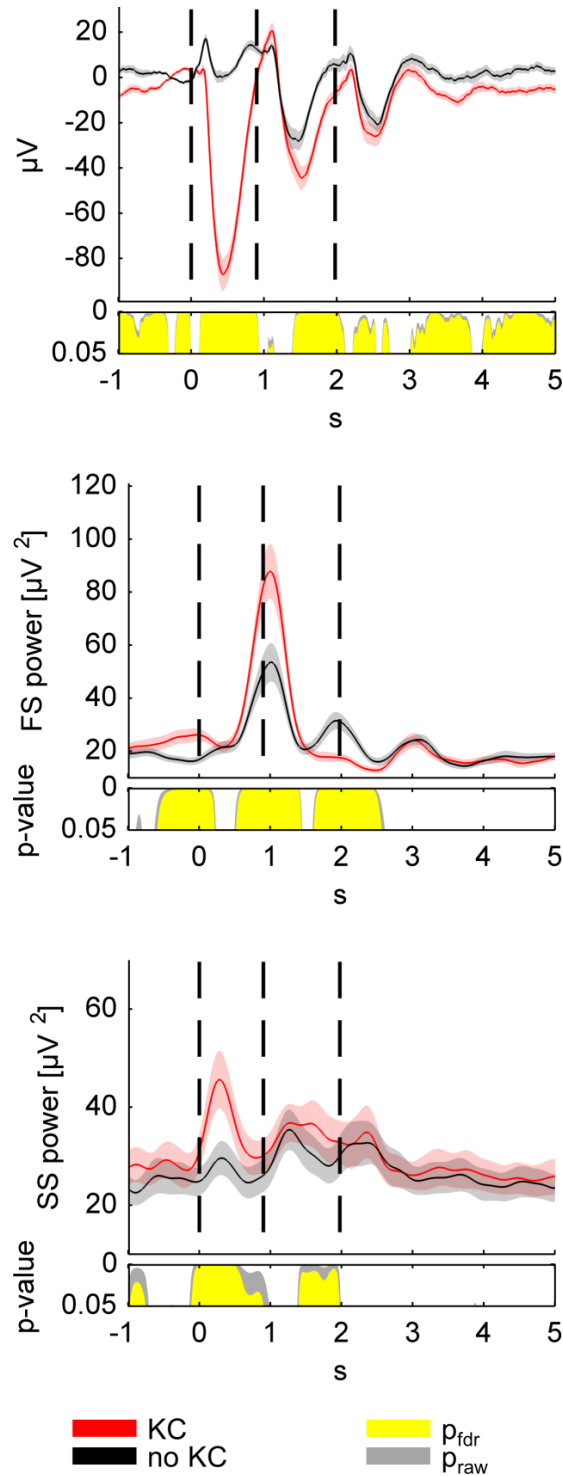
Figure 6.3.: EEG responses to click sequences: evoked KC versus no KC after the first click.
(Top) Mean (±SEM) event-related response at Cz averaged for the wide-band EEG signal, (middle) fast
spindle power (FS, $12 - 15$ Hz) and (bottom) slow spindle power (SS, $9 - 12$ Hz), time-locked to the
first click of each sequence ($t = 0$ s) for (red) successfully evoked KC after the first click and (black)
missing KC after the first click. Note that after the second and third click KCs may occur in both cases.
Vertical dashed lines indicate clicks. Time axis is adjusted for individual interstimulus intervals such that
the second click occurs at 940 ms. Baseline has not been removed. Bottom panels indicate significant
differences between conditions (P-values): yellow – corrected using false discovery rate (P_{fdr}); grey –
uncorrected (P_{raw}).
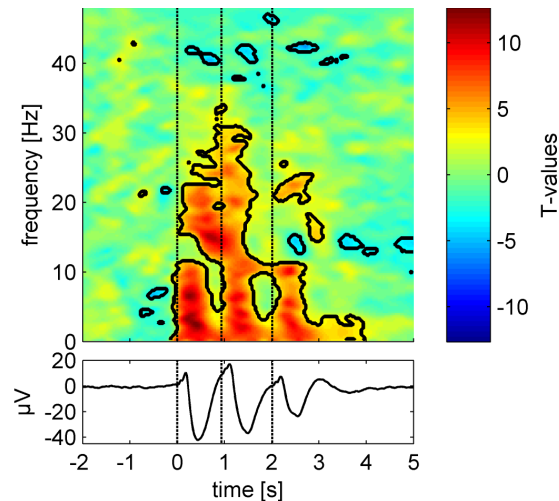
Figure 6.4.: Time-frequency representation of the response to click sequences at Cz. (Top) T-values (Stimulation vs. Sham) time-locked to the first click of each sequence ($t = 0$ s) in interval [-2,5] s are shown. Black contours indicate regions with P_{fdr}<0.05. (Bottom) Mean event-related response averaged for the wide-band EEG signal, time-locked to the first click of each sequence ($t = 0$ s), for the Stimulation condition. (Top, Bottom) Vertical dashed lines indicate clicks. Time axis is adjusted for individual interstimulus intervals such that the second click occurs at 940 ms.

6.2.1. Differential effects on slow-wave power and spindle power

Stimulation had opposite effects on SOs and spindles. While power in SO, delta and SWA bands was increased throughout non-REM sleep of the stimulation epochs ($F_{1,20} = 7.6, P = 0.012$; $F_{1,20} = 4.5, P = 0.047$; $F_{1,20} = 7.7, P = 0.012$), power in slow and fast spindle bands decreased during this time ($F_{1,20} = 17.6, P < 0.001$; $F_{1,20} = 25.1, P < 0.001$; see Figure 6.3, bottom row). The effect on SO power was strongest in frontal regions and exhibited a lateralization to the right hemisphere. Slow spindle power was altered mainly at central leads and fast spindle power at centro-parietal leads (Figure 6.3, top row).

In addition to the stimulation period, we evaluated EEG power during N2 epochs between sleep onset and beginning of the stimulation (pre-stimulation period) and non-REM sleep epochs of the post-stimulation period (see Figure 6.1B for definitions). As could be expected, power in N2 epochs preceding the stimulation period did not differ between conditions ($P > 0.24$ for all ANOVA condition main effects and condition $\times$ topography interaction). Hence, we can rule out that the changes observed during the stimulation period are due to a preexisting baseline offset.

During post-stimulation non-REM sleep epochs power in SO, delta and SWA bands was also increased, despite absence of stimulation. The presence of this effect depended on electrode site (condition $\times$ topography interaction: SO, $F_{20,400} = 3.64, P = 0.036$; delta, $F_{20,400} = 3.41, P = 0.041$; SWA, $F_{20,400} = 3.85, P = 0.028$). The suppression of slow spindle power also extended beyond acute stimulation into the post-stimulation non-REM sleep epochs (condition main effect: $F_{20,400} = 4.44, P = 0.048$). However, post-hoc t-tests did not reveal any significant effects, neither for any electrode site nor for any frequency band ($P_{fdr} > 0.18$ at all electrodes). Figure 6.5 summarizes therefore the overall time course of power across the three periods of nocturnal sleep in the different frequency bands. Neither baseline nor rebound effects are evident for any of the six frequency bands.
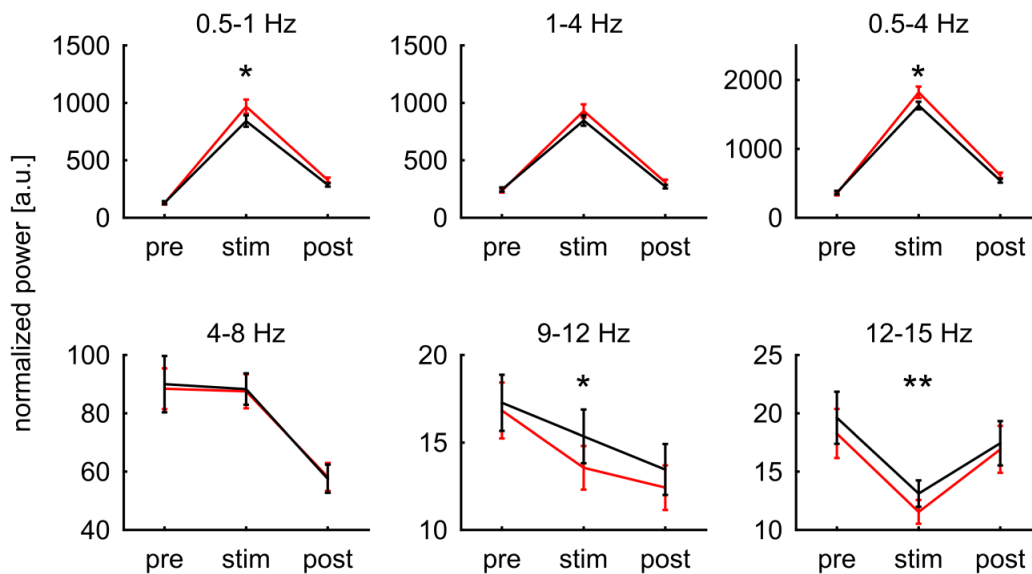
Figure 6.5.: Spectral power at Cz across the night. Mean (±SEM) of normalized spectral power over course of night at Cz averaged over subjects, for Stimulation (red) and Sham (black) condition. "pre": N2 epochs of the pre-stimulation period. "stim": Non-REM sleep epochs with clicks during the 210 min stimulation period, i.e., the stimulation epochs. "post": Non-REM sleep epochs after stimulation period, i.e., the post-stimulation period. $^{*}P_{\text{fdr}} < 0.05$, $^{**}P_{\text{fdr}} < 0.01$, paired t-test.

6.2.2. Within-sequence-interval and inter-sequence-interval spindle power

To further characterize the decrease in spindle power within the stimulation period, we calculated separately mean spindle power for the within-sequence-intervals and inter-sequence-intervals (see Figure 6.1B for definitions). The results are given in Figure 6.6A. The decrease in fast and slow spindle power is confined to the time between click sequences. Spindle power in the inter-sequence-intervals is lower in the Stimulation than the Sham condition (fast spindles: 19.1±7 μV^2 vs. 25.8±9.9 μV^2, P<0.001; slow spindles: 25.6±14.8 μV^2, $P < 0.001$), whereas power levels of within-sequence-intervals are similar ($P > 0.31$). For the Stimulation condition only spindle power in within-sequence-intervals is higher than in inter-sequence-intervals (fast spindles: 26.1 ± 9.1 μV^2 vs. 19.1 ± 7 μV^2, $P < 0.001$; slow spindles: 31.2 ± 17.5 μV^2 vs. 25.6 ± 14.8 μV^2, $P < 0.001$).

Surprisingly, within the stimulation period fast spindle power during positive half-waves of SOs was not affected ($36.1 \pm 11.8 \mu V^2$ vs.$35.7 \pm 11.9 \mu V^2$, $P = 0.83$), but power decreased in the case of slow spindles (30.4 ± 15.4 vs. 35 ± 21.3, $P = 0.012$; depicted in Figure 6.2B middle/bottom and Figure 6.6B, see "Relations between spindles and SOs" in Methods).

This analysis is closely related to the mean vector length, M, a common measure for quantification of phase-amplitude coupling. Since spindle power in positive half-waves of SOs remains similar across conditions despite an overall decrease of spindle power in the Stimulation condition, we expect the mean vector length to be higher in the Stimulation condition. Indeed, this is what happens (Stimulation: $M = 0.09 \pm 0.03$, Sham: $M = 0.07 \pm 0.03$, $P = 0.004$). The phase at which fast spindles are coupled strongest to the slow oscillation does not differ between conditions (Stimulation: $\varphi^* = -24 \pm 0.28$, Sham: $\varphi^* = -0.19 \pm 0.30$, confidence interval CI=[-0.11, 0.02], paired sample test for angular data (Zar, 1999)).

We also repeated the analysis separately for the sequences where the first click successfully evoked a KC and for those where it did not. The spindle power in within-sequence and inter-
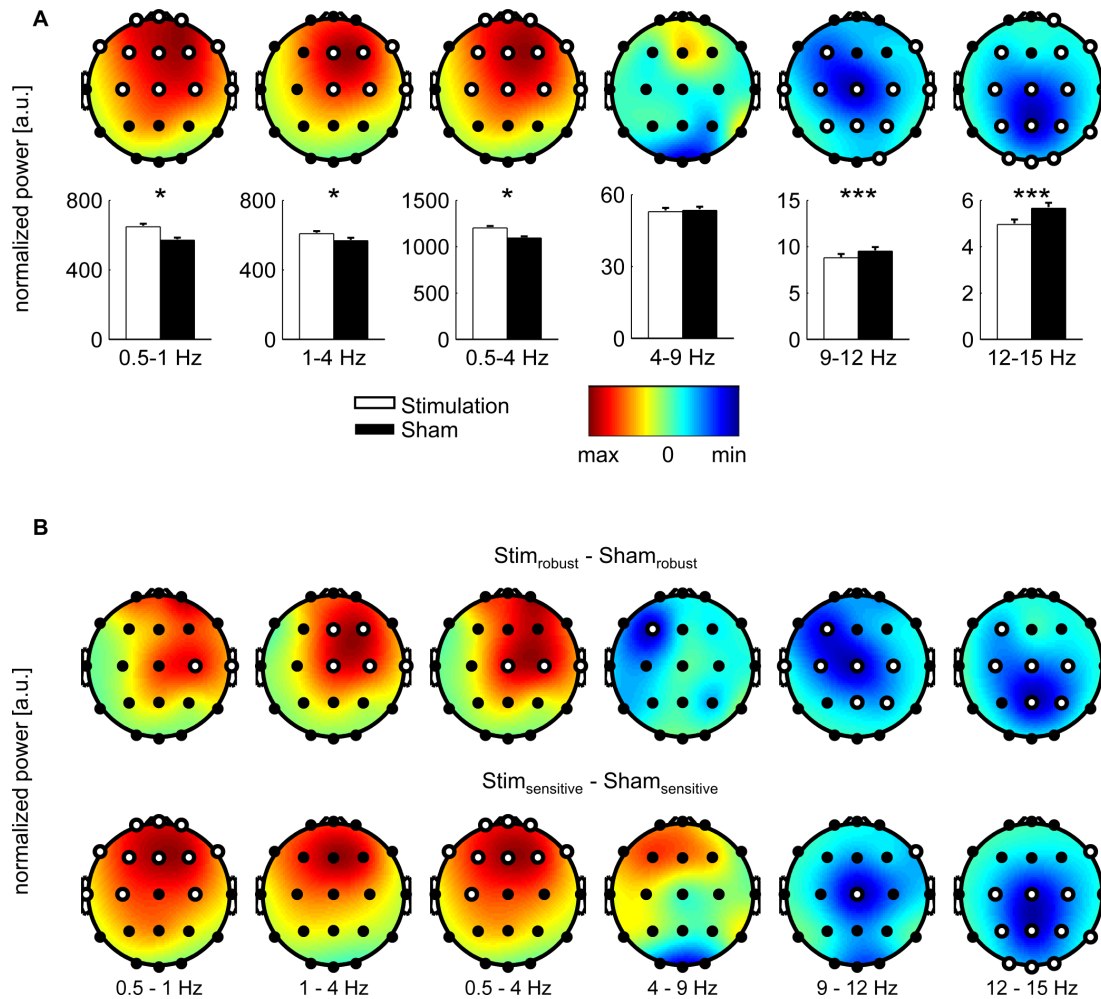
Figure 6.6.: Topographical distribution of stimulation efficiency. (A, top row) Difference (Stimulation-Sham) of normalized spectral power in SO, delta, SWA, theta, slow spindle and fast spindle band for the 210 min stimulation period. Electrode locations with a significant difference ($P_{\mathrm{fdr}} < 0.05$, paired t-test, corrected for multiple comparisons) are depicted as white circles. (A, bottom row) Mean ($\pm$SEM) of normalized spectral power averaged over all subjects and all electrodes, for the Stimulation (white) and Sham (black bars) conditions. Frequency bands apply to top and bottom rows. (B) Same as in A, but for (top) robust and (bottom) sensitive responders. $^{*}P < 0.05$, $^{***}P < 0.001$.

sequence intervals for the "KC" and "no KC" cases are depicted in Figure 7C. A suppression of spindle power in the inter-sequence intervals as compared to the within-sequence intervals is present in both the "KC" as well as "no KC" group for fast and slow spindles. When the first click successfully evoked a KC, however, power in within-sequence intervals was higher for fast and slow spindles. In addition, for fast spindles the decrease in power in the inter-sequence interval was also more pronounced in the KC group.
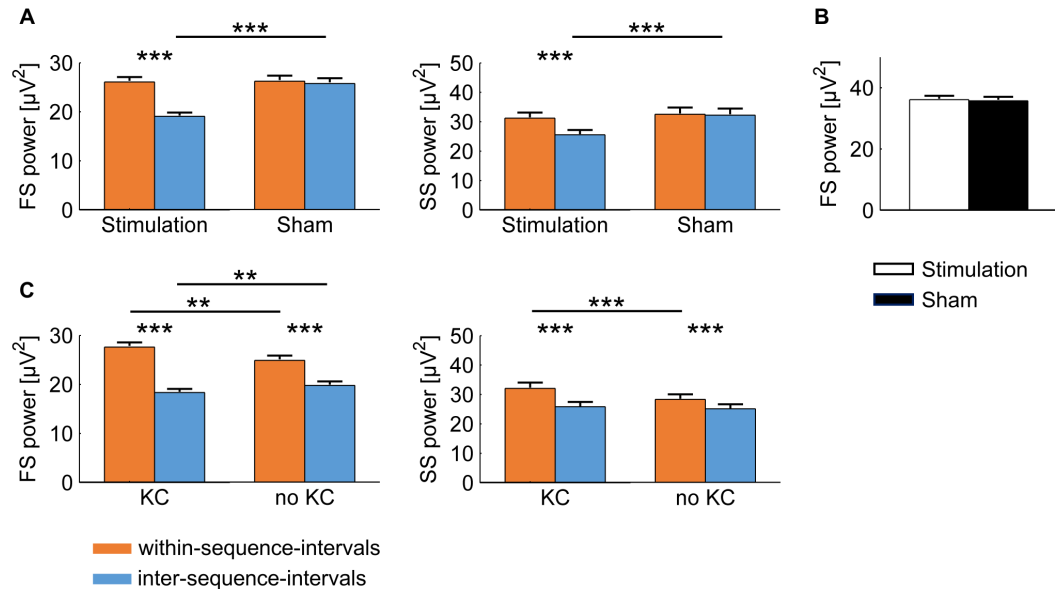
Figure 6.7.: Stimulation-related decrease in spindle power. (A) Mean ($\pm$SEM) of fast spindle power (left) and slow spindle power (right) in within-sequence-intervals (red) and inter-sequence-intervals (blue) for Stimulation and Sham condition. See Figure 6.1 for definition of the intervals. (B) Mean ($\pm$SEM) of fast spindle power during positive half-waves of offline detected SOs in the 210 min stimulation period for Stimulation (white) and Sham (black) condition. (C) Separately for the Stimulation condition only, mean ($\pm$SEM) of fast spindle power (left) and slow spindle power (right) in within-sequence-intervals (red) and inter-sequence-intervals (blue) for sequences where the first click successfully evoked a KC ("KC") as compared to click sequences where it did not ("no KC"). (A, B, C) Power is calculated from time series of instantaneous power, without normalization. $^*P < 0.05$, $^{**}P < 0.01$, $^{***}P < 0.001$.

6.2.3. Open-loop stimulation does not improve memory consolidation

Open-loop auditory stimulation did not affect overnight retention, i.e., the difference in the number of words recalled when tested after sleep and the number recalled at learning before sleep, compared to Sham (26.0 ± 8.3 vs. 25.8 ± 1.8 word pairs, $P = 0.89$, see Figure 6.2D). Learning performance before sleep did not differ significantly between conditions (Stimulation vs. Sham: 61.3 ± 20.6 vs 62.3 ± 19.4 word pairs, $P = 0.74$). Control measures of sleep quality, mood and tiredness (SF-A, PANAS, SSS) were comparable across conditions (all $P > 0.13$). Similarly, the measures of general cognitive ability (DST, RWT) did not exhibit significant differences ($P > 0.12$, see Table 6.1). The PVT differs between conditions ($P = 0.05$, interaction condition $\times$ time, see also Table 6.1) due to a baseline difference in the evening, in which performance in the Sham condition was slightly better than in the Stimulation condition ($\text{PVT}_{ev,Stim} = 309.0 \pm 27.0$ ms, $\text{PVT}_{ev,Sham} = 304.3 \pm 24.6$ ms).

Table 6.1.: Overview of control measures. Mean $\pm$ SD, *paired t-test, **two-way ANOVA (condition $\times$ time)

Test	Stimulation		Sham		*P*-value
	evening	morning	evening	morning	
SF-A	n.a.	3.2 ± 0.5	n.a.	3.2 ± 0.6	0.8*
SSS	4.3 ± 1.1	3.5 ± 0.9	4.2 ± 1.1	3.3 ± 1.0	0.75**
PANAS (P)	21.1 ± 5.4	21.4 ± 6.5	21.1 ± 4.3	23.6 ± 6.2	0.12**
PANAS (N)	11.8 ± 3.3	11.4 ± 2.2	11.7 ± 2.7	11.5 ± 2.5	0.59**
PVT	309.0 ± 27.0	305.0 ± 21.3	304.3 ± 24.6	307.6 ± 21.5	0.05**
DST	n.a.	20.9 ± 4.1	n.a.	21.5 ± 4.8	0.57*
RWT	n.a.	37.3 ± 8.6	n.a.	36.2 ± 8.5	0.45*

Table 6.2.: Overview of control measures. Mean $\pm$ SD, *paired t-test, **two-way ANOVA (condition $\times$ time)

Parameter	Stimulation	Sham	*P*-value
Whole night			
SPT (min)	398.8 ± 8.9	401.0 ± 6.3	0.67
W (%)	2.2 ± 0.7	1.9 ± 0.5	0.74
N1 (%)	7.6 ± 0.9	8.2 ± 0.9	0.41
N2 (%)	46.8 ± 1.5	48.3 ± 1.3	0.24
N3 (%)	25.9 ± 1.8	23.5 ± 1.5	0.04
REM (%)	17.5 ± 0.9	18.0 ± 1.0	0.88
MA (%)	7.4 ± 0.5	7.4 ± 0.6	0.85
Stimulation period			
W (%)	1.7 ± 0.8	1.3 ± 0.6	0.45
N1 (%)	4.4 ± 0.8	4.5 ± 0.7	0.45
N2 (%)	39.7 ± 2.5	41.9 ± 2.0	0.15
N3 (%)	46.5 ± 3.2	45.1 ± 2.6	0.74
REM (%)	7.6 ± 1.3	7.2 ± 1.2	0.71
MA (%)	7.2 ± 0.7	7.0 ± 0.7	0.99
Post-stimulation period			
W (%)	2.5 ± 1.1	1.7 ± 0.4	0.27
N1 (%)	7.8 ± 1.1	8.4 ± 1.0	0.64
N2 (%)	49.6 ± 1.8	52.3 ± 1.5	0.24
N3 (%)	15.0 ± 2.1	11.4 ± 1.5	0.10
REM (%)	25.1 ± 1.4	26.3 ± 1.6	0.39
MA (%)	7.5 ± 0.6	7.9 ± 0.7	0.71

Table 6.3.: Correlations of memory performance with sleep parameters. Displayed *P*-values are not corrected. None is significant after correcting for multiple comparisons. Sleep stages were given in percent of sleep period time (first N1 until awakening). EEG power in the different bands is calculated using non-REM sleep epochs of the whole night.

	Overnight retention			
	Stimulation		Sham	
Sleep stage	ρ	*P*-value	ρ	*P*-value
W	0.03	0.89	-0.03	0.91
N1	0.26	0.26	0.53	0.01
N2	0.08	0.71	0.05	0.83
N3	-0.12	0.61	-0.48	0.03
REM	-0.18	0.42	0.18	0.45
AI	0.43	0.05	0.29	0.20
Power				
SO	-0.07	0.76	-0.3	0.18
Delta	-0.16	0.50	-0.41	0.06
SWA	-0.12	0.61	-0.37	0.10
Theta	-0.30	0.19	-0.52	0.02
slow spindle	-0.25	0.28	-0.35	0.13
fast spindle	-0.09	0.69	-0.46	0.04

6.2.4. Sleep architecture

There were no significant differences in sleep architecture between conditions for the full night, except for N3, in which subjects spent more time during the "Stimulation" condition ($P = 0.04$, Wilcoxon signed-rank test, see Table 6.2). However, analysis of the N3 duration in the stimulation period and the remaining period of nocturnal sleep with a two-way ANOVA (factors time and condition), failed to reach significance (condition: $F_{1,20} = 3.4, P = 0.08$; time $\times$ condition: $F_{1,20} = 0.353, P = 0.56$). We also failed to find any significant correlation for either condition between overnight retention of word pairs and time (percentage) spent in individual sleep stages or in EEG power within the six frequency bands at electrode Cz using Pearson correlations after correcting for multiple comparisons ($P > 0.12$) (Table 6.3).

6.2.5. Comparison of "robust" and "sensitive" responders

Eight out of twenty-one subjects had frequent arousals in the beginning of the night, possibly linked to stimulation. Therefore, most of the stimuli occurred towards the end of the 210 min stimulation period. It has been reported that reactivation processes during sleep seem to be strongest at early portions of non-REM sleep (Bendor and Wilson, 2012). Furthermore, SOs appear to be more global during early fractions of sleep (Nir et al., 2011). Hence, we investigated whether the timing issue had an effect on memory consolidation and oscillatory activity associated with auditory stimulation. We split the participants into the two groups "robust" (13 subjects) and "sensitive" (8 subjects). A 3-way ANOVA with factors time, condition and responder type, however, did not reveal any significant influence of responder type on the overnight consolidation of word pairs (time $\times$ condition $\times$ type: $F_{1,19} = 0.373, P = 0.55$).

Interestingly, the efficacy of the stimulation in the SO and SWA bands indeed differed between the groups, revealing a stronger impact on the sensitive responders (SO, main effect condition: $F_{1,19} = 12.2, P = 0.002$, interaction condition $\times$ topography $\times$ type: $F_{1,19} = 5.0, P = 0.001$; SWA, main effect condition: $F_{1,19} = 10.6, P = 0.004$, interaction condition $\times$ topography $\times$ type: $F_{1,19} = 3.6, P = 0.005$). There were no significant differences between responder types in any other frequency band. Figure 6.6B depicts the topographies of both responder types. The changes in slow and fast spindle activity are independent of responder type. Further, we re-analyzed separately for robust and sensitive responders spindle power in within-sequence and inter-sequence intervals and fast spindle power during putative slow oscillation up states. The pattern of results does not differ between the groups (Figure 6.8).
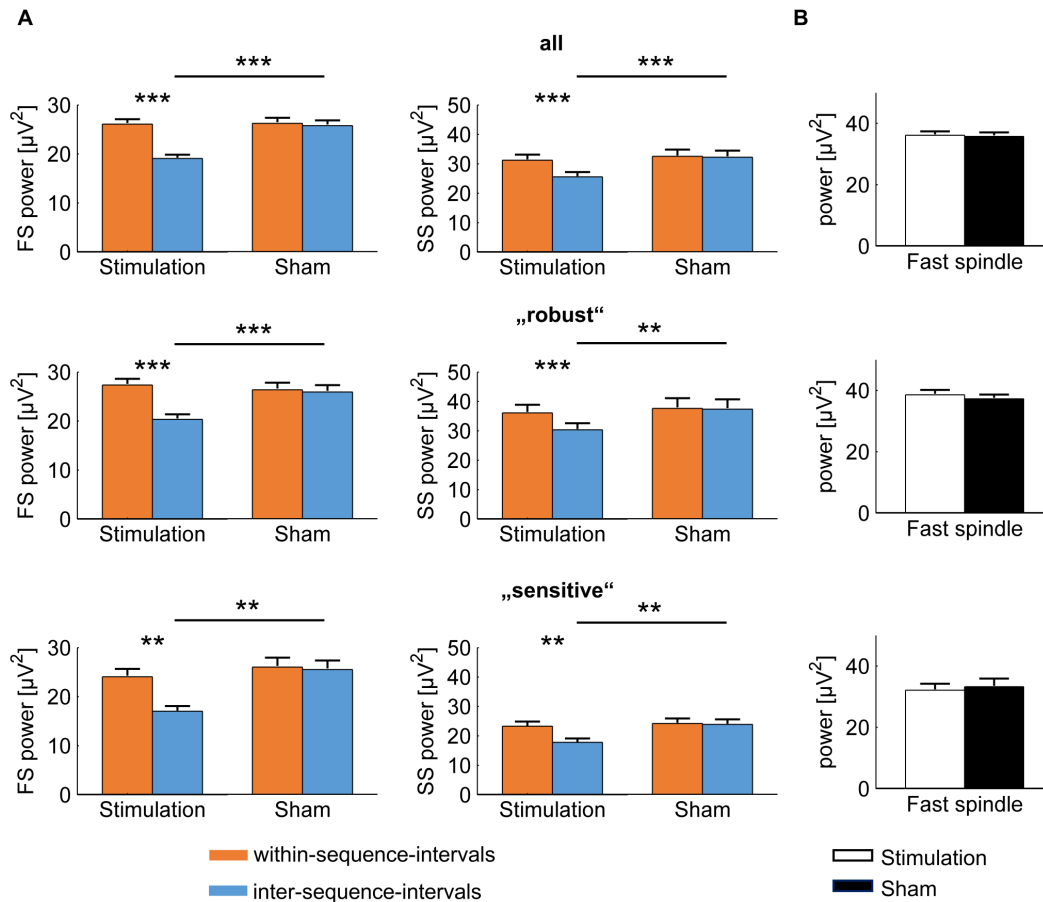
Figure 6.8.: Stimulation-related decrease in spindle power: robust vs. sensitive responders. (A) Mean ($\pm$SEM) of fast spindle power (FS, left) and slow spindle power (SS, right) in within-sequence-intervals (red) and inter-sequence-intervals (blue) for Stimulation and Sham conditions. The top row is for "all" subjects ($n = 21$), the middle row for "robust" responders ($n = 13$), and the bottom row for "sensitive" responders ($n = 8$). Definitions for the intervals are shown in Figure 1. (B) Mean ($\pm$SEM) of fast spindle power during the positive half-waves of offline detected SOs in the 210 min stimulation period for Stimulation (white) and Sham (black) conditions. The top row is for all subjects ($n = 21$), the middle row for "robust" ($n = 13$), and the bottom row for "sensitive" responders ($n = 8$). (A,B) Power was calculated from time series of instantaneous power, without normalization (see Materials & Methods). $^*P < 0.05$, $^{**}P < 0.01$, $^{***}P < 0.001$.

6.3. Discussion

In this study, we investigated whether it is possible to improve the overnight consolidation of declarative memories with a modified version of the auditory closed-loop stimulation paradigm (Ngo et al., 2013, 2015), which is phase-independent. We found that open-loop stimulation with sequences of three clicks evoked SOs, lead to an increase in SO power and a decrease in slow and fast spindle power, but did not alter the overnight retention of word pairs. Similar to the closed-loop stimulation we found that only the first click in a sequence evoked a strong spindle response. We attribute this effect to the mechanisms of endogenous spindle termination and the refractory period between spindles. This has been ascribed to 1) an upregulation of the hyperpolarization-activated nonspecific cation current, Ih, in thalamocortical cells (Lüthi and McCormick, 1998) or 2) depolarization in thalamocortical cells by cortical feedback which is no longer phase-locked with inhibitory postsynaptic potentials (Bonjean et al., 2011). Both mechanisms prevent the de-inactivation of the low threshold T-type Ca^{2+} channels involved in spindle initiation.

Notably, open-loop stimulation caused an overall decrease of spindle power in the stimulation period, whereas this has not been reported for the phase-dependent version (Ngo et al., 2013, 2015).

The observed decrease in spindle power suggests that open-loop stimulation disturbs ongoing endogenous spindle generation. This has also been found with electric stimulation in the latero-posterior thalamic nucleus of anesthetized cats, where a locally induced spindle, out-of-phase with the endogenous rhythm, prevented the occurrence of the next endogenous spindle in the same location (Contreras et al., 1997).

Our results suggest that open-loop stimulation disturbs spindle generation. This has also been observed with electric stimulation in the lateroposterior thalamic nucleus of anesthetized cats, where a locally induced spindle, out-of-phase with the endogenous rhythm, prevented the occurrence of the next endogenous spindle in the same location (Contreras et al., 1997). In order to generate spindles, neurons in the reticular nucleus have to be sufficiently hyperpolarized, so that low-threshold Ca^{2+} currents can deinactivate and initiate bursting (Astori et al., 2011; Lee et al., 2013). On the other hand, a much increased level of hyperpolarization prevents spindle oscillations and instead gives rise to thalamic delta oscillations (Nunez et al., 1992). Auditory stimulation was shown to have a net excitatory, i.e., depolarizing, effect on its thalamic targets (Yu et al., 2004). Thus, open-loop stimulation might reduce spindle power by preventing a re-polarization of the membrane potential in thalamic nuclei. The main advantage of closed-loop stimulation over open-loop stimulation is that the first click by design always occurs during an up state. In this situation, many thalamic nuclei are already depolarized due to the cortical up state (Sheroziya and Timofeev, 2014) and excitatory sensory inputs may cause only little additional depolarization relative to a hyperpolarized state. Hence, auditory closed-loop stimulation is less likely to disturb the endogenous spindle generating mechanisms. A further comparative observation to the study by Ngo et al. (2013) is that clicks were always preceded by an endogenous SO, i.e., were preceded by an endogenous spindle with high probability (Mölle et al., 2002; Steriade, 2006). Surprisingly, in Ngo et al. the spindle response following the first click was even stronger than that of the preceding endogenous spindle (Ngo et al., 2013). This suggests that there is no absolute refractory period of the spindle generating network, as also noted in (Contreras et al., 1997). There, strong stimuli could trigger a spindle at any time, even during an ongoing spindle sequence, because only a fraction of neurons participated in each spindle (Contreras and Steriade, 1996; Destexhe et al., 1996a). Combined MEG-EEG recordings suggest that spindles are only visible in the EEG when they involve larger parts of the cortex (Dehghani et al., 2011). Thus, the fact that an external auditory click can evoke a strong spindle response directly after an endogenous spindle event indicates that it recruits otherwise

silent neurons into a spindle oscillation and/or increases thalamic synchrony. It would be interesting to see whether a sequence of sensory stimuli of different modality might overcome the suppressive effect of open-loop sensory stimulation on spindle power during sleep.

Several studies report a positive correlation between spindle power and overnight retention (Gais et al., 2002; Schabus et al., 2004; Fogel and Smith, 2011; Tamminen et al., 2013). Interestingly, in the present study, memory performance of the Stimulation night was similar to that of the Sham night, although power in the slow and fast spindle band was markedly decreased throughout the stimulation period and no rebound of SO or spindle power occurred in the post-stimulation period. One could argue that, albeit statistically significant, the effect was not strong enough to influence the behavioral outcome. Alternatively, it could be that specific aspects of spindle activity are responsible for its efficacy with respect to memory consolidation and those are not altered by open-loop stimulation. In the present study, fast spindle power during positive half-waves of SOs remained at the same level as in the Sham condition and the reduction of fast spindle power is restricted to the intervals between click sequences only. Thus the relative timing of spindles and SOs, which is critical for memory consolidation (Mölle et al., 2009; Cox et al., 2012; Ngo et al., 2013) was mostly not perturbed during the stimulation period. Finally, others have demonstrated that SO and spindle rhythms by themselves may induce long-term plasticity and therefore may independently contribute to memory consolidation (Rosanova and Ulrich, 2005; Chauvette et al., 2012). Hence, in the present study a positive effect of increased SO power on memory consolidation might offset a detrimental effect of decreased spindle power. However, at least in humans enhancing slow-wave activity alone by pharmacological means (without increasing sleep spindle activity) does not improve overnight memory consolidation (Feld et al., 2013). Also, benzodiazepines which are known to enhance sleep spindle activity and suppress slow-wave activity (Brunner et al., 1991; Arbon et al., 2015) have inconsistent effects on memory consolidation (Meléndez et al., 2005; Mednick et al., 2013; Hall-Porter et al., 2014). Thus, at least some findings indicate that neither enhancing slow-wave nor spindle activity alone might be sufficient to enhance later memory performance. In contrast, increasing slow-wave and spindle activity simultaneously has shown a benefit (Marshall et al., 2006; Ngo et al., 2013, 2015).

7. Summary

In the preceding chapters, thalamocortical dynamics were modeled mathematically and probed via auditory stimulation in an experiment.

First, we validated a neural network model and a mean-field model of slow oscillatory activity in brain slice in vitro by reproducing the experiment of Shu et al. (2003). Then, we characterized their response to stimuli by means of a phase response curve. The PRCs of the different models were qualitatively similar, thus encouraging the use of mean-field models, as they are easier to analyze than networks of spiking neurons. Using the derived PRC, a 2D network of phase oscillators predicts the emergence of wave patterns and entrainment of these wave patterns to external stimuli in brain slice in vitro (Figure 2.8). These results apply when the slow oscillation has the form of a relaxation oscillation.

This insight spurred the development of a more flexible model, that can more directly relate to EEG data and unifies the multiple manifestations of slow oscillations. we presented a thalamocortical neural mass model which generates K-complexes, slow wave activity (<4 Hz) and fast spindles (12-15 Hz). A slow firing rate adaptation in the cortical neural mass and mechanisms for rebound bursts in the thalamic neural mass accounted for sleep specific dynamics. The model allows the investigation of responses to auditory stimulation during wake and non-REM sleep. In particular, it reproduces EEG data of open-loop and closed-loop auditory stimulation of recent sleep studies in humans (Ngo et al., 2013; Weigenand et al., 2016).

In chapter 3, we presented an algorithm for parameter estimation in nonlinear stochastic dynamical systems. It reliably identifies the dynamic regime and bifurcations of a model that most likely generate the observed data. It is the key component that enabled the inferences of dynamic determinants of K-complexes and slow oscillations.

In the model, transitioning from wake to non-REM sleep corresponds to approaching a Hopf bifurcation, which manifests in the EEG by the slowing of frequencies and an increase in amplitudes. A canard phenomenon and the associated homoclinic orbit determine the shape of K-complexes and slow oscillations. Importantly, a K-complex is a transient event, which corresponds to a single excursion along the homoclinic orbit. In contrast, slow oscillations are noise-driven oscillations around a stable focus.

The significance of the thalamocortical model of chapter 4 is that it introduces a differentiated view on cortical slow oscillation dynamics in common experimental conditions. The term slow oscillation has been used indiscriminately in the experimental literature for a variety of different phenomena, e.g., irregular or regular switching between two stable states, relaxation oscillations, occasional population spikes or reversed spikes. Moreover, these dynamic regimes were often claimed to be similar to the acitivity expressed during natural slow-wave sleep in vivo.

The cortex model reconciles these different observations and suggests that during natural sleep the cortex remains predominantly in the active state and only transiently assumes the silent state. A stable silent state, hyperregular relaxation oscillations or genuine bistability are rather found in anesthesia, coma and slice preparations and belong to other parameters of the same system (bifurcation diagram in Figure 4.2). This view is supported by the thalamocortical

model's ability to capture the phase-coupling between spindles and slow oscillations, and evoked responses.

However, adding more brain structures increases the parameter space, especially the number of unknown parameters. This limits the identifiability of system parameters and, hence, the information that can be gained from a mechanistic model. Thus, keeping models simple becomes more important. A step in this direction is chapter 5, where we illustrated the proposed K-complex mechanism in the Fitzhugh-Nagumo model, which can be regarded as a minimal model.

The thalamocortical model predicted, that the cortical response produced by closed-loop stimulation can also be achieved with a simpler open-loop protocol that does not require real-time feedback, while reaping the same positive effects on memory consolidation. Hence, we designed and applied sequences of three clicks during deep non-REM sleep to achieve a quasi-phase-dependent open-loop stimulation. This stimulation was successful in eliciting slow oscillation power in the stimulation period. However, memory consolidation did not differ from the sham control condition. Even more surprising, fast and slow spindle power were markedly decreased during the stimulation period. During putative up states fast spindle power remained, however, at sham levels. We conclude that concurrence of slow oscillations and fast spindles suffices to maintain memory consolidation at sham levels despite an overall decreased spindle activity.

8. Outlook

Following the investigation of the dynamical mechanisms of slow oscillations and K-complexes, the next step is to investigate their computational role. The brain is close to optimal with respect to several measures, e.g., it responds quickly, robustly, and accurately to stimuli in various environments. At the same time, it is stable with respect to noise and degradation of its constituting components and maximizes memory capacity. The mere presence of different mental states, like wakefulness, non-REM and REM sleep, strongly suggests that these multiple processes are partly conflicting optimization targets which cannot be optimized simultaneously. Indeed, it has been proven that there is a fundamental trade-off between energy consumption, speed and precision in neural communication (Lan et al., 2012; Govern and ten Wolde, 2014; Lahiri et al., 2016). Moreover, there are tradeoffs between storing proximal and distal memories. A memory system must be organized hierarchically and span multiple time scales in order to provide long and short term memory, which has been formalized by Fusi and Abbott (2007); Roxin and Fusi (2013); Lahiri and Ganguli (2013). The transfer of memories to their long-term store is thought to involve gist abstraction, which denotes the process of reducing memories to their essential features, devoid of contextual details. It needs to be investigated whether encoding, retrieval and gist abstraction are mutually exclusive, or if not, under which conditions they can co-occur. Further, it remains to be shown how the temporal network dynamics of wake, slow-wave sleep and REM sleep, provide optimal conditions for functions like the formation of long-term memory, the optimization of the memory representation, recall of memories and inference. While the role of sleep in the formation of long-term memories and the ability to generalize is still under debate among experimentalists (Nettersheim et al., 2015; Neske, 2016; Werchan and Gómez, 2014), these theoretical considerations are largely independent of that.

The slow oscillation should be viewed in light of this context, instead of just being considered the mediator in the thalamocortical-hippocampal dialogue, coordinating hippocampal sharp wave ripples and thalamic spindles. This peculiar oscillation may in itself play a decisive role and directly cause the changes in cortical representations leading to memory consolidation and gist abstraction. One of the many open questions is which objective function is optimized by the recurrent networks during slow oscillations. Slow oscillation dynamics have a profound impact on calcium dynamics and spike shape (Massimini and Amzica, 2001; Crochet et al., 2005; Boucetta et al., 2013), which are known to affect spike timing dependent plasticity (Aihara et al., 2007; Krieg and Triesch, 2014). Consequently, network dynamics, single neuron dynamics and synaptic plasticity rules must be optimized jointly. According to the generation mechanism pursued in this thesis slow oscillations are a result of increased slow inhibitory feedback. Notably, this increase does not take place in sudden discrete steps, but smooth transitions between sleep stages. Interestingly, adaptation currents are one way to implement decorrelation of input and output in neurons (Wang, 2003) and, hence, predictive coding. Underlying the typical alternation between sleep stages could be a systematic sweep across timescales of adaptation currents to optimize a predictive coding target. I propose to call this the "timescale sweep hypothesis". This offers a new perspective on infra-slow oscillations, which consequently could play an active role in memory consolidation and transformation.

The question whether synaptic learning rules actually differ significantly between wake and sleep is crucial for inferring the computational role of the cortical slow oscillation. Such a

change seems plausible given the dramatic changes in the neuromodulator levels throughout states of vigilance and the known dependence of plasticity mechanisms on neuromodulators. This still has to be quantified systematically in experiments. Taking into account the conclusions of this thesis it is important that these experiments are performed in naturally waking and sleeping animals.

Regarding gist abstraction and the gaining of insight by a night of sleep, it is not clear which structures participate in this process. In particular, the role of the hippocampus remains to be elucidated. It might well be that gist abstraction is independent of the hippocampus or other sub-cortical structures, and is a purely cortical process, linked to the slow oscillation.

A. Network model

In the original model by Compte et al. (2003) 1024 pyramidal neurons (see paragraph A) and 256 interneurons (see Table A.1) are distributed equidistantly along a line of 5mm. The probability that two neurons, separated by a distance x, are connected is

$$P(x) = (\frac{1}{\sqrt{2\pi\sigma^2}}) \exp(-x^2/2\sigma^2) \tag{A.1}$$

with a synaptic footprint of $\sigma = 250\mu$m for excitatory connections and $\sigma = 125\mu$m for inhibitory connections. The equations governing the synapses can be found in Table A.2. Each neuron makes 20 ± 5 connections to other neurons. In the simulations I used 256 pyramidal neurons and 64 interneurons. The network length and synaptic footprint was linearly scaled to preserve the properties of the original model. We applied periodic boundary conditions.

Regular spiking pyramidal neurons   The gating variables have the form

$$\frac{\mathrm{d}m}{\mathrm{d}t} = \phi\left[\alpha_x(V)(1-m) - \beta_m(V)m\right]$$

or

$$\frac{\mathrm{d}m}{\mathrm{d}t} = \phi\left[m_\infty(V) - m\right]/\tau_m(V)$$

Somatic voltage:

$$C_\mathrm{m}A_\mathrm{s}\frac{\mathrm{d}V_\mathrm{s}}{\mathrm{d}t} = -A_\mathrm{s}(I_\mathrm{L} + I_\mathrm{Na} + I_\mathrm{K} + I_\mathrm{A} + I_\mathrm{KS} + I_\mathrm{KNa}) - I_\mathrm{syn,s} - g_\mathrm{sd}(V_\mathrm{s} - V_\mathrm{d}) + I_\mathrm{ext}$$

C_m	$1\mu\mathrm{F/cm}^2$	A_s	$0.015\mathrm{mm}^2$
g_sd	$(1.75 \pm 0.1)\mu\mathrm{S}$	A_d	$0.035\mathrm{mm}^2$
V_L	$(-60.95 \pm 0.3)\mathrm{mV}$	g_L	$(0.067 \pm 0.0067)\mathrm{mS/cm}^2$
g_Na	$50\mathrm{mS/cm}^2$	V_Na	$55\mathrm{mV}$
ϕ	4	g_K	$10.5\mathrm{mS/cm}^2$
V_K	$-100\mathrm{mV}$	g_A	$1\mathrm{mS/cm}^2$
τ_{h_A}	$15\mathrm{ms}$	g_AR	$0.0257\mathrm{mS/cm}^2$
g_NaP	$0.0686\mathrm{mS/cm}^2$	g_Ca	$0.43\mathrm{mS/cm}^2$
V_Ca	$120\mathrm{mV}$	g_KCa	$0.57\mathrm{mS/cm}^2$
α_Ca	$0.005\mu\mathrm{M/(nA \cdot ms)}$	τ_Ca	$150\mathrm{ms}$
R_pump	$0.018\mathrm{mM/ms}$	$[\mathrm{Na}^+]_\mathrm{eq}$	$9.5\mathrm{mM}$

A. Network model

Dendritic voltage:

$$C_{\mathrm{m}}A_{\mathrm{d}}\frac{\mathrm{d}V_{\mathrm{d}}}{\mathrm{d}t} = -A_{\mathrm{d}}(I_{\mathrm{Ca}} + I_{\mathrm{KCa}} + I_{\mathrm{NaP}} + I_{\mathrm{AR}}) - I_{\mathrm{syn,d}} - g_{\mathrm{sd}}(V_{\mathrm{d}} - V_{\mathrm{s}}) + I_{\mathrm{ext}}$$

Leak current:

$$I_L = g_{\mathrm{L}}(V - V_{\mathrm{L}})$$

Spiking Na$^+$ current:

$$I_{\mathrm{Na}} = g_{\mathrm{Na}}m_{\mathrm{Na},\infty}^3 h_{\mathrm{Na}}(V - V_{\mathrm{Na}})$$
$$m_{\mathrm{Na},\infty} = \alpha_{m_{\mathrm{Na}}}/(\alpha_{m_{\mathrm{Na}}} + \beta_{m_{\mathrm{Na}}})$$
$$\alpha_{m_{\mathrm{Na}}} = 0.1(V + 33)/[1 - \exp(-(V + 33)/10]$$
$$\beta_{m_{\mathrm{Na}}} = 4\exp(-(V + 53.7)/12)$$
$$\frac{\mathrm{d}h_{\mathrm{Na}}}{\mathrm{d}t} = \phi\left[\alpha_{h_{\mathrm{Na}}}(V)(1 - h_{\mathrm{Na}}) - \beta_{h_{\mathrm{Na}}}(V)h_{\mathrm{Na}}\right]$$
$$\alpha_{h_{\mathrm{Na}}} = 0.07\exp(-(V + 50)/10)$$
$$\beta_{h_{\mathrm{Na}}} = 1/[1 + \exp(-(V + 20)/10)]$$

Spiking K$^+$ current:

$$I_{\mathrm{K}} = g_{\mathrm{K}}h_{\mathrm{K}}^4(V - V_{\mathrm{K}})$$
$$\frac{\mathrm{d}h_{\mathrm{K}}}{\mathrm{d}t} = \phi\left[\alpha_{h_{\mathrm{K}}}(V)(1 - h_{\mathrm{K}}) - \beta_{h_{\mathrm{K}}}(V)h_{\mathrm{K}}\right]$$
$$\alpha_{h_{\mathrm{K}}} = 0.01(V + 34)/[1 - \exp(-(V + 34)/10)]$$
$$\beta_{h_{\mathrm{K}}} = 0.125[\exp(-(V + 44)/25)]$$

Fast inactivating current:

$$I_{\mathrm{A}} = g_{\mathrm{A}}m_{\mathrm{A},\infty}h_{\mathrm{A}}(V - V_{\mathrm{K}})$$
$$m_{\mathrm{A},\infty} = 1/[1 + \exp(-(V + 50)/20)]$$
$$\frac{\mathrm{d}h_{\mathrm{A}}}{\mathrm{d}t} = (h_{\mathrm{A},\infty}(V) - h_{\mathrm{A}})/\tau_{h_{\mathrm{A}}}$$
$$h_{\mathrm{A},\infty} = 1/[\exp(-(V + 80)/6)]$$

Non-inactivating K$^+$-channel:

$$I_{\mathrm{KS}} = g_{\mathrm{KS}}m_{\mathrm{KS}}(V - V_{\mathrm{K}})$$
$$g_{\mathrm{KS}} = 0.576\mathrm{mS/cm}^2$$
$$\frac{\mathrm{d}m_{\mathrm{KS}}}{\mathrm{d}t} = (m_{\mathrm{KS},\infty}(V) - m_{\mathrm{KS}})/\tau_{m_{\mathrm{KS}}}$$
$$m_{\mathrm{KS},\infty} = 1/[1 + \exp(-(V + 34.5)/6.5]$$
$$\tau_{m_{\mathrm{KS}}} = 8/[\exp(-(V + 55)/30) + \exp((V + 55)/30)]$$

Non-inactivating Na$^+$ channel:

$$I_{\mathrm{NaP}} = g_{\mathrm{NaP}}m_{\mathrm{NaP},\infty}^3(V - V_{\mathrm{Na}})$$
$$m_{\mathrm{NaP},\infty} = 1/[1 + \exp(-(V + 55.7)/7.7)]$$

Hyperpolarization de-inactivated channel:

$$I_{\mathrm{AR}} = g_{\mathrm{AR}}h_{\mathrm{AR},\infty}(V - V_{\mathrm{K}})$$
$$h_{\mathrm{AR},\infty} = 1/[1 + \exp((V + 75)/4]$$

High-threshold Ca^{2+}-channel:

$$I_{\mathrm{Ca}} = g_{\mathrm{Ca}}m_{\mathrm{Ca},\infty}^2(V - V_{\mathrm{Ca}})$$
$$m_{\mathrm{Ca},\infty} = 1/[1 + \exp(-(V + 20)/9)]$$

Ca^{2+} dependent K$^+$ channel:

$$I_{\mathrm{KCa}} = g_{\mathrm{KCa}}[\mathrm{Ca}^{2+}]/([\mathrm{Ca}^{2+}] + K_D)(V - V_{\mathrm{K}})$$
$$\mathrm{d}[\mathrm{Ca}^{2+}]/\mathrm{d}t = -\alpha_{\mathrm{Ca}}A_d I_{\mathrm{Ca}} - [\mathrm{Ca}^{2+}]/\tau_{\mathrm{Ca}}$$

Na$^+$ dependent K$^+$ channel:

$$I_{\mathrm{KNa}} = g_{\mathrm{KNa}}w_{\infty}([\mathrm{Na}^+])(V - V_{\mathrm{K}})$$
$$g_{\mathrm{KNa}} = 1.33\mathrm{mS/cm}^2$$
$$w_{\infty} = 0.37/[1 + (38.7/[\mathrm{Na}^+])^{3.5}]$$

Na$^+$ dynamics:

$$\mathrm{d}[\mathrm{Na}^+]/\mathrm{d}t = -\alpha_{\mathrm{Na}}(A_{\mathrm{s}}I_{\mathrm{Na}} + A_{\mathrm{d}}I_{\mathrm{NaP}})$$
$$\alpha_{\mathrm{Na}} = 0.01\mathrm{mM/(nA \cdot ms)} - R_{\mathrm{pump}}\{[\mathrm{Na}^+]^3/([\mathrm{Na}^+]^3 + 15^3) -$$
$$[\mathrm{Na}^+]_{\mathrm{eq}}^3/([\mathrm{Na}^+]_{\mathrm{eq}}^3 + 15^3)\}$$

<div align="center">Table A.1.: Fast-spiking inhibitory interneurons</div>

description	equations	parameters
somatic voltage	$C_\mathrm{m} A_\mathrm{i} \frac{\mathrm{d}V_\mathrm{i}}{\mathrm{d}t} = -A_\mathrm{i}(I_\mathrm{L}+I_\mathrm{Na}+I_\mathrm{K})-I_\mathrm{syn,i} + I_\mathrm{ext}$	$A_\mathrm{i} = 0.02 \text{ mm}^2$
		$g_\mathrm{Na} = 35 \text{ mS/cm}^2$
leak current	$I_\mathrm{L} = g_\mathrm{L}(V - V_\mathrm{L})$	$g_\mathrm{L} = (0.1025 \pm 0.0025)\text{mS/cm}^2$
		$V_\mathrm{L} = (-63.8 \pm 0.15)\text{mV}$
spiking sodium current	$I_\mathrm{Na} = g_\mathrm{Na} m_\mathrm{Na,\infty} h_\mathrm{Na}(V - V_\mathrm{Na})$	$g_\mathrm{Na} = 35 \text{ mS/cm}^2$
	$m_\mathrm{Na,\infty} = \alpha_{m_\mathrm{Na}}/(\alpha_{m_\mathrm{Na}} + \beta_{m_\mathrm{Na}})$	$V_\mathrm{Na} = 55 \text{ mV}$
	$\alpha_{m_\mathrm{Na}} = 0.5(V + 35)/[1 - \exp(-(V + 35)/10)]$	
	$\beta_{m_\mathrm{Na}} = 20 \exp(-(V + 60)/18)$	
	$\frac{\mathrm{d}h_\mathrm{Na}}{\mathrm{d}t} = \alpha_{h_\mathrm{Na}}(V)(1 - h_\mathrm{Na}) - \beta_{h_\mathrm{Na}}(V)h_\mathrm{Na}$	
	$\alpha_{h_\mathrm{Na}} = 0.35 \exp(-(V + 58)/20)$	
	$\beta_{h_\mathrm{Na}} = 5/[1 + \exp(-(V + 28)/10)]$	
slow potassium current	$I_\mathrm{K} = g_\mathrm{K} m_\mathrm{K}^4(V - V_k)$	$g_\mathrm{K} = 9 \text{ mS/cm}^2$
	$\frac{\mathrm{d}m_\mathrm{K}}{\mathrm{d}t} = \alpha_{m_\mathrm{K}}(V)(1 - m_\mathrm{K}) - \beta_{m_\mathrm{K}}(V)m_\mathrm{K}$	$V_\mathrm{K} = -90\text{mV}$
	$\alpha_{m_\mathrm{K}} = 0.05(V + 34)/[1 - \exp(-(V + 34)/10)]$	
	$\beta_{m_\mathrm{K}} = 0.625 \exp(-(V+44)/80)$	

Table A.2.: Synapses

description	equations	parameters
AMPA synapses	$I_\mathrm{syn} = g_\mathrm{syn} s (V - V_\mathrm{syn})$ $\frac{\mathrm{d}s}{\mathrm{d}t} = \alpha f(V_\mathrm{pre}) - s/\tau$ $f(V_\mathrm{pre}) = 1/\left[1 + \exp(-(V\mathrm{pre} - 20)/2)\right]$	$\alpha = 3.48$ $\tau = 2\mathrm{ms}$ $V_\mathrm{syn} = 0\mathrm{V}$ $g_\mathrm{EE}^\mathrm{AMPA} = 5.4\mathrm{nS}$ $g_\mathrm{EI}^\mathrm{AMPA} = 2.25\mathrm{nS}$
NMDA synapses	$\frac{\mathrm{d}s}{\mathrm{d}t} = \alpha_s (1 - s) x - s/\tau_\mathrm{s}$ $\frac{\mathrm{d}x}{\mathrm{d}t} = \alpha_x f(V_\mathrm{pre}) - x/\tau_\mathrm{x}$ $f(V_\mathrm{pre}) = 1/\left[1 + \exp(-(V\mathrm{pre} - 20)/2)\right]$	$\alpha_\mathrm{s} = 0.5$ $\tau_\mathrm{s} = 100\mathrm{ms}$ $\alpha_\mathrm{x} = 3.48$ $\tau_\mathrm{x} = 2\mathrm{ms}$ $V_\mathrm{syn} = 0\mathrm{mV}$ $g_\mathrm{EE}^\mathrm{NMDA} = 0.9\mathrm{nS}$ $g_\mathrm{EI}^\mathrm{NMDA} = 0.5\mathrm{nS}$
GABA synapses	$I_\mathrm{syn} = g_\mathrm{syn} s (V - V_\mathrm{syn})$ $\frac{\mathrm{d}s}{\mathrm{d}t} = \alpha f(V_\mathrm{pre}) - s/\tau$ $f(V_\mathrm{pre}) = 1/\left[1 + \exp(-(V\mathrm{pre} - 20)/2)\right]$	$\alpha = 1$ $\tau = 10\mathrm{ms}$ $V_\mathrm{syn} = -70\mathrm{mV}$ $g_\mathrm{IE} = 4.15\mathrm{nS}$

B. Cortex model

This table defines all constants used within the model, that are not described elsewhere.

Table B.1.: Parameters of cortex model

τ_e, τ_i	30 ms	membrane rise time
Q_e^{max}	0.03 ms^{-1}	maximal firing rate
Q_i^{max}	0.06 ms^{-1}	maximal firing rate
θ_e, θ_i	-58.5 mV	firing threshold
σ_i	6 mV	firing rate deviation
γ_e	0.07 ms^{-1}	synaptic rate constant
γ_i	0.0586 ms^{-1}	synaptic rate constant
N_{ee}	120	connectivity e-e
N_{ei}	72	connectivity e-i
N_{ie}	90	connectivity i-e
N_{ii}	90	connectivity i-i
C_m	1 μF/cm^2	membrane capacity
g_L	1 mS/cm^2	channel conductivity
E_{Le}, E_{Li}	-66,-64 mV	reversal potential
E_K	-100 mV	reversal potential
E_{AMPA}	0 mV	reversal potential
E_{GABA}	-70 mV	reversal potential
α_{Na}	2 mM/ mA ms	sodium influx
τ_{Na}	1 ms	sodium time constant
R_{pump}	0.09 mM ms^{-1}	sodium pump capacity
Na_{eq}	9.5 mM	sodium resting state
ϕ_n	0.12 ms^{-1}	background noise standard deviation

The basic neural column described in Methods is given by the following set of equations:

$$\tau_e \dot{V}_e = -I_L - I_{AMPA}(s_{ee}) - I_{GABA}(s_{ie}) - \tau_e C_m^{-1} I_{KNA},$$
$$\tau_i \dot{V}_i = -I_L - I_{AMPA}(s_{ei}) - I_{GABA}(s_{ii}),$$
$$\ddot{s}_{ee} = \gamma_e^2 \left(N_{ee} Q_e(V_e) + \phi_n - s_{ee} \right) - 2\gamma_e \dot{s}_{ee},$$
$$\ddot{s}_{ie} = \gamma_i^2 \left(N_{ie} Q_i(V_i) \qquad - s_{ie} \right) - 2\gamma_i \dot{s}_{ie},$$
$$\ddot{s}_{ei} = \gamma_e^2 \left(N_{ei} Q_e(V_e) + \phi_n' - s_{ei} \right) - 2\gamma_e \dot{s}_{ei},$$
$$\ddot{s}_{ii} = \gamma_i^2 \left(N_{ii} Q_i(V_i) \qquad - s_{ii} \right) - 2\gamma_i \dot{s}_{ii},$$
$$[\dot{Na}] = (\alpha_{Na} Q_e(V_e) - Na_{pump}([Na]))/\tau_{Na}.$$

The currents are given by

$$I_L = g_L(V_k - E_L),$$
$$I_{AMPA} = g_{AMPA}s_{ek}(V_k - E_{AMPA}),$$
$$I_{GABA} = g_{GABA}s_{ik}(V_k - E_{GABA}),$$
$$I_{\mathrm{KNa}} = g_{\mathrm{KNa}}\frac{0.37}{1 + \left(\frac{38.7}{[\mathrm{Na}]}\right)^{3.5}}(V_e - E_K).$$

The sodium pump is described by

$$\mathrm{Na}_{\mathrm{pump}}([\mathrm{Na}]) = R_{\mathrm{pump}}\left(\frac{[Na]^3}{[Na]^3 + 3375} - \frac{[Na]_{eq}^3}{[Na]_{eq}^3 + 3375}\right).$$

C. Thalamocortical model

This table describes all symbols used within the model.

Table C.1.: Symbol description

C_m	Membrane capacitance in the HH model	Q_k^{max}	Maximal firing rate of population k
θ_k	Firing threshold of population k (half activation)	σ_k	Default gain coefficient of the firing rate function of population k (inverse neural gain)
τ_k	Membrane time constant of population k	γ_m	Synaptic rate constant of synapse type m
ν	Axonal rate constant	N_{kl}	Connectivity constant from presynaptic population l to postsynaptic population k
w_X	Input rate of synaptic channel of type X	$\bar{g}_X$	Conductivity of ion channel X
E_X	Nernst reversal potential of channel X	α_{Na}	Sodium influx through firing rate
τ_{Na}	Time constant of sodium extrusion	R_{pump}	Strength of the sodium pump
$\mathrm{Na_{eq}}$	Resting state sodium equilibrium	α_{Ca}	Calcium influx rate
τ_{Ca}	Calcium time constant	$\mathrm{Ca_0}$	Calcium resting state concentration
k_j	Reaction velocity of h-current	n_P	Number of calcium binding sites
g_{inc}	Conductivity scaling of h-current	ϕ_0	Mean background noise
ϕ_C^{sd}	Standard deviation of cortical background noise	ϕ_T^{sd}	Standard deviation of thalamic background noise

C_m	1 μF/cm^2		
τ_p, τ_i	30 ms	τ_t, τ_r	20 ms
$Q_p^{\max}$	$30 \cdot 10^{-3}$ ms^{-1}	$Q_i^{\max}$	$60 \cdot 10^{-3}$ ms^{-1}
$Q_t^{\max}, Q_r^{\max}$	$400 \cdot 10^{-3}$ ms^{-1}	θ	-58.5 mV
σ_p	4 mV	$\sigma_i, \sigma_t, \sigma_r$	6 mV
γ_e	$70 \cdot 10^{-3}$ ms^{-1}	γ_g	$58.6 \cdot 10^{-3}$ ms^{-1}
γ_r	$100 \cdot 10^{-3}$ ms^{-1}	ν	$120 \cdot 10^{-3}$ ms^{-1}
N_{pp}	120	N_{ip}	72
N_{pi}, N_{ii}	90	N_{tp}, N_{rp}	2.6
N_{rt}	3	N_{tr}	5
N_{rr}	19	N_{pt}, N_{it}	2.5
$w_{\text{AMPA}}, w_{\text{GABA}}$	1 ms	$\bar{g}_{\text{T}}^{t}$	3 mS/cm^2
$\bar{g}_{\text{T}}^{r}$	2.3 mS/cm^2	$\bar{g}_{\text{KNa}}$	1.33 mS/cm^2
$E_{\text{L}}^{p}, E_{\text{L}}^{i}$	-64 mV	$E_{\text{L}}^{t}, E_{\text{L}}^{r}$	-70 mV
E_{K}	-100 mV	E_{Ca}	120 mV
E_{Ca}	-40 mV	E_{AMPA}	0 mV
E_{GABA}	-70 mV	α_{Na}	2 mM/mA ms
τ_{Na}	1.7 ms	R_{pump}	0.09 mM ms^{-1}
Na_{eq}	9.5 mM	α_{Ca}	$51.8 \cdot 10^{-6}$ mM/mA ms
τ_{Ca}	10 ms	Ca_0	$2.4 \cdot 10^{-4}$ mM
k_2	$4 \cdot 10^{-4}$ ms^{-1}	k_3	$1 \cdot 10^{-1}$ ms^{-1}
k_4	$1 \cdot 10^{-3}$ ms^{-1}	n_P	4
g_{inc}	2	ϕ_0	0 ms^{-1}
ϕ_C^{sd}	$120 \cdot 10^{-3}$ ms^{-1}	ϕ_T^{sd}	$10 \cdot 10^{-3}$ ms^{-1}

C. Thalamocortical model

The complete mathematical description of the full thalamocortical model is

$$
\begin{aligned}
\tau_p \dot{V}_p &= -J_{\mathrm{L}}^p - J_{\mathrm{AMPA}}(s_{ep}) - J_{\mathrm{GABA}}(s_{gp}) - C_m^{-1}\tau_p I_{\mathrm{KNa}}, \\
\tau_i \dot{V}_i &= -J_{\mathrm{L}}^k - J_{\mathrm{AMPA}}(s_{ei}) - J_{\mathrm{GABA}}(s_{gi}), \\
\tau_t \dot{V}_t &= -J_{\mathrm{L}}^t - J_{\mathrm{AMPA}}(s_{et}) - J_{\mathrm{GABA}}(s_{rt}) - C_m^{-1}\tau_t (I_{\mathrm{LK}}^t - I_{\mathrm{T}}^t - I_{\mathrm{h}}), \\
\tau_r \dot{V}_r &= -J_{\mathrm{L}}^r - J_{\mathrm{AMPA}}(s_{er}) - J_{\mathrm{GABA}}(s_{rr}) - C_m^{-1}\tau_r (I_{\mathrm{LK}}^r - I_{\mathrm{T}}^r), \\
\ddot{s}_{ep} &= \gamma_e^2 \left(N_{pp}Q_p(V_p) + N_{pt}\phi_t + \phi_n - s_{ep} \right) - 2\gamma_e \dot{s}_{ep}, \\
\ddot{s}_{ei} &= \gamma_e^2 \left(N_{ip}Q_p(V_p) + N_{it}\phi_t + \phi_n' - s_{ei} \right) - 2\gamma_e \dot{s}_{ei}, \\
\ddot{s}_{et} &= \gamma_e^2 \left(\qquad\qquad N_{tp}\phi_p + \phi_n'' - s_{et} \right) - 2\gamma_e \dot{s}_{et}, \\
\ddot{s}_{er} &= \gamma_e^2 \left(N_{rt}Q_t(V_t) + N_{rp}\phi_p \quad - s_{er} \right) - 2\gamma_e \dot{s}_{er}, \\
\ddot{s}_{gp} &= \gamma_g^2 \left(N_{pi}Q_i(V_i) \qquad - s_{gp} \right) - 2\gamma_g \dot{s}_{gp}, \\
\ddot{s}_{gi} &= \gamma_g^2 \left(N_{ii}Q_i(V_i) \qquad - s_{gi} \right) - 2\gamma_g \dot{s}_{gi}, \\
\ddot{s}_{rt} &= \gamma_r^2 \left(N_{tr}Q_r(V_r) \qquad - s_{it} \right) - 2\gamma_r \dot{s}_{rt}, \\
\ddot{s}_{rr} &= \gamma_r^2 \left(N_{rr}Q_r(V_r) \qquad - s_{rr} \right) - 2\gamma_r \dot{s}_{rr}, \\
\ddot{\phi}_p &= \nu^2 \left(Q_p(V_p) \qquad\quad - \phi_p \right) - 2\nu \dot{\phi}_p, \\
\ddot{\phi}_t &= \nu^2 \left(Q_t(V_t) \qquad\quad - \phi_t \right) - 2\nu \dot{\phi}_t, \\
\dot{h}_{\mathrm{T}}^t &= (h_\infty^t - h_{\mathrm{T}}^t)/\tau_{\mathrm{h}}^t, \\
\dot{h}_{\mathrm{T}}^r &= (h_\infty^r - h_{\mathrm{T}}^r)/\tau_{\mathrm{h}}^r, \\
\dot{m}_{\mathrm{h}1} &= (m_\infty^h(1 - m_{\mathrm{h}2}) - m_{\mathrm{h}1})/\tau_m^{\mathrm{h}} - k_3 P_{\mathrm{h}} m_{\mathrm{h}1} + k_4 m_{\mathrm{h}2}, \\
\dot{m}_{\mathrm{h}2} &= k_3 P_{\mathrm{h}} m_{\mathrm{h}1} - k_4 m_{\mathrm{h}2}, \\
[\dot{\mathrm{Ca}}] &= \alpha_{\mathrm{Ca}} I_{\mathrm{T}}^t - ([\mathrm{Ca}] - \mathrm{Ca}_0)/\tau_{\mathrm{Ca}}, \\
[\dot{\mathrm{Na}}] &= (\alpha_{\mathrm{Na}} Q_p(V_p) - \mathrm{Na}_{\mathrm{pump}}([\mathrm{Na}]))/\tau_{\mathrm{Na}}.
\end{aligned}
\tag{C.1}
$$

The currents are given by the following equations:

$$
\begin{aligned}
J_{\mathrm{L}}^k &= (V_i - E_{\mathrm{L}}^k), \\
J_{\mathrm{AMPA}}(s_{ek}) &= w_{\mathrm{AMPA}} s_{ek}(V_k - E_{\mathrm{AMPA}}), \\
J_{\mathrm{GABA}}(s_{gk}) &= w_{\mathrm{GABA}} s_{gk}(V_k - E_{\mathrm{GABA}}), \\
J_{\mathrm{GABA}}(s_{rk}) &= w_{\mathrm{GABA}} s_{rk}(V_k - E_{\mathrm{GABA}}), \\
I_{\mathrm{LK}}^k &= \bar{g}_{\mathrm{LK}}(V_i - E_{\mathrm{K}}^k), \\
I_{\mathrm{T}}^t &= \bar{g}_{\mathrm{T}}^t m_\infty^t m_\infty^t h^t (V_t - E_{\mathrm{Ca}}), \\
I_{\mathrm{T}}^r &= \bar{g}_{\mathrm{T}}^r m_\infty^r m_\infty^t h^r (V_r - E_{\mathrm{Ca}}), \\
I_{\mathrm{h}} &= \bar{g}_{\mathrm{h}}(m_{\mathrm{h}1} + g_{inc} m_{\mathrm{h}2})(V_t - E_{\mathrm{h}}), \\
I_{\mathrm{KNa}} &= \bar{g}_{\mathrm{KNa}} \frac{0.37}{1 + \left(\frac{38.7}{[\mathrm{Na}]} \right)^{3.5}} (V_p - E_{\mathrm{K}}).
\end{aligned}
\tag{C.2}
$$

The gating functions are

$$m_\infty^t = \frac{1}{1 + \exp(-(V_t + 59)/6.2))},$$

$$m_\infty^r = \frac{1}{1 + \exp(-(V_r + 52)/7.4))},$$

$$h_\infty^t = \frac{1}{1 + \exp((V_t + 81)/4))},$$

$$h_\infty^r = \frac{1}{1 + \exp((V_r + 80)/5))}, \tag{C.3}$$

$$\tau_h^t = (30.8 + (211.4 + \exp((V_t + 115.2)/5))/(1 + \exp((V_t + 86)/3.2)))/3^{1.2},$$

$$\tau_h^r = (85 + 1/(\exp((V_r + 48)/4) + \exp(-(V_r + 407)/50)))/3^{1.2},$$

$$m_\infty^h = \frac{1}{1 + \exp((V_t + 75)/5.5))},$$

$$\tau_m^h = (20 + 1000/(\exp((V_t + 71.5)/14.2) + \exp(-(V_t + 89)/11.6))),$$

$$P_h = k_1[\mathrm{Ca}]^{n_P}/(k_1[\mathrm{Ca}]^{n_P} + k_2).$$

The sodium pump is given by

$$\mathrm{Na_{pump}}([\mathrm{Na}]) = R_{\mathrm{pump}} \left(\frac{[\mathrm{Na}]^3}{[\mathrm{Na}]^3 + 3375} - \frac{[\mathrm{Na_0}]^3}{[\mathrm{Na_0}]^3 + 3375} \right). \tag{C.4}$$

Finally, the firing rate function obeys

$$Q_k = \frac{Q_k^{\max}}{1 + \exp(-(V_k - \theta)/\sigma_k)}. \tag{C.5}$$

D. Behavioral data

PANAS

subject	age	gender	PAL Stim ev	PAL Stim mo	PAL Sham ev	PAL Sham mo	PosAff Stim ev	PosAff Stim mo	PosAff Sham ev	PosAff Sham mo	NegAff Stim ev	NegAff Stim mo	NegAff Sham ev	NegAff Sham mo	PVT Stim ev	PVT Stim mo	PVT Sham ev	PVT Sham mo	SSS Stim ev	SSS Stim mo	SSS Sham ev	SSS Sham mo	RWT Stim	RWT Sham	DST Stim	DST Sham	SF-A Stim	SF-A Sham
1	25	female	69	93	89	103	26	20	21	15	12	11	12	11	274	286	284	302	5	3	3	5	42	45	23	29	3.6	2.7
2	22	male	72	92	59	89	31	25	26	23	14	20	14	10	297	300	307	314	6	5	4	4	37	35	25	23	3.4	3.7
3	24	female	48	77	80	95	19	24	17	24	10	10	10	10	290	289	285	303	3	4	3	3	39	30	23	20	3.3	3.2
4	27	male	57	75	47	75	22	17	16	26	10	10	10	10	270	262	243	243	5	3	5	2	46	35	15	24	4.3	2.9
5	18	male	61	91	40	67	28	42	30	42	19	17	19	17	393	361	365	353	4	2	2	4	18	24	18	20	3.7	4.8
6	20	female	71	99	78	104	26	30	25	24	12	11	11	10	317	329	328	333	3	4	3	4	55	55	17	18	2.4	2.8
7	23	male	28	44	46	56	21	18	21	18	11	10	11	10	355	316	328	323	4	4	4	3	28	25	20	21	2.8	3.6
8	20	female	75	93	73	99	32	25	20	32	11	12	11	12	297	301	321	297	3	4	6	3	48	49	27	27	3.1	4.2
9	25	male	61	87	46	68	13	13	13	14	10	10	10	10	297	288	290	319	3	3	5	3	26	26	18	21	2.6	2.7
10	19	female	71	97	83	102	21	23	22	28	12	11	12	11	317	316	307	302	5	5	2	2	28	43	24	28	3.6	2.3
11	23	male	25	66	42	73	20	23	24	25	10	10	10	10	307	308	298	320	2	5	5	4	28	27	15	19	3.4	3.1
12	23	male	90	109	79	105	26	27	27	28	10	10	10	12	310	300	318	320	5	3	5	3	38	28	24	30	2.8	3.1
13	20	male	36	75	50	91	25	17	25	21	11	10	11	10	312	311	308	306	3	4	2	5	38	34	17	14	3.3	3.2
14	20	female	89	109	76	108	17	19	23	23	10	10	10	10	300	289	280	281	6	2	4	3	45	40	22	17	3.1	3.2
15	28	male	74	115	71	110	16	17	21	22	11	13	10	10	303	308	282	305	3	4	4	3	47	38	24	26	2.6	3.1
16	24	female	67	90	78	94	14	19	14	20	12	13	11	11	297	295	313	320	5	4	5	3	37	46	25	28	2.8	2.7
17	23	female	44	69	35	61	22	18	20	22	12	11	12	11	317	314	303	310	6	4	5	3	39	30	18	17	3.7	3.1
18	22	female	86	109	90	110	17	19	22	20	10	11	10	10	340	342	330	321	3	4	5	4	39	34	17	16	3	3.7
19	21	female	38	66	30	56	17	14	21	18	18	16	14	16	303	287	304	297	5	4	5	5	37	42	22	17	3.1	2.2
20	19	male	89	102	74	109	15	15	16	20	11	10	11	10	290	299	289	292	5	3	5	5	37	42	29	18	2.9	3.1
21	21	male	36	76	43	75	19	25	20	25	10	10	10	10	303	306	310	300	5	3	5	5	32	32	16	18	3.6	2.8

ev, evening; **mo**, morning

References

Abbott, L. F. and van Vreeswijk, C. (1993). Asynchronous states in networks of pulse-coupled oscillators. *Physical Review E*, 48(2):1483.

Acebrón, J. A., Bonilla, L. L., Vicente, C. J., Ritort, F., and Spigler, R. (2005). The Kuramoto model: A simple paradigm for synchronization phenomena. *Reviews of modern physics*, 77(1):137.

Achermann, P. and Borbély, A. (1997). Low-frequency (<1Hz) oscillations in the human sleep electroencephalogram. *Neuroscience*, 81(1):213–222.

Achuthan, S., Butera, R. J., and Canavier, C. C. (2010). Synaptic and intrinsic determinants of the phase resetting curve for weak coupling. *Journal of Computational Neuroscience*, 30(2):373–390.

Agmon, A. and Connors, B. W. (1992). Correlation between intrinsic firing patterns and thalamocortical synaptic responses of neurons in mouse barrel cortex. *The Journal of Neuroscience*, 12(1):319–329.

Aihara, T., Abiru, Y., Yamazaki, Y., Watanabe, H., Fukushima, Y., and Tsukada, M. (2007). The relation between spike-timing dependent plasticity and Ca2+ dynamics in the hippocampal CA1 network. *Neuroscience*, 145(1):80–87.

Alzheimer, C., Schwindt, P. C., and Crill, W. E. (1993). Modal gating of Na+ channels as a mechanism of persistent Na+ current in pyramidal neurons from rat and cat sensorimotor cortex. *The Journal of Neuroscience*, 13(2):660–673.

Amzica, F. and Steriade, M. (1997a). Cellular substrates and laminar profile of sleep K-complex. *Neuroscience*, 82(3):671–686.

Amzica, F. and Steriade, M. (1997b). The K-complex: Its slow (< 1-Hz) rhythmicity and relation to delta waves. *Neurology*, 49(4):952.

Amzica, F. and Steriade, M. (1998). Electrophysiological correlates of sleep delta waves1. *Electroencephalography and clinical neurophysiology*, 107(2):69–83.

Anderer, P., Klösch, G., Gruber, G., Trenker, E., Pascual-Marqui, R. D., Zeitlhofer, J., Barbanoj, M. J., Rappelsberger, P., and Saletu, B. (2001). Low-resolution brain electromagnetic tomography revealed simultaneously active frontal and parietal sleep spindle sources in the human cortex. *Neuroscience*, 103(3):581–592.

Andrillon, T., Nir, Y., Staba, R., Ferrarelli, F., Cirelli, C., Tononi, G., and Fried, I. (2011). Sleep Spindles in Humans: Insights from Intracranial EEG and Unit Recordings. *The Journal of Neuroscience*, 31(49):17821–17834.

Antic, S. D., Zhou, W. L., Moore, A. R., Short, S. M., and Ikonomu, K. D. (2010). The decade of the dendritic NMDA spike. *Journal of Neuroscience Research*.

REFERENCES

Antonenko, D., Diekelmann, S., Olsen, C., Born, J., and Mölle, M. (2013). Napping to renew learning capacity: Enhanced encoding after stimulation of sleep slow oscillations. *European Journal of Neuroscience*, 37(7):1142–1151.

Anwyl, R. (1999). Metabotropic glutamate receptors: Electrophysiological properties and role in plasticity. *Brain Research Reviews*, 29(1):83–120.

Arbon, E. L., Knurowska, M., and Dijk, D.-J. (2015). Randomised clinical trial of the effects of prolonged-release melatonin, temazepam and zolpidem on slow-wave activity during sleep in healthy people. *Journal of Psychopharmacology*, 29(7):764–776.

Aschenbrenner, S., Tucha, O., and Lange, K. (2000). Regensburg word fluency test. *Hogrefe, Göttingen*.

Astori, S., Wimmer, R. D., Prosser, H. M., Corti, C., Corsi, M., Liaudet, N., Volterra, A., Franken, P., Adelman, J. P., and Luthi, A. (2011). The CaV3.3 calcium channel is the major sleep spindle pacemaker in thalamus. *Proceedings of the National Academy of Sciences*, 108(33):13823–13828.

Ayoub, A., Aumann, D., Hörschelmann, A., Kouchekmanesch, A., Paul, P., Born, J., and Marshall, L. (2013). Differential Effects on Fast and Slow Spindle Activity, and the Sleep Slow Oscillation in Humans with Carbamazepine and Flunarizine to Antagonize Voltage-Dependent Na+ and Ca2+ Channel Activity. *SLEEP*.

Ayoub, A., Mölle, M., Preissl, H., and Born, J. (2012). Grouping of MEG gamma oscillations by EEG sleep spindles. *NeuroImage*, 59(2):1491–1500.

Bal, T. and McCormick, D. A. (1996). What stops synchronized thalamocortical oscillations? *Neuron*, 17(2):297–308.

Ball, G. J., Gloor, P., and Schaul, N. (1977). The cortical electromicrophysiology of pathological delta waves in the electroencephalogram of cats. *Electroencephalography and Clinical Neurophysiology*, 43(3):346–361.

Barak, O. and Tsodyks, M. (2007). Persistent Activity in Neural Networks with Dynamic Synapses. *PLOS Comput Biol*, 3(2):e35.

Barthó, P., Slézia, A., Mátyás, F., Faradzs-Zade, L., Ulbert, I., Harris, K. D., and Acsády, L. (2014). Ongoing Network State Controls the Length of Sleep Spindles via Inhibitory Activity. *Neuron*, 82(6):1367–1379.

Bastien, C. and Campbell, K. (1994). Effects of rate of tone-pip stimulation on the evoked K-Complex. *Journal of Sleep Research*, 3(2):65–72.

Bastien, C. H., Crowley, K. E., and Colrain, I. M. (2002). Evoked potential components unique to non-REM sleep: Relationship to evoked K-complexes and vertex sharp waves. *International Journal of Psychophysiology*, 46(3):257–274.

Bazhenov, M., Timofeev, I., Steriade, M., and Sejnowski, T. J. (2002). Model of thalamocortical slow-wave sleep oscillations and transitions to activated states. *The Journal of Neuroscience*, 22(19):8691.

Bekkers, J. M. and Stevens, C. F. (1995). Quantal analysis of EPSCs recorded from small numbers of synapses in hippocampal cultures. *Journal of Neurophysiology*, 73(3):1145–1156.

Bendor, D. and Wilson, M. A. (2012). Biasing the content of hippocampal replay during sleep. *Nature Neuroscience*, 15(10):1439–1444.

Benita, J. M., Guillamon, A., Deco, G., and Sanchez-Vives, M. V. (2012). Synaptic depression and slow oscillatory activity in a biophysical network model of the cerebral cortex. *Frontiers in Computational Neuroscience*, 6.

Benjamini, Y. and Hochberg, Y. (1995). Controlling the False Discovery Rate: A Practical and Powerful Approach to Multiple Testing. *Journal of the Royal Statistical Society. Series B (Methodological)*, 57(1):289–300.

Benoit, E., Callot, J. L., Diener, F., Diener, M., and others (1981). Chasse au canard (première partie). *Collectanea Mathematica*, 32(1):37–76.

Bergmann, T. O., Mölle, M., Marshall, L., Kaya-Yildiz, L., Born, J., and Siebner, H. R. (2008). A local signature of LTP- and LTD-like plasticity in human NREM sleep. *European Journal of Neuroscience*, 27(9):2241–2249.

Biggio, M., Storace, M., and Mattia, M. (2013). Non-instantaneous synaptic transmission in spiking neuron networks and equivalence with delay distribution. *BMC Neuroscience*, 14(Suppl 1):P267.

Biktasheva, I. V., Barkley, D., Biktashev, V. N., and Foulkes, A. J. (2010). Computation of the drift velocity of spiral waves using response functions. *Physical Review E*, 81(6):066202.

Bischoff, U., Vogel, W., and Safronov, B. V. (1998). Na+-activated K+ channels in small dorsal root ganglion neurones of rat. *The Journal of Physiology*, 510(3):743–754.

Bojak, I. and Liley, D. T. J. (2005). Modeling the effects of anesthesia on the electroencephalogram. *Physical Review E*, 71(4).

Bonjean, M., Baker, T., Bazhenov, M., Cash, S., Halgren, E., and Sejnowski, T. (2012). Interactions between Core and Matrix Thalamocortical Projections in Human Sleep Spindle Synchronization. *The Journal of Neuroscience*, 32(15):5250–5263.

Bonjean, M., Baker, T., Lemieux, M., Timofeev, I., Sejnowski, T., and Bazhenov, M. (2011). Corticothalamic Feedback Controls Sleep Spindle Duration In Vivo. *The Journal of Neuroscience*, 31(25):9124.

Borisyuk, R. M. and Kirillov, A. B. (1992). Bifurcation analysis of a neural network model. *Biological Cybernetics*, 66(4):319–325.

Botella-Soler, V., Valderrama, M., Crépon, B., Navarro, V., and Le Van Quyen, M. (2012). Large-Scale Cortical Dynamics of Sleep Slow Waves. *PLoS One*, 7(2):e30757.

Boucetta, S., Crochet, S., Chauvette, S., Seigneur, J., and Timofeev, I. (2013). Extracellular Ca2+ fluctuations in vivo affect afterhyperpolarization potential and modify firing patterns of neocortical neurons. *Experimental Neurology*, 245:5–14.

Boustani, S. E. and Destexhe, A. (2009). Does brain activity stem from high-dimensional chaotic dynamics? Evidence from the human electroencephalogram, cat cerebral cortex and artificial neuronal networks. *arXiv preprint arXiv:0904.4217*.

Brunner, D. P., Dijk, D.-J., Münch, M., and Borbély, A. A. (1991). Effect of zolpidem on sleep and sleep EEG spectra in healthy young men. *Psychopharmacology*, 104(1):1–5.

Buzsáki, G. (2015). Hippocampal sharp wave-ripple: A cognitive biomarker for episodic memory and planning. *Hippocampus*, 25(10):1073–1188.

REFERENCES

Buzsáki, G., Anastassiou, C. A., and Koch, C. (2012). The origin of extracellular fields and currents — EEG, ECoG, LFP and spikes. *Nature Reviews Neuroscience*, 13(6):407–420.

Canolty, R. T., Edwards, E., Dalal, S. S., Soltani, M., Nagarajan, S. S., Kirsch, H. E., Berger, M. S., Barbaro, N. M., and Knight, R. T. (2006). High Gamma Power Is Phase-Locked to Theta Oscillations in Human Neocortex. *Science*, 313(5793):1626–1628.

Carracedo, L. M., Kjeldsen, H., Cunnington, L., Jenkins, A., Schofield, I., Cunningham, M. O., Davies, C. H., Traub, R. D., and Whittington, M. A. (2013). A Neocortical Delta Rhythm Facilitates Reciprocal Interlaminar Interactions via Nested Theta Rhythms. *The Journal of Neuroscience*, 33(26):10750–10761.

Cash, S. S., Halgren, E., Dehghani, N., Rossetti, A. O., Thesen, T., Wang, C., Devinsky, O., Kuzniecky, R., Doyle, W., Madsen, J. R., Bromfield, E., Eross, L., Halasz, P., Karmos, G., Csercsa, R., Wittner, L., and Ulbert, I. (2009). The Human K-Complex Represents an Isolated Cortical Down-State. *Science*, 324(5930):1084–1087.

Castro-Alamancos, M. A. and Favero, M. (2015). NMDA receptors are the basis for persistent network activity in neocortex slices. *Journal of Neurophysiology*, 113(10):3816–3826.

Chalifoux, J. R. and Carter, A. G. (2011). Glutamate Spillover Promotes the Generation of NMDA Spikes. *The Journal of Neuroscience*, 31(45):16435–16446.

Chauvette, S., Crochet, S., Volgushev, M., and Timofeev, I. (2011). Properties of Slow Oscillation during Slow-Wave Sleep and Anesthesia in Cats. *The Journal of Neuroscience*, 31(42):14998–15008.

Chauvette, S., Seigneur, J., and Timofeev, I. (2012). Sleep Oscillations in the Thalamocortical System Induce Long-Term Neuronal Plasticity. *Neuron*, 75(6):1105–1113.

Chauvette, S., Volgushev, M., and Timofeev, I. (2010). Origin of Active States in Local Neocortical Networks during Slow Sleep Oscillation. *Cerebral Cortex*, 20(11):2660–2674.

Chen, J.-Y., Chauvette, S., Skorheim, S., Timofeev, I., and Bazhenov, M. (2012). Interneuron-mediated inhibition synchronizes neuronal activity during slow oscillation. *The Journal of Physiology*, 590(16):3987–4010.

Chen, X., Leischner, U., Rochefort, N. L., Nelken, I., and Konnerth, A. (2011). Functional mapping of single spines in cortical neurons in vivo. *Nature*, 475(7357):501–505.

Clemens, Z., Mölle, M., Eross, L., Barsi, P., Halasz, P., and Born, J. (2007). Temporal coupling of parahippocampal ripples, sleep spindles and slow oscillations in humans. *Brain*, 130(11):2868–2878.

Clement, E. A., Richard, A., Thwaites, M., Ailon, J., Peters, S., and Dickson, C. T. (2008). Cyclic and Sleep-Like Spontaneous Alternations of Brain State Under Urethane Anaesthesia. *PLoS One*, 3(4):e2004.

Colrain, I. (2005). The K-complex: A 7-decade history. *Sleep*, 28(2):255–273.

Compte, A., Reig, R., Descalzo, V., Harvey, M., Puccini, G., and Sanchez-Vives, M. (2008). Spontaneous high-frequency (10–80 Hz) oscillations during up states in the cerebral cortex in vitro. *The Journal of Neuroscience*, 28(51):13828–13844.

Compte, A., Sanchez-Vives, M. V., McCormick, D. A., and Wang, X.-J. (2003). Cellular and Network Mechanisms of Slow Oscillatory Activity ($<$1 Hz) and Wave Propagations in a Cortical Network Model. *Journal of Neurophysiology*, 89(5):2707–2725.

Cona, F., Lacanna, M., and Ursino, M. (2014). A thalamo-cortical neural mass model for the simulation of brain rhythms during sleep. *Journal of Computational Neuroscience*, 37(1):125–148.

Contreras, D., Destexhe, A., Sejnowski, T. J., and Steriade, M. (1996a). Control of Spatiotemporal Coherence of a Thalamic Oscillation by Corticothalamic Feedback. *Science*, 274(5288):771 –774.

Contreras, D., Destexhe, A., Sejnowski, T. J., and Steriade, M. (1997). Spatiotemporal Patterns of Spindle Oscillations in Cortex and Thalamus. *The Journal of Neuroscience*, 17(3):1179–1196.

Contreras, D. and Steriade, M. (1995). Cellular Basis of EEG Slow Rhythms: A Study of Dynamic Corticothalamic Relationships. *The Journal of Neuroscience*, 15(1):604–622.

Contreras, D. and Steriade, M. (1996). Spindle oscillation in cats: The role of corticothalamic feedback in a thalamically generated rhythm. *The Journal of physiology*, 490(Pt 1):159–179.

Contreras, D., Timofeev, I., and Steriade, M. (1996b). Mechanisms of long-lasting hyperpolarizations underlying slow sleep oscillations in cat corticothalamic networks. *The Journal of Physiology*, 494(Pt 1):251.

Coombes, S. (2005). Waves, bumps, and patterns in neural field theories. *Biological Cybernetics*, 93(2):91–108.

Cortes, J. M., Desroches, M., Rodrigues, S., Veltz, R., Munoz, M. A., and Sejnowski, T. J. (2013). Short-term synaptic plasticity in the deterministic Tsodyks-Markram model leads to unpredictable network dynamics. *Proceedings of the National Academy of Sciences*, 110(41):16610–16615.

Cossart, R., Aronov, D., and Yuste, R. (2003). Attractor dynamics of network UP states in the neocortex. *Nature*, 423(6937):283–288.

Costa, M. S., Weigenand, A., Ngo, H.-V. V., Marshall, L., Born, J., Martinetz, T., and Claussen, J. C. (2016). A Thalamocortical Neural Mass Model of the EEG during NREM Sleep and Its Response to Auditory Stimulation. *PLoS Computational Biology*, 12(9):e1005022.

Cox, R., Hofman, W. F., and Talamini, L. M. (2012). Involvement of spindles in memory consolidation is slow wave sleep-specific. *Learning & Memory*, 19(7):264–267.

Crochet, S., Chauvette, S., Boucetta, S., and Timofeev, I. (2005). Modulation of synaptic transmission in neocortex by network activities. *European Journal of Neuroscience*, 21(4):1030–1044.

Crunelli, V. and Hughes, S. W. (2010). The slow (<1 Hz) rhythm of non-REM sleep: A dialogue between three cardinal oscillators. *Nature Neuroscience*, 13(1):9–17.

Csercsa, R., Dombovári, B., Fabó, D., Wittner, L., Erőss, L., Entz, L., Sólyom, A., Rásonyi, G., Szűcs, A., Kelemen, A., Jakus, R., Juhos, V., Grand, L., Magony, A., Halász, P., Freund, T. F., Maglóczky, Z., Cash, S. S., Papp, L., Karmos, G., Halgren, E., and Ulbert, I. (2010). Laminar analysis of slow wave activity in humans. *Brain*, 133(9):2814 –2829.

Cueni, L., Canepari, M., Luján, R., Emmenegger, Y., Watanabe, M., Bond, C. T., Franken, P., Adelman, J. P., and Lüthi, A. (2008). T-type Ca2+ channels, SK2 channels and SERCAs gate sleep-related oscillations in thalamic dendrites. *Nature Neuroscience*, 11(6):683–692.

REFERENCES

Cunningham, M. O., Pervouchine, D. D., Racca, C., Kopell, N. J., Davies, C. H., Jones, R. S. G., Traub, R. D., and Whittington, M. A. (2006). Neuronal metabolism governs cortical network response state. *Proceedings of the National Academy of Sciences*, 103(14):5597–5601.

Curto, C., Sakata, S., Marguet, S., Itskov, V., and Harris, K. D. (2009). A simple model of cortical dynamics explains variability and state dependence of sensory responses in urethane-anesthetized auditory cortex. *The Journal of Neuroscience*, 29(34):10600.

Dang-Vu, T. T., Desseilles, M., Laureys, S., Degueldre, C., Perrin, F., Phillips, C., Maquet, P., and Peigneux, P. (2005). Cerebral correlates of delta waves during non-REM sleep revisited. *NeuroImage*, 28(1):14–21.

Dang-Vu, T. T., Schabus, M., Desseilles, M., Albouy, G., Boly, M., Darsaud, A., Gais, S., Rauchs, G., Sterpenich, V., Vandewalle, G., Carrier, J., Moonen, G., Balteau, E., Degueldre, C., Luxen, A., Phillips, C., and Maquet, P. (2008). Spontaneous neural activity during human slow wave sleep. 105(39):15160–15165.

Daunizeau, J., Friston, K., and Kiebel, S. (2009). Variational Bayesian identification and prediction of stochastic nonlinear dynamic causal models. *Physica D: Nonlinear Phenomena*, 238(21):2089–2118.

David, F., Schmiedt, J. T., Taylor, H. L., Orban, G., Di Giovanni, G., Uebele, V. N., Renger, J. J., Lambert, R. C., Leresche, N., and Crunelli, V. (2013). Essential Thalamic Contribution to Slow Waves of Natural Sleep. *The Journal of Neuroscience*, 33(50):19599–19610.

David, O. and Friston, K. J. (2003). A neural mass model for MEG/EEG:. *NeuroImage*, 20(3):1743–1755.

Deco, G. and Jirsa, V. K. (2012). Ongoing Cortical Activity at Rest: Criticality, Multistability, and Ghost Attractors. *The Journal of Neuroscience*, 32(10):3366–3375.

Deco, G., Jirsa, V. K., Robinson, P. A., Breakspear, M., and Friston, K. (2008). The Dynamic Brain: From Spiking Neurons to Neural Masses and Cortical Fields. *PLoS Computational Biology*, 4(8):e1000092.

Deco, G., Martí, D., Ledberg, A., Reig, R., and Sanchez Vives, M. V. (2009). Effective Reduced Diffusion-Models: A Data Driven Approach to the Analysis of Neuronal Dynamics. *PLoS Comput Biol*, 5(12):e1000587.

Dehghani, N., Cash, S. S., and Halgren, E. (2011). Emergence of synchronous EEG spindles from asynchronous MEG spindles. *Human Brain Mapping*, 32(12):2217–2227.

Delorme, A. and Makeig, S. (2004). EEGLAB: An open source toolbox for analysis of single-trial EEG dynamics including independent component analysis. *Journal of Neuroscience Methods*, 134(1):9–21.

Destexhe, A., Bal, T., McCormick, D. A., and Sejnowski, T. J. (1996a). Ionic mechanisms underlying synchronized oscillations and propagating waves in a model of ferret thalamic slices. *Journal of Neurophysiology*, 76(3):2049–2070.

Destexhe, A., Contreras, D., Sejnowski, T. J., and Steriade, M. (1994). A model of spindle rhythmicity in the isolated thalamic reticular nucleus. *Journal of Neurophysiology*, 72(2):803–818.

Destexhe, A., Contreras, D., and Steriade, M. (1999). Spatiotemporal Analysis of Local Field Potentials and Unit Discharges in Cat Cerebral Cortex during Natural Wake and Sleep States. *The Journal of Neuroscience*, 19(11):4595–4608.

Destexhe, A., Contreras, D., Steriade, M., Sejnowski, T. J., and Huguenard, J. R. (1996b). In vivo, in vitro, and computational analysis of dendritic calcium currents in thalamic reticular neurons. *The Journal of Neuroscience*, 16(1):169–185.

Destexhe, A., Neubig, M., Ulrich, D., and Huguenard, J. (1998). Dendritic Low-Threshold Calcium Currents in Thalamic Relay Cells. *The Journal of Neuroscience*, 18(10):3574–3588.

Destexhe, A. and Sejnowski, T. J. (2003). Interactions between membrane conductances underlying thalamocortical slow-wave oscillations. *Physiological reviews*, 83(4):1401–1453.

Diekelmann, S. and Born, J. (2010). The memory function of sleep. *Nat Rev Neurosci*, 11(2):114–126.

Dijk, D.-J., Hayes, B., and Czeisler, C. A. (1993). Dynamics of electroencephalographic sleep spindles and slow wave activity in men: Effect of sleep deprivation. *Brain Research*, 626(1–2):190–199.

Diniz Behn, C. G. and Booth, V. (2010). Simulating Microinjection Experiments in a Novel Model of the Rat Sleep-Wake Regulatory Network. *Journal of Neurophysiology*, 103(4):1937–1953.

Disney, A. A., Aoki, C., and Hawken, M. J. (2007). Gain Modulation by Nicotine in Macaque V1. *Neuron*, 56(4):701–713.

Dossi, R. C., Nunez, A., and Steriade, M. (1992). Electrophysiology of a slow (0.5-4 Hz) intrinsic oscillation of cat thalamocortical neurones in vivo. *The Journal of physiology*, 447(1):215–234.

Dudai, Y., Karni, A., and Born, J. (2015). The Consolidation and Transformation of Memory. *Neuron*, 88(1):20–32.

Eckhaus, W. (1983). Relaxation oscillations including a standard chase on French ducks. In *Asymptotic Analysis II—*, pages 449–494. Springer.

Egea, J. A., Henriques, D., Cokelaer, T., Villaverde, A. F., MacNamara, A., Danciu, D.-P., Banga, J. R., and Saez-Rodriguez, J. (2014). MEIGO: An open-source software suite based on metaheuristics for global optimization in systems biology and bioinformatics. *BMC Bioinformatics*, 15:136.

Ego-Stengel, V. and Wilson, M. A. (2010). Disruption of ripple-associated hippocampal activity during rest impairs spatial learning in the rat. *Hippocampus*, 20(1):1–10.

Esser, S. K., Hill, S. L., and Tononi, G. (2007). Sleep Homeostasis and Cortical Synchronization: I. Modeling the Effects of Synaptic Strength on Sleep Slow Waves. *Sleep*, 30(12):1617–1630.

Evans, B. M. (1976). Patterns of arousal in comatose patients. *Journal of Neurology, Neurosurgery & Psychiatry*, 39(4):392–402.

Favero, M. and Castro-Alamancos, M. A. (2013). Synaptic Cooperativity Regulates Persistent Network Activity in Neocortex. *The Journal of Neuroscience*, 33(7):3151–3163.

REFERENCES

Featherstone, D. E. and Shippy, S. A. (2008). Regulation of Synaptic Transmission by Ambient Extracellular Glutamate. *The Neuroscientist*, 14(2):171–181.

Feld, G. B., Wilhelm, I., Ma, Y., Groch, S., Binkofski, F., Mölle, M., and Born, J. (2013). Slow Wave Sleep Induced by GABA Agonist Tiagabine Fails to Benefit Memory Consolidation. *SLEEP*, 36(9):1317.

Fogel, S. M. and Smith, C. T. (2011). The function of the sleep spindle: A physiological index of intelligence and a mechanism for sleep-dependent memory consolidation. *Neuroscience & Biobehavioral Reviews*, 35(5):1154–1165.

Foster, B. L., Bojak, I., and Liley, D. T. J. (2011). Understanding the effects of anesthetic agents on the EEG through neural field theory. pages 4709–4712. IEEE.

Fowler, M. J., Sullivan, M. J., and Ekstrand, B. R. (1973). Sleep and Memory. *Science*, 179(4070):302–304.

Frauscher, B., von Ellenrieder, N., Dubeau, F., and Gotman, J. (2015). Scalp spindles are associated with widespread intracranial activity with unexpectedly low synchrony. *NeuroImage*, 105:1–12.

Fröhlich, F., Bazhenov, M., Timofeev, I., Steriade, M., and Sejnowski, T. J. (2006). Slow State Transitions of Sustained Neural Oscillations by Activity-Dependent Modulation of Intrinsic Excitability. *The Journal of Neuroscience*, 26(23):6153 –6162.

Fröhlich, F. and McCormick, D. A. (2010). Endogenous Electric Fields May Guide Neocortical Network Activity. *Neuron*, 67(1):129–143.

Fucke, T., Suchanek, D., Nawrot, M. P., Seamari, Y., Heck, D. H., Aertsen, A., and Boucsein, C. (2011). Stereotypical spatiotemporal activity patterns during slow-wave activity in the neocortex. *Journal of Neurophysiology*, 106(6):3035–3044.

Fusi, S. and Abbott, L. F. (2007). Limits on the memory storage capacity of bounded synapses. *Nature Neuroscience*.

Gais, S., Mölle, M., Helms, K., and Born, J. (2002). Learning-Dependent Increases in Sleep Spindle Density. *The Journal of Neuroscience*, 22(15):6830–6834.

Gentet, L. J. and Ulrich, D. (2004). Electrophysiological characterization of synaptic connections between layer VI cortical cells and neurons of the nucleus reticularis thalami in juvenile rats. *European Journal of Neuroscience*, 19(3):625–633.

Georgiou, T. (2007). Distances and Riemannian Metrics for Spectral Density Functions. *IEEE Transactions on Signal Processing*, 55(8):3995–4003.

Georgiou, T., Karlsson, J., and Takyar, M. (2009). Metrics for Power Spectra: An Axiomatic Approach. *IEEE Transactions on Signal Processing*, 57(3):859–867.

Ghorbani, M., Mehta, M., Bruinsma, R., and Levine, A. (2012). Nonlinear-dynamics theory of up-down transitions in neocortical neural networks. *Physical Review E*, 85(2).

Girardeau, G., Benchenane, K., Wiener, S. I., Buzsáki, G., and Zugaro, M. B. (2009). Selective suppression of hippocampal ripples impairs spatial memory. *Nature Neuroscience*, 12(10):1222–1223.

Golomb, D., Wang, X. J., and Rinzel, J. (1994). Synchronization properties of spindle oscillations in a thalamic reticular nucleus model. *Journal of Neurophysiology*, 72(3):1109–1126.

Görtelmeyer, R. (1981). Schlaffragebogen SF-A und SF-B. Internationale Skalen für Psychiatrie. *Beltz, Weinheim*.

Govern, C. C. and ten Wolde, P. R. (2014). Energy Dissipation and Noise Correlations in Biochemical Sensing. *Physical Review Letters*, 113(25):258102.

Granada, A., Hennig, R., Ronacher, B., Kramer, A., and Herzel, H. (2009). Chapter 1 Phase Response CurvesElucidating the Dynamics of Coupled Oscillators. In *Methods in Enzymology*, volume 454, pages 1–27. Elsevier.

Grannan, E. R., Kleinfeld, D., and Sompolinsky, H. (1993). Stimulus-dependent synchronization of neuronal assemblies. *Neural computation*, 5(4):550–569.

Groh, A., Bokor, H., Mease, R. A., Plattner, V. M., Hangya, B., Stroh, A., Deschenes, M., and Acsády, L. (2014). Convergence of Cortical and Sensory Driver Inputs on Single Thalamocortical Cells. *Cerebral Cortex*, 24(12):3167–3179.

Gulledge, A. T., Bucci, D. J., Zhang, S. S., Matsui, M., and Yeh, H. H. (2009). M1 Receptors Mediate Cholinergic Modulation of Excitability in Neocortical Pyramidal Neurons. *The Journal of Neuroscience*, 29(31):9888–9902.

Haider, B., Duque, A., Hasenstaub, A., and McCormick, D. (2006). Neocortical network activity in vivo is generated through a dynamic balance of excitation and inhibition. *The Journal of neuroscience*, 26(17):4535.

Halassa, M. M., Siegle, J. H., Ritt, J. T., Ting, J. T., Feng, G., and Moore, C. I. (2011). Selective optical drive of thalamic reticular nucleus generates thalamic bursts and cortical spindles. *Nature Neuroscience*, 14(9):1118–1120.

Hall-Porter, J. M., Schweitzer, P. K., Eisenstein, R. D., Ahmed, H. A. H., and Walsh, J. K. (2014). The Effect of Two Benzodiazepine Receptor Agonist Hypnotics on Sleep-Dependent Memory Consolidation. *Journal of Clinical Sleep Medicine*, 10(1):27.

Hangya, B., Tihanyi, B. T., Entz, L., Fabó, D., Erőss, L., Wittner, L., Jakus, R., Varga, V., Freund, T. F., and Ulbert, I. (2011). Complex Propagation Patterns Characterize Human Cortical Activity during Slow-Wave Sleep. *The Journal of Neuroscience*, 31(24):8770.

Hashemi, M., Hutt, A., and Sleigh, J. (2014). Anesthetic action on extra-synaptic receptors: Effects in neural population models of EEG activity. *Frontiers in Systems Neuroscience*, 8.

Hasselmo, M. E. and Giocomo, L. M. (2006). Cholinergic modulation of cortical function. *Journal of Molecular Neuroscience*, 30(1):133–135.

Hill, S. and Tononi, G. (2005). Modeling Sleep and Wakefulness in the Thalamocortical System. *Journal of Neurophysiology*, 93(3):1671–1698.

Himanen, S.-L., Virkkala, J., Huhtala, H., and Hasan, J. (2002). Spindle frequencies in sleep EEG show U-shape within first four NREM sleep episodes. *Journal of Sleep Research*, 11(1):35–42.

Hirata, A. and Castro-Alamancos, M. A. (2010). Neocortex Network Activation and Deactivation States Controlled by the Thalamus. *Journal of Neurophysiology*, 103(3):1147–1157.

Hoddes, E., Zarcone, V., Smythe, H., Phillips, R., and Dement, W. C. (1973). Quantification of Sleepiness: A New Approach. *Psychophysiology*, 10(4):431–436.

Holcman, D. and Tsodyks, M. (2006). The Emergence of Up and Down States in Cortical Networks. *PLoS Comput Biol*, 2(3):e23.

REFERENCES

Hromadka, T., Zador, A. M., and DeWeese, M. R. (2013). Up states are rare in awake auditory cortex. *Journal of Neurophysiology*, 109(8):1989–1995.

Huber, R., Felice Ghilardi, M., Massimini, M., and Tononi, G. (2004). Local sleep and learning. *Nature*, 430(6995):78–81.

Huber, R., Ghilardi, M. F., Massimini, M., Ferrarelli, F., Riedner, B. A., Peterson, M. J., and Tononi, G. (2006). Arm immobilization causes cortical plastic changes and locally decreases sleep slow wave activity. *Nature Neuroscience*, 9:1169–1176.

Hughes, S. W., Cope, D. W., Blethyn, K. L., and Crunelli, V. (2002). Cellular mechanisms of the slow (< 1 Hz) oscillation in thalamocortical neurons in vitro. *Neuron*, 33(6):947–958.

Huguenard, J. R. (1996). Low-threshold calcium currents in central nervous system neurons. *Annual review of physiology*, 58(1):329–348.

Iber, C., Ancoli-Israel, S., Chesson, A. L., and Quan, S. F. (2007). *The AASM Manual for the Scoring of Sleep and Associated Events: Rules, Terminology and Technical Specifications*. American Academy of Sleep Medicine, Westchester, IL.

Izhikevich, E. M. (2000). Phase equations for relaxation oscillators. *SIAM Journal on Applied Mathematics*, 60(5):1789–1804.

Jansen, B. H., Zouridakis, G., and Brandt, M. E. (1993). A neurophysiologically-based mathematical model of flash visual evoked potentials. *Biological Cybernetics*, 68(3):275–283.

Ji, D. and Wilson, M. A. (2007). Coordinated memory replay in the visual cortex and hippocampus during sleep. *Nature Neuroscience*, 10(1):100–107.

Jirsa, V. K. (2009). Neural field dynamics with local and global connectivity and time delay. *Philosophical Transactions of the Royal Society of London A: Mathematical, Physical and Engineering Sciences*, 367(1891):1131–1143.

Jobert, M., Poiseau, E., Jähnig, P., Schulz, H., and Kubicki, S. (1992). Topographical Analysis of Sleep Spindle Activity. *Neuropsychobiology*, 26(4):210–217.

Jones, E. G. (2001). The thalamic matrix and thalamocortical synchrony. *Trends in Neurosciences*, 24(10):595–601.

Jones, E. G. (2002). Thalamic circuitry and thalamocortical synchrony. *Philosophical Transactions of the Royal Society B: Biological Sciences*, 357(1428):1659–1673.

Kang, S., Kitano, K., and Fukai, T. (2004). Self-organized two-state membrane potential transitions in a network of realistically modeled cortical neurons. *Neural Networks*, 17(3):307–312.

Kay, A. R., Sugimori, M., and Llinás, R. (1998). Kinetic and stochastic properties of a persistent sodium current in mature guinea pig cerebellar Purkinje cells. *Journal of neurophysiology*, 80(3):1167–1179.

Kazakov, V. A. and Lavrov, A. M. (1994). Orthogonal polynomial expansion of Pearson's probability densities for non-Markov processes. *Radiophysics and Quantum Electronics*, 37(12):1012–1016.

Kerr, C. C., Rennie, C. J., and Robinson, P. A. (2007). Physiology-based modeling of cortical auditory evoked potentials. *Biological Cybernetics*, 98(2):171–184.

Kim, D., Hwang, E., Lee, M., Sung, H., and Choi, J. H. (2015). Characterization of Topographically Specific Sleep Spindles in Mice. *SLEEP*.

Kim, U. and Mccormick, D. A. (1998). Functional and Ionic Properties of a Slow After-hyperpolarization in Ferret Perigeniculate Neurons In Vitro. *Journal of Neurophysiology*, 80(3):1222–1235.

Kleinhans, D., Friedrich, R. M., Nawroth, A., and Peinke, J. (2005). Estimation of Drift and Diffusion Functions of Stochastic Processes. Technical report.

Knight, B. W. (1972). The relationship between the firing rate of a single neuron and the level of activity in a population of neurons experimental evidence for resonant enhancement in the population response. *The Journal of General Physiology*, 59(6):767–778.

Knoblauch, V., Martens, W. L., Wirz-Justice, A., and Cajochen, C. (2003). Human sleep spindle characteristics after sleep deprivation. *Clinical Neurophysiology*, 114(12):2258–2267.

Ko, T.-W. and Ermentrout, G. (2009). Phase-response curves of coupled oscillators. *Physical Review E*, 79(1).

Kori, H., Kawamura, Y., Nakao, H., Arai, K., and Kuramoto, Y. (2009). Collective-phase description of coupled oscillators with general network structure. *Physical Review E*, 80(3).

Krieg, D. and Triesch, J. (2014). A unifying theory of synaptic long-term plasticity based on a sparse distribution of synaptic strength. *Frontiers in Synaptic Neuroscience*, 6.

Krishnamurthy, P., Silberberg, G., and Lansner, A. (2012). A Cortical Attractor Network with Martinotti Cells Driven by Facilitating Synapses. *PLoS One*, 7(4):e30752.

Kumar, R., Bose, A., and Mallick, B. N. (2012). A Mathematical Model towards Understanding the Mechanism of Neuronal Regulation of Wake-NREMS-REMS States. *PLoS One*, 7(8):e42059.

Kurth, S., Ringli, M., Geiger, A., LeBourgeois, M., Jenni, O. G., and Huber, R. (2010). Mapping of Cortical Activity in the First Two Decades of Life: A High-Density Sleep Electroencephalogram Study. *The Journal of Neuroscience*, 30(40):13211–13219.

Lahiri, S. and Ganguli, S. (2013). A memory frontier for complex synapses. In *Advances in Neural Information Processing Systems*, pages 1034–1042.

Lahiri, S., Sohl-Dickstein, J., and Ganguli, S. (2016). A universal tradeoff between power, precision and speed in physical communication. *arXiv:1603.07758*.

Lan, G., Sartori, P., Neumann, S., Sourjik, V., and Tu, Y. (2012). The energy–speed–accuracy trade-off in sensory adaptation. *Nature Physics*, 8(5):422–428.

Landsness, E. C., Crupi, D., Hulse, B. K., Peterson, M. J., Huber, R., Ansari, H., Coen, M., Cirelli, C., Benca, R. M., Ghilardi, M. F., and others (2009). Sleep-dependent improvement in visuomotor learning: A causal role for slow waves. *Sleep*, 32(10):1273–1284.

Langdon, A. J., Breakspear, M., and Coombes, S. (2012). Phase-locked cluster oscillations in periodically forced integrate-and-fire-or-burst neuronal populations. *Physical Review E*, 86(6).

Laurino, M., Menicucci, D., Piarulli, A., Mastorci, F., Bedini, R., Allegrini, P., and Gemignani, A. (2014). Disentangling different functional roles of evoked K-complex components: Mapping the sleeping brain while quenching sensory processing. *NeuroImage*, 86:433–445.

REFERENCES

Le Bon-Jego, M. and Yuste, R. (2007). Persistently active, pacemaker-like neurons in neocortex. *Frontiers in Neuroscience*, 1(1):123.

Le Van Quyen, M., Staba, R., Bragin, A., Dickson, C., Valderrama, M., Fried, I., and Engel, J. (2010). Large-scale microelectrode recordings of high-frequency gamma oscillations in human cortex during sleep. *The Journal of Neuroscience*, 30(23):7770.

Lee, J., Song, K., Lee, K., Hong, J., Lee, H., Chae, S., Cheong, E., and Shin, H.-S. (2013). Sleep spindles are generated in the absence of T-type calcium channel-mediated low-threshold burst firing of thalamocortical neurons. *Proceedings of the National Academy of Sciences*, 110(50):20266–20271.

Lemieux, M., Chen, J.-Y., Lonjers, P., Bazhenov, M., and Timofeev, I. (2014). The Impact of Cortical Deafferentation on the Neocortical Slow Oscillation. *The Journal of Neuroscience*, 34(16):5689–5703.

Léna, I., Parrot, S., Deschaux, O., Muffat-Joly, S., Sauvinet, V., Renaud, B., Suaud-Chagny, M. f., and Gottesmann, C. (2005). Variations in extracellular levels of dopamine, noradrenaline, glutamate, and aspartate across the sleep–wake cycle in the medial prefrontal cortex and nucleus accumbens of freely moving rats. *Journal of Neuroscience Research*, 81(6):891–899.

Leresche, N., Lightowler, S., Soltesz, I., Jassik-Gerschenfeld, D., and Crunelli, V. (1991). Low-frequency oscillatory activities intrinsic to rat and cat thalamocortical cells. *The Journal of Physiology*, 441(1):155–174.

Levnajić, Z. and Pikovsky, A. (2010). Phase resetting of collective rhythm in ensembles of oscillators. *Physical Review E*, 82(5).

Li, Y. and Wong, K. M. (2013). Riemannian Distances for Signal Classification by Power Spectral Density. *IEEE Journal of Selected Topics in Signal Processing*, 7(4):655–669.

Liley, D. T., Cadusch, P. J., and Dafilis, M. P. (2002). A spatially continuous mean field theory of electrocortical activity. *Network: Computation in Neural Systems*, 13(1):67–113.

Liley, D. T., Cadusch, P. J., and Wright, J. J. (1999). A continuum theory of electro-cortical activity. *Neurocomputing*, 26:795–800.

Llinás, R. and Jahnsen, H. (1982). Electrophysiology of mammalian thalamic neurones in vitro. *Nature*, 297(5865):406–408.

Lopes da Silva, F. H., Hoeks, A., Smits, H., and Zetterberg, L. H. (1974). Model of brain rhythmic activity. *Kybernetik*, 15(1):27–37.

Lőrincz, M. L., Gunner, D., Bao, Y., Connelly, W. M., Isaac, J. T., Hughes, S. W., and Crunelli, V. (2015). A Distinct Class of Slow ($\sim$0.2–2 Hz) Intrinsically Bursting Layer 5 Pyramidal Neurons Determines UP/DOWN State Dynamics in the Neocortex. *The Journal of Neuroscience*, 35(14):5442–5458.

Loxley, P. N. and Robinson, P. A. (2007). Spike-rate adaptation and neuronal bursting in a mean-field model of brain activity. *Biological Cybernetics*, 97(2):113–122.

Lüthi, A. and McCormick, D. A. (1998). Periodicity of Thalamic Synchronized Oscillations: The Role of Ca^{2+} -Mediated Upregulation of I_h. *Neuron*, 20(3):553–563.

Lüthi, A. and McCormick, D. A. (1999). Modulation of a pacemaker current through Ca2+-induced stimulation of cAMP production. *Nature Neuroscience*, 2(7):634–641.

Lydic, R. and Baghdoyan, H. A. (2005). Sleep, Anesthesiology, and the Neurobiology of Arousal State Control. *The Journal of the American Society of Anesthesiologists*, 103(6):1268–1295.

Lytton, W. W., Destexhe, A., and Sejnowski, T. J. (1996). Control of slow oscillations in the thalamocortical neuron: A computer model. *Neuroscience*, 70(3):673–684.

Markram, H., Lübke, J., Frotscher, M., and Sakmann, B. (1997). Regulation of synaptic efficacy by coincidence of postsynaptic APs and EPSPs. *Science*, 275(5297):213.

Markram, H., Wang, Y., and Tsodyks, M. (1998). Differential signaling via the same axon of neocortical pyramidal neurons. *Proceedings of the National Academy of Sciences*, 95(9):5323–5328.

Marreiros, A. C., Daunizeau, J., Kiebel, S. J., and Friston, K. J. (2008). Population dynamics: Variance and the sigmoid activation function. *Neuroimage*, 42(1):147–157.

Marshall, L., Helgadottir, H., Molle, M., and Born, J. (2006). Boosting slow oscillations during sleep potentiates memory. *Nature*, 444(7119):610–613.

Massimini, M. (2002). EEG Slow (1 Hz) Waves Are Associated With Nonstationarity of Thalamo-Cortical Sensory Processing in the Sleeping Human. *Journal of Neurophysiology*, 89:1205–1213.

Massimini, M. and Amzica, F. (2001). Extracellular Calcium Fluctuations and Intracellular Potentials in the Cortex During the Slow Sleep Oscillation. *Journal of Neurophysiology*, 85(3):1346–1350.

Massimini, M., Ferrarelli, F., Esser, S. K., Riedner, B. A., Huber, R., Murphy, M., Peterson, M. J., and Tononi, G. (2007). Triggering sleep slow waves by transcranial magnetic stimulation. *Proceedings of the National Academy of Sciences*, 104(20):8496–8501.

Massimini, M., Huber, R., Ferrarelli, F., Hill, S., and Tononi, G. (2004). The sleep slow oscillation as a traveling wave. *The Journal of Neuroscience*, 24(31):6862.

Mattia, M. and Sanchez-Vives, M. V. (2011). Exploring the spectrum of dynamical regimes and timescales in spontaneous cortical activity. *Cognitive Neurodynamics*, 6(3):239–250.

Mayer, J., Schuster, H., and Claussen, J. (2006). Role of inhibitory feedback for information processing in thalamocortical circuits. *Physical Review E*, 73(3).

Mayer, J., Schuster, H. G., Claussen, J. C., and Molle, M. (2007). Corticothalamic Projections Control Synchronization in Locally Coupled Bistable Thalamic Oscillators. *Physical Review Letters*, 99(6):068102–4.

McCormick, D. A. (1989). Cholinergic and noradrenergic modulation of thalamocortical processing. *Trends in Neurosciences*, 12(6):215–221.

McCormick, D. A. (1992). Neurotransmitter actions in the thalamus and cerebral cortex and their role in neuromodulation of thalamocortical activity. *Progress in Neurobiology*, 39(4):337–388.

McCormick, D. A. and Pape, H. C. (1990). Properties of a hyperpolarization-activated cation current and its role in rhythmic oscillation in thalamic relay neurones. *The Journal of Physiology*, 431(1):291–318.

REFERENCES

Mednick, S. C., McDevitt, E. A., Walsh, J. K., Wamsley, E., Paulus, M., Kanady, J. C., and Drummond, S. P. A. (2013). The Critical Role of Sleep Spindles in Hippocampal-Dependent Memory: A Pharmacology Study. *The Journal of Neuroscience*, 33(10):4494–4504.

Mehaffey, W. H. (2005). Deterministic Multiplicative Gain Control with Active Dendrites. *The Journal of Neuroscience*, 25(43):9968–9977.

Mejias, J. F., Kappen, H. J., and Torres, J. J. (2010). Irregular Dynamics in Up and Down Cortical States. *PLoS One*, 5(11):e13651.

Melamed, O., Barak, O., Silberberg, G., Markram, H., and Tsodyks, M. (2008). Slow oscillations in neural networks with facilitating synapses. *Journal of Computational Neuroscience*, 25(2):308–316.

Meléndez, J., Galli, I., Boric, K., Ortega, A., Zuñiga, L., Henríquez-Roldán, C. F., and Cárdenas, A. M. (2005). Zolpidem and triazolam do not affect the nocturnal sleep-induced memory improvement. *Psychopharmacology*, 181(1):21–26.

Menicucci, D., Piarulli, A., Allegrini, P., Laurino, M., Mastorci, F., Sebastiani, L., Bedini, R., and Gemignani, A. (2013). Fragments of wake-like activity frame down-states of sleep slow oscillations in humans: New vistas for studying homeostatic processes during sleep. *International Journal of Psychophysiology*, 89(2):151–157.

Metherate, R. and Ashe, J. H. (1993). Ionic flux contributions to neocortical slow waves and nucleus basalis-mediated activation: Whole-cell recordings in vivo. *The Journal of Neuroscience*, 13(12):5312–5323.

Millman, D., Mihalas, S., Kirkwood, A., and Niebur, E. (2010). Self-organized criticality occurs in non-conservative neuronal networks during 'up' states. *Nature Physics*, 6(10):801–805.

Milojkovic, B. A., Radojicic, M. S., and Antic, S. D. (2005). A Strict Correlation Between Dendritic and Somatic Plateau Depolarizations in the Rat Prefrontal Cortex Pyramidal Neurons. *The Journal of Neuroscience*, 25(15):3940–3951.

Milojkovic, B. A., Zhou, W.-L., and Antic, S. D. (2007). Voltage and calcium transients in basal dendrites of the rat prefrontal cortex. *The Journal of Physiology*, 585(2):447–468.

Mittmann, T. and Alzheimer, C. (1998). Muscarinic Inhibition of Persistent Na+ Current in Rat Neocortical Pyramidal Neurons. *Journal of Neurophysiology*, 79(3):1579–1582.

Moakher, M. (2005). A differential geometric approach to the geometric mean of symmetric positive-definite matrices. *SIAM Journal on Matrix Analysis and Applications*, 26(3):735–747.

Mohajerani, M. H., McVea, D. A., Fingas, M., and Murphy, T. H. (2010). Mirrored Bilateral Slow-Wave Cortical Activity within Local Circuits Revealed by Fast Bihemispheric Voltage-Sensitive Dye Imaging in Anesthetized and Awake Mice. *The Journal of Neuroscience*, 30(10):3745–3751.

Molaee-Ardekani, B. (2007). Brain activity modeling in general anesthesia: Enhancing local mean-field models using a slow adaptive firing rate. *Physical Review E*, 76(4).

Mölle, M., Bergmann, T. O., Marshall, L., and Born, J. (2011). Fast and Slow Spindles during the Sleep Slow Oscillation: Disparate Coalescence and Engagement in Memory Processing. *Sleep*, 34(10):1411–1421.

Mölle, M., Eschenko, O., Gais, S., Sara, S. J., and Born, J. (2009). The influence of learning on sleep slow oscillations and associated spindles and ripples in humans and rats. *European Journal of Neuroscience*, 29(5):1071–1081.

Mölle, M., Marshall, L., Gais, S., and Born, J. (2002). Grouping of spindle activity during slow oscillations in human non-rapid eye movement sleep. *The Journal of Neuroscience*, 22(24):10941.

Mölle, M., Yeshenko, O., Marshall, L., Sara, S. J., and Born, J. (2006). Hippocampal Sharp Wave-Ripples Linked to Slow Oscillations in Rat Slow-Wave Sleep. *Journal of Neurophysiology*, 96(1):62 –70.

Mongillo, G., Barak, O., and Tsodyks, M. (2008). Synaptic Theory of Working Memory. *Science*, 319(5869):1543–1546.

Mukovski, M., Chauvette, S., Timofeev, I., and Volgushev, M. (2007). Detection of Active and Silent States in Neocortical Neurons from the Field Potential Signal during Slow-Wave Sleep. *Cerebral Cortex*, 17(2):400–414.

Murphy, M., Riedner, B. A., Huber, R., Massimini, M., Ferrarelli, F., and Tononi, G. (2009). Source modeling sleep slow waves. *Proceedings of the National Academy of Sciences*, 106(5):1608–1613.

Nakagawa, T. T., Woolrich, M., Luckhoo, H., Joensson, M., Mohseni, H., Kringelbach, M. L., Jirsa, V., and Deco, G. (2014). How delays matter in an oscillatory whole-brain spiking-neuron network model for MEG alpha-rhythms at rest. *NeuroImage*, 87:383–394.

Neske, G. T. (2016). The Slow Oscillation in Cortical and Thalamic Networks: Mechanisms and Functions. *Frontiers in Neural Circuits*, 9.

Neske, G. T., Patrick, S. L., and Connors, B. W. (2015). Contributions of Diverse Excitatory and Inhibitory Neurons to Recurrent Network Activity in Cerebral Cortex. *The Journal of Neuroscience*, 35(3):1089–1105.

Nettersheim, A., Hallschmid, M., Born, J., and Diekelmann, S. (2015). The Role of Sleep in Motor Sequence Consolidation: Stabilization Rather Than Enhancement. *The Journal of Neuroscience*, 35(17):6696–6702.

Ngo, H.-V. V., Köhler, J., Mayer, J., Claussen, J. C., and Schuster, H. G. (2010). Triggering up states in all-to-all coupled neurons. *Europhysics Letters*, 89(6):68002.

Ngo, H.-V. V., Martinetz, T., Born, J., and Mölle, M. (2013). Auditory Closed-Loop Stimulation of the Sleep Slow Oscillation Enhances Memory. *Neuron*, 78(3):545–553.

Ngo, H.-V. V., Miedema, A., Faude, I., Martinetz, T., Mölle, M., and Born, J. (2015). Driving Sleep Slow Oscillations by Auditory Closed-Loop Stimulation—A Self-Limiting Process. *The Journal of Neuroscience*, 35(17):6630–6638.

Nicoll, R. A., Malenka, R. C., and Kauer, J. A. (1990). Functional comparison of neurotransmitter receptor subtypes in mammalian central nervous system. *Physiological Reviews*, 70(2):513–565.

Niknazar, M., Krishnan, G. P., Bazhenov, M., and Mednick, S. C. (2015). Coupling of Thalamocortical Sleep Oscillations Are Important for Memory Consolidation in Humans. *PLoS ONE*, 10(12):e0144720.

REFERENCES

Nir, Y., Staba, R. J., Andrillon, T., Vyazovskiy, V. V., Cirelli, C., Fried, I., and Tononi, G. (2011). Regional Slow Waves and Spindles in Human Sleep. *Neuron*, 70(1):153–169.

Nunez, A., Curró Dossi, R., Contreras, D., and Steriade, M. (1992). Intracellular evidence for incompatibility between spindle and delta oscillations in thalamocortical neurons of cat. *Neuroscience*, 48(1):75–85.

Okun, M. and Lampl, I. (2008). Instantaneous correlation of excitation and inhibition during ongoing and sensory-evoked activities. *Nature Neuroscience*, 11:535–537.

Olbrich, E. and Achermann, P. (2005). Analysis of oscillatory patterns in the human sleep EEG using a novel detection algorithm. *Journal of Sleep Research*, 14(4):337–346.

Olbrich, E. and Achermann, P. (2008). Analysis of the Temporal Organization of Sleep Spindles in the Human Sleep EEG Using a Phenomenological Modeling Approach. *Journal of Biological Physics*, 34(3-4):341–349.

Olcese, U., Esser, S. K., and Tononi, G. (2010). Sleep and synaptic renormalization: A computational study. *Journal of Neurophysiology*, page jn.00593.2010.

Panas, D., Malinowska, U., Piotrowski, T., Żygierewicz, J., and Suffczyński, P. (2013). Statistical Analysis of Sleep Spindle Occurrences. *PLoS One*, 8(4):e59318.

Paré, D., Lebel, E., and Lang, E. J. (1997). Differential Impact of Miniature Synaptic Potentials on the Soma and Dendrites of Pyramidal Neurons In Vivo. *Journal of Neurophysiology*, 78(3):1735–1739.

Parga, N. and Abbott, L. F. (2007). Network model of spontaneous activity exhibiting synchronous transitions between up and down states. *Frontiers in Neuroscience*, 1(1):57.

Patel, A. J., Honoré, E., Lesage, F., Fink, M., Romey, G., and Lazdunski, M. (1999). Inhalational anesthetics activate two-pore-domain background K + channels. *Nature Neuroscience*, 2(5):422–426.

Perez Velazquez, J., Galán, R., Dominguez, L., Leshchenko, Y., Lo, S., Belkas, J., and Erra, R. (2007). Phase response curves in the characterization of epileptiform activity. *Physical Review E*, 76(6).

Peter-Derex, L., Comte, J.-C., Mauguière, F., and Salin, P. A. (2012). Density and Frequency Caudo-Rostral Gradients of Sleep Spindles Recorded in the Human Cortex. *SLEEP*.

Peyrache, A., Battaglia, F. P., and Destexhe, A. (2011). Inhibition recruitment in prefrontal cortex during sleep spindles and gating of hippocampal inputs. *Proceedings of the National Academy of Sciences*, 108(41):17207–17212.

Peyrache, A., Dehghani, N., Eskandar, E. N., Madsen, J. R., Anderson, W. S., Donoghue, J. A., Hochberg, L. R., Halgren, E., Cash, S. S., and Destexhe, A. (2012). Spatiotemporal dynamics of neocortical excitation and inhibition during human sleep. *Proceedings of the National Academy of Sciences*, 109(5):1731–1736.

Peyrache, A., Khamassi, M., Benchenane, K., Wiener, S. I., and Battaglia, F. P. (2009). Replay of rule-learning related neural patterns in the prefrontal cortex during sleep. *Nature Neuroscience*, 12(7):919–926.

Phillips, A. and Robinson, P. (2007). A quantitative model of sleep-wake dynamics based on the physiology of the brainstem ascending arousal system. *Journal of Biological Rhythms*, 22(2):167–179.

Piantoni, G., Astill, R. G., Raymann, R. J., Vis, J. C., Coppens, J. E., and Van Someren, E. J. (2013). Modulation of gamma and spindle-range power by slow oscillations in scalp sleep EEG of children. *International Journal of Psychophysiology*, 89(2):252–258.

Plihal, W. and Born, J. (1997). Effects of Early and Late Nocturnal Sleep on Declarative and Procedural Memory. *Journal of Cognitive Neuroscience*, 9(4):534–547.

Polack, P.-O., Friedman, J., and Golshani, P. (2013). Cellular mechanisms of brain state–dependent gain modulation in visual cortex. *Nature Neuroscience*, 16(9):1331–1339.

Poskanzer, K. E. and Yuste, R. (2011). Astrocytic Regulation of Cortical UP States. *Proceedings of the National Academy of Sciences*, 108(45):18453–18458.

Poskanzer, K. E. and Yuste, R. (2016). Astrocytes regulate cortical state switching in vivo. *Proceedings of the National Academy of Sciences*, 113(19):E2675–E2684.

Radman, T., Su, Y., An, J. H., Parra, L. C., and Bikson, M. (2007). Spike Timing Amplifies the Effect of Electric Fields on Neurons: Implications for Endogenous Field Effects. *The Journal of Neuroscience*, 27(11):3030 –3036.

Rasch, B. and Born, J. (2013). About Sleep's Role in Memory. *Physiological Reviews*, 93(2):681–766.

Reato, D., Rahman, A., Bikson, M., and Parra, L. C. (2010). Low-Intensity Electrical Stimulation Affects Network Dynamics by Modulating Population Rate and Spike Timing. *The Journal of Neuroscience*, 30(45):15067.

Reig, R. and Sanchez-Vives, M. V. (2007). Synaptic transmission and plasticity in an active cortical network. *PLoS One*, 2(8):670.

Rempe, M. J., Best, J., and Terman, D. (2009). A mathematical model of the sleep/wake cycle. *Journal of Mathematical Biology*, 60(5):615–644.

Reyes, A., Lujan, R., Rozov, A., Burnashev, N., Somogyi, P., and Sakmann, B. (1998). Target-cell-specific facilitation and depression in neocortical circuits. *Nature Neuroscience*, 1(4):279–285.

Rigas, P. and Castro-Alamancos, M. A. (2007). Thalamocortical Up States: Differential Effects of Intrinsic and Extrinsic Cortical Inputs on Persistent Activity. *J. Neurosci.*, 27(16):4261–4272.

Robinson, P. (2011). Neural field theory of synaptic plasticity. *Journal of Theoretical Biology*, 285(1):156–163.

Robinson, P. A., Rennie, C. J., and Rowe, D. L. (2002). Dynamics of large-scale brain activity in normal arousal states and epileptic seizures. *Physical Review E*, 65(4).

Robinson, P. A., Rennie, C. J., and Wright, J. J. (1997). Propagation and stability of waves of electrical activity in the cerebral cortex. *Physical Review E*, 56(1):826.

Rosanova, M. and Ulrich, D. (2005). Pattern-Specific Associative Long-Term Potentiation Induced by a Sleep Spindle-Related Spike Train. *The Journal of Neuroscience*, 25(41):9398–9405.

Roux, F., Wibral, M., Singer, W., Aru, J., and Uhlhaas, P. J. (2013). The Phase of Thalamic Alpha Activity Modulates Cortical Gamma-Band Activity: Evidence from Resting-State MEG Recordings. *The Journal of Neuroscience*, 33(45):17827–17835.

REFERENCES

Rovó, Z., Mátyás, F., Barthó, P., Slézia, A., Lecci, S., Pellegrini, C., Astori, S., Dávid, C., Hangya, B., Lüthi, A., and Acsády, L. (2014). Phasic, Nonsynaptic GABA-A Receptor-Mediated Inhibition Entrains Thalamocortical Oscillations. *The Journal of Neuroscience*, 34(21):7137–7147.

Roxin, A. and Fusi, S. (2013). Efficient Partitioning of Memory Systems and Its Importance for Memory Consolidation. *PLoS Computational Biology*, 9(7):e1003146.

Rudolph, M., Pospischil, M., Timofeev, I., and Destexhe, A. (2007). Inhibition Determines Membrane Potential Dynamics and Controls Action Potential Generation in Awake and Sleeping Cat Cortex. *J. Neurosci.*, 27(20):5280–5290.

Ruiz-Mejias, M., Ciria-Suarez, L., Mattia, M., and Sanchez-Vives, M. V. (2011). Slow and fast rhythms generated in the cerebral cortex of the anesthetized mouse. *Journal of Neurophysiology*, 106(6):2910–2921.

Sakata, S. and Harris, K. D. (2009). Laminar Structure of Spontaneous and Sensory-Evoked Population Activity in Auditory Cortex. *Neuron*, 64(3):404–418.

Salami, M., Itami, C., Tsumoto, T., and Kimura, F. (2003). Change of conduction velocity by regional myelination yields constant latency irrespective of distance between thalamus and cortex. *Proceedings of the National Academy of Sciences*, 100(10):6174–6179.

Sanchez-Vives, M., Reig, R., Winograd, M., and Descalzo, V. (2007). An active cortical network in vitro. *Mechanisms of spontaneous active states in neocortex*, pages 23–44.

Sanchez-Vives, M. V., Descalzo, V. F., Reig, R., Figueroa, N. A., Compte, A., and Gallego, R. (2008). Rhythmic spontaneous activity in the piriform cortex. *Cerebral Cortex*, 18(5):1179.

Sanchez-Vives, M. V., Mattia, M., Compte, A., Perez-Zabalza, M., Winograd, M., Descalzo, V. F., and Reig, R. (2010). Inhibitory Modulation of Cortical Up States. *Journal of Neurophysiology*, 104(3):1314–1324.

Sanchez-Vives, M. V. and McCormick, D. A. (2000). Cellular and network mechanisms of rhythmic recurrent activity in neocortex. *Nature neuroscience*, 3(10):1027–1034.

Särkkä, S. (2013). *Bayesian Filtering and Smoothing*, volume 3. Cambridge University Press.

Schabus, M., Gruber, G., Parapatics, S., Sauter, C., Klosch, G., Anderer, P., Klimesch, W., Saletu, B., and Zeitlhofer, J. (2004). Sleep spindles and their significance for declarative memory consolidation. *Sleep*, 27(8):1479–1485.

Schwindt, P. C., Spain, W. J., and Crill, W. E. (1989). Long-lasting reduction of excitability by a sodium-dependent potassium current in cat neocortical neurons. *Journal of Neurophysiology*, 61(2):233–244.

Schwindt, P. C., Spain, W. J., Foehring, R. C., Chubb, M. C., and Crill, W. E. (1988a). Slow conductances in neurons from cat sensorimotor cortex in vitro and their role in slow excitability changes. *Journal of Neurophysiology*, 59(2):450–467.

Schwindt, P. C., Spain, W. J., Foehring, R. C., Stafstrom, C. E., Chubb, M. C., and Crill, W. E. (1988b). Multiple potassium conductances and their functions in neurons from cat sensorimotor cortex in vitro. *Journal of Neurophysiology*, 59(2):424–449.

Seamari, Y., Narváez, J. A., Vico, F. J., Lobo, D., and Sanchez-Vives, M. V. (2007). Robust Off- and Online Separation of Intracellularly Recorded Up and Down Cortical States. *PLoS ONE*, 2(9):e888.

Sherman, S. M. (2005). Thalamic relays and cortical functioning. In *Progress in Brain Research*, volume 149, pages 107–126. Elsevier.

Sheroziya, M. and Timofeev, I. (2014). Global Intracellular Slow-Wave Dynamics of the Thalamocortical System. *The Journal of Neuroscience*, 34(26):8875–8893.

Shilnikov, A. and Cymbalyuk, G. (2005). Transition between Tonic Spiking and Bursting in a Neuron Model via the Blue-Sky Catastrophe. *Physical Review Letters*, 94(4).

Shu, Y., Hasenstaub, A., and McCormick, D. A. (2003). Turning on and off recurrent balanced cortical activity. *Nature*, 423(6937):288–293.

Silberberg, G. and Markram, H. (2007). Disynaptic Inhibition between Neocortical Pyramidal Cells Mediated by Martinotti Cells. *Neuron*, 53(5):735–746.

Sirota, A., Csicsvari, J., Buhl, D., and Buzsáki, G. (2003). Communication between neocortex and hippocampus during sleep in rodents. *Proceedings of the National Academy of Sciences of the United States of America*, 100(4):2065 –2069.

Slezia, A., Hangya, B., Ulbert, I., and Acsady, L. (2011). Phase Advancement and Nucleus-Specific Timing of Thalamocortical Activity during Slow Cortical Oscillation. *Journal of Neuroscience*, 31(2):607–617.

Smeal, R. M., Ermentrout, G. B., and White, J. A. (2010). Phase-response curves and synchronized neural networks. *Philosophical Transactions of the Royal Society B: Biological Sciences*, 365(1551):2407–2422.

Soltesz, I., Lightowler, S., Leresche, N., Jassik-Gerschenfeld, D., Pollard, C. E., and Crunelli, V. (1991). Two inward currents and the transformation of low-frequency oscillations of rat and cat thalamocortical cells. *The Journal of Physiology*, 441(1):175–197.

Soma, S., Shimegi, S., Osaki, H., and Sato, H. (2012). Cholinergic modulation of response gain in the primary visual cortex of the macaque. *Journal of Neurophysiology*, 107(1):283–291.

Sotero, R. C. and Trujillo-Barreto, N. J. (2008). Biophysical model for integrating neuronal activity, EEG, fMRI and metabolism. *NeuroImage*, 39(1):290–309.

Squire, L. R. (2009). The Legacy of Patient H.M. for Neuroscience. *Neuron*, 61(1):6–9.

Staresina, B. P., Bergmann, T. O., Bonnefond, M., van der Meij, R., Jensen, O., Deuker, L., Elger, C. E., Axmacher, N., and Fell, J. (2015). Hierarchical nesting of slow oscillations, spindles and ripples in the human hippocampus during sleep. *Nature Neuroscience*, 18(11):1679–1686.

Steriade, M. (2003). The corticothalamic system in sleep. *Frontiers in Bioscience*, 8:d878–d899.

Steriade, M. (2004). Acetylcholine systems and rhythmic activities during the waking–sleep cycle. In *Progress in Brain Research*, volume 145, pages 179–196. Elsevier.

Steriade, M. (2006). Grouping of brain rhythms in corticothalamic systems. *Neuroscience*, 137(4):1087–1106.

Steriade, M. and Amzica, F. (1998). Slow sleep oscillation, rhythmic K-complexes, and their paroxysmal developments. *Journal of Sleep Research*, 7(S1):30–35.

REFERENCES

Steriade, M., Contreras, D., Amzica, F., and Timofeev, I. (1996). Synchronization of fast (30-40 Hz) spontaneous oscillations in intrathalamic and thalamocortical networks. *The Journal of Neuroscience*, 16(8):2788–2808.

Steriade, M., Contreras, D., Dossi, R. C., and Nunez, A. (1993a). The slow (< 1 Hz) oscillation in reticular thalamic and thalamocortical neurons: Scenario of sleep rhythm generation in interacting thalamic and neocortical networks. *The Journal of Neuroscience*, 13(8):3284–3299.

Steriade, M. and Deschenes, M. (1984). The thalamus as a neuronal oscillator. *Brain Research Reviews*, 8(1):1–63.

Steriade, M., Deschenes, M., Domich, L., and Mulle, C. (1985). Abolition of spindle oscillations in thalamic neurons disconnected from nucleus reticularis thalami. *Journal of Neurophysiology*, 54(6):1473–1497.

Steriade, M., Domich, L., Oakson, G., and Deschenes, M. (1987). The deafferented reticular thalamic nucleus generates spindle rhythmicity. *Journal of Neurophysiology*, 57(1):260–273.

Steriade, M., Dossi, R. C., and Nunez, A. (1991). Network modulation of a slow intrinsic oscillation of cat thalamocortical neurons implicated in sleep delta waves: Cortically induced synchronization and brainstem cholinergic suppression. *The Journal of Neuroscience*, 11(10):3200–3217.

Steriade, M., Gloor, P., Llinás, R. R., Lopes da Silva, F. H., and Mesulam, M. M. (1990). Basic mechanisms of cerebral rhythmic activities. *Electroencephalography and Clinical Neurophysiology*, 76(6):481–508.

Steriade, M. and Llinás, R. R. (1988). The functional states of the thalamus and the associated neuronal interplay. *Physiological Reviews*, 68(3):649–742.

Steriade, M., Nunez, A., and Amzica, F. (1993b). A novel slow (< 1 Hz) oscillation of neocortical neurons in vivo: Depolarizing and hyperpolarizing components. *The Journal of Neuroscience*, 13(8):3252–3265.

Steriade, M., Timofeev, I., and Grenier, F. (2001). Natural Waking and Sleep States: A View From Inside Neocortical Neurons. *Journal of Neurophysiology*, 85(5):1969–1985.

Steyn-Ross, D. A., Steyn-Ross, M. L., Sleigh, J. W., Wilson, M. T., Gillies, I. P., and Wright, J. J. (2005). The Sleep Cycle Modelled as a Cortical Phase Transition. *Journal of Biological Physics*, 31(3-4):547–569.

Steyn-Ross, M. (2005). Proposed mechanism for learning and memory erasure in a white-noise-driven sleeping cortex. *Physical Review E*, 72(6).

Steyn-Ross, M. L., Steyn-Ross, D. A., and Sleigh, J. W. (2013). Interacting Turing-Hopf Instabilities Drive Symmetry-Breaking Transitions in a Mean-Field Model of the Cortex: A Mechanism for the Slow Oscillation. *Physical Review X*, 3(2).

Steyn-Ross, M. L., Steyn-Ross, D. A., Sleigh, J. W., and Liley, D. T. J. (1999). Theoretical electroencephalogram stationary spectrum for a white-noise-driven cortex: Evidence for a general anesthetic-induced phase transition. *Physical Review E*, 60(6):7299.

Steyn-Ross, M. L., Steyn-Ross, D. A., Sleigh, J. W., and Wilcocks, L. C. (2001). Toward a theory of the general-anesthetic-induced phase transition of the cerebral cortex. I. A thermodynamics analogy. *Physical Review E*, 64(1):011917.

Suffczynski, P., Kalitzin, S., and Lopes Da Silva, F. H. (2004). Dynamics of non-convulsive epileptic phenomena modeled by a bistable neuronal network. *Neuroscience*, 126(2):467–484.

Sullivan, D., Mizuseki, K., Sorgi, A., and Buzsaki, G. (2014). Comparison of Sleep Spindles and Theta Oscillations in the Hippocampus. *Journal of Neuroscience*, 34(2):662–674.

Swadlow, H. A. (2000). Information flow along neocortical axons. In *Time and the Brain. Conceptual Advances in Brain Research.* Harwood Academic Publishers, Amsterdam.

Tabak, J., Rinzel, J., and Bertram, R. (2011). Quantifying the Relative Contributions of Divisive and Subtractive Feedback to Rhythm Generation. *PLoS Computational Biology*, 7(4):e1001124.

Talley, E. M. and Bayliss, D. A. (2002). Modulation of TASK-1 (Kcnk3) and TASK-3 (Kcnk9) Potassium Channels: Anesthetics and neurotransmitters share a molecular site of action. *Journal of Biological Chemistry*, 277(20):17733–17742.

Tamakawa, Y. (2005). A Quartet Neural System Model Orchestrating Sleep and Wakefulness Mechanisms. *Journal of Neurophysiology*, 95(4):2055–2069.

Tamminen, J., Ralph, M. A. L., and Lewis, P. A. (2013). The Role of Sleep Spindles and Slow-Wave Activity in Integrating New Information in Semantic Memory. *The Journal of Neuroscience*, 33(39):15376–15381.

Taub, A. H., Katz, Y., and Lampl, I. (2013). Cortical Balance of Excitation and Inhibition Is Regulated by the Rate of Synaptic Activity. *The Journal of Neuroscience*, 33(36):14359–14368.

Tewes, U. (1991). HAWIE–R: Hamburg–Wechsler Intelligence Test for Adults: Handbook and testing instructions. *Stuttgart, Germany: Huber*.

Thomson, A. M., Deuchars, J., and West, D. C. (1993). Single axon excitatory postsynaptic potentials in neocortical interneurons exhibit pronounced paired pulse facilitation. *Neuroscience*, 54(2):347–360.

Thurley, K., Senn, W., and Lüscher, H.-R. (2008). Dopamine Increases the Gain of the Input-Output Response of Rat Prefrontal Pyramidal Neurons. *Journal of Neurophysiology*, 99(6):2985–2997.

Timmons, S., Geisert, E., Stewart, A., Lorenzon, N., and Foehring, R. (2004). $a2$-Adrenergic receptor-mediated modulation of calcium current in neocortical pyramidal neurons. *Brain Research*, 1014(1-2):184–196.

Timofeev, I. and Bazhenov, M. (2005). Mechanisms and biological role of thalamocortical oscillations. *Trends in chronobiology research*, pages 1–47.

Timofeev, I., Bazhenov, M., Sejnowski, T. J., and Steriade, M. (2001a). Contribution of intrinsic and synaptic factors in the desynchronization of thalamic oscillatory activity. *Thalamus & Related Systems*, 1(1):53–69.

Timofeev, I., Grenier, F., Bazhenov, M., Sejnowski, T., and Steriade, M. (2000). Origin of Slow Cortical Oscillations in Deafferented Cortical Slabs. *Cerebral Cortex*, 10(12):1185–1199.

Timofeev, I., Grenier, F., and Steriade, M. (2001b). Disfacilitation and active inhibition in the neocortex during the natural sleep-wake cycle: An intracellular study. *Proceedings of the National Academy of Sciences*, 98(4):1924–1929.

REFERENCES

Timofeev, I. and Steriade, M. (1996). Low-frequency rhythms in the thalamus of intact-cortex and decorticated cats. *Journal of Neurophysiology*, 76(6):4152–4168.

Tononi, G. and Cirelli, C. (2014). Sleep and the Price of Plasticity: From Synaptic and Cellular Homeostasis to Memory Consolidation and Integration. *Neuron*, 81(1):12–34.

Tort, A. B. L., Komorowski, R., Eichenbaum, H., and Kopell, N. (2010). Measuring Phase-Amplitude Coupling Between Neuronal Oscillations of Different Frequencies. *Journal of Neurophysiology*, 104(2):1195–1210.

Traub, R. D., Contreras, D., Cunningham, M. O., Murray, H., LeBeau, F. E. N., Roopun, A., Bibbig, A., Wilent, W. B., Higley, M. J., and Whittington, M. A. (2005). Single-Column Thalamocortical Network Model Exhibiting Gamma Oscillations, Sleep Spindles, and Epileptogenic Bursts. *Journal of Neurophysiology*, 93(4):2194–2232.

Tsodyks, M., Pawelzik, K., and Markram, H. (1998). Neural Networks with Dynamic Synapses. *Neural Computation*, 10(4):821–835.

Ulrich, D. and Huguenard, J. R. (1997). GABAA-receptor-mediated rebound burst firing and burst shunting in thalamus. *Journal of neurophysiology*, 78(3):1748–1751.

Valencia, M., Artieda, J., Bolam, J. P., and Mena-Segovia, J. (2013). Dynamic Interaction of Spindles and Gamma Activity during Cortical Slow Oscillations and Its Modulation by Subcortical Afferents. *PLoS One*, 8(7):e67540.

van Vreeswijk, C. and Sompolinsky, H. (1998). Chaotic balanced state in a model of cortical circuits. *Neural computation*, 10(6):1321–1371.

Varkonyi, P. L. and Holmes, P. (2008). On Synchronization and Traveling Waves in Chains of Relaxation Oscillators with an Application to Lamprey CPG. *SIAM Journal on Applied Dynamical Systems*, 7:766.

Verleger, R., Rose, M., Wagner, U., Yordanova, J., and Kolev, V. (2013). Insights into sleep's role for insight: Studies with the number reduction task. *Advances in Cognitive Psychology*, 9(4):160–172.

Vijayan, S., Hale, G. J., Moore, C. I., Brown, E. N., and Wilson, M. (2010). Activity in the Barrel Cortex During Active Behavior and Sleep. *Journal of Neurophysiology*, 103(4):2074–2084.

Villablanca, J. (1972). Sleep-wakefulness, EEG and behavioral studies of chronic cats without the thalamus: The"athalamic" cat. *Archives Italiennes de Biologie*, 110(3):383–411.

Volgushev, M., Chauvette, S., Mukovski, M., and Timofeev, I. (2006). Precise long-range synchronization of activity and silence in neocortical neurons during slow-wave sleep. *Journal of Neuroscience*, 26(21):5665.

Volgushev, M., Chauvette, S., and Timofeev, I. (2011). Long-range correlation of the membrane potential in neocortical neurons during slow oscillation. In *Progress in Brain Research*, volume 193, pages 181–199. Elsevier.

Von Krosigk, M., Bal, T., and McCormick, D. A. (1993). Cellular mechanisms of a synchronized oscillation in the thalamus. *Science*, 261:361–361.

Voss, H. U., Timmer, J., and Kurths, J. (2004). Nonlinear dynamical system identification from uncertain and indirect measurements. *International Journal of Bifurcation and Chaos*, 14(06):1905–1933.

Vyazovskiy, V. V. and Harris, K. D. (2013). Sleep and the single neuron: The role of global slow oscillations in individual cell rest. *Nature Reviews Neuroscience*, 14(6):443–451.

Vyazovskiy, V. V., Olcese, U., Lazimy, Y. M., Faraguna, U., Esser, S. K., Williams, J. C., Cirelli, C., and Tononi, G. (2009). Cortical Firing and Sleep Homeostasis. *Neuron*, 63(6):865–878.

Walker, M. P. and Stickgold, R. (2004). Sleep-Dependent Learning and Memory Consolidation. *Neuron*, 44(1):121–133.

Wan, E. A. and Van Der Merwe, R. (2000). The unscented Kalman filter for nonlinear estimation. In *Adaptive Systems for Signal Processing, Communications, and Control Symposium*, pages 153–158. IEEE.

Wang, Q., Kulkarni, S. R., and Verdu, S. (2009). Divergence Estimation for Multidimensional Densities Via k-Nearest-Neighbor Distances. *IEEE Transactions on Information Theory*, 55(5):2392–2405.

Wang, X.-J. (2003). Adaptation and Temporal Decorrelation by Single Neurons in the Primary Visual Cortex. *Journal of Neurophysiology*, 89(6):3279–3293.

Waters, J. and Helmchen, F. (2006). Background synaptic activity is sparse in neocortex. *The Journal of Neuroscience*, 26(32):8267.

Watson, B. O., MacLean, J. N., and Yuste, R. (2008). UP States Protect Ongoing Cortical Activity from Thalamic Inputs. *PLoS One*, 3(12):e3971.

Watson, D., Clark, L. A., and Tellegen, A. (1988). Development and validation of brief measures of positive and negative affect: The PANAS scales. *Journal of Personality and Social Psychology*, 54(6):1063.

Wei, Y., Krishnan, G. P., and Bazhenov, M. (2016). Synaptic Mechanisms of Memory Consolidation during Sleep Slow Oscillations. *The Journal of Neuroscience*, 36(15):4231–4247.

Weigenand, A., Martinetz, T., and Claussen, J. C. (2012). The phase response of the cortical slow oscillation. *Cognitive Neurodynamics*, 6(4):367–375.

Weigenand, A., Mölle, M., Werner, F., Martinetz, T., and Marshall, L. (2016). Timing matters: Open-loop stimulation does not improve overnight consolidation of word pairs in humans. *European Journal of Neuroscience*, 44(6):2357–2368.

Weigenand, A., Schellenberger Costa, M., Ngo, H.-V. V., Claussen, J. C., and Martinetz, T. (2014). Characterization of K-Complexes and Slow Wave Activity in a Neural Mass Model. *PLoS Computational Biology*, 10(11):e1003923.

Wendling, F., Bartolomei, F., Bellanger, J. J., and Chauvel, P. (2002). Epileptic fast activity can be explained by a model of impaired GABAergic dendritic inhibition. *European Journal of Neuroscience*, 15(9):1499–1508.

Wennberg, R. (2010). Intracranial cortical localization of the human K-complex. *Clinical Neurophysiology*, 121(8):1176–1186.

Werchan, D. M. and Gómez, R. L. (2014). Wakefulness (Not Sleep) Promotes Generalization of Word Learning in 2.5-Year-Old Children. *Child Development*, 85(2):429–436.

Williams, S. R., Tóth, T. I., Turner, J. P., Hughes, S. W., and Crunelli, V. (1997). The 'window' component of the low threshold Ca2+ current produces input signal amplification and bistability in cat and rat thalamocortical neurones. *The Journal of Physiology*, 505(3):689–705.

REFERENCES

Wilson, H. R. and Cowan, J. D. (1973). A mathematical theory of the functional dynamics of cortical and thalamic nervous tissue. *Kybernetik*, 13(2):55–80.

Wilson, M. and McNaughton, B. (1994). Reactivation of hippocampal ensemble memories during sleep. *Science*, 265(5172):676.

Wilson, M. T., Barry, M., Reynolds, J. N. J., Crump, W. P., Steyn-Ross, D. A., Steyn-Ross, M. L., and Sleigh, J. W. (2010). An analysis of the transitions between down and up states of the cortical slow oscillation under urethane anaesthesia. *Journal of Biological Physics*, 36(3):245–259.

Wilson, M. T., Steyn-Ross, D. A., Sleigh, J. W., Steyn-Ross, M. L., Wilcocks, L. C., and Gillies, I. P. (2006). The K-complex and slow oscillation in terms of a mean-field cortical model. *Journal of Computational Neuroscience*, 21(3):243–257.

Wilson, M. T., Steyn-Ross, M. L., Steyn-Ross, D. A., and Sleigh, J. W. (2005). Predictions and simulations of cortical dynamics during natural sleep using a continuum approach. *Physical Review E*, 72(5):051910.

Winocur, G. and Moscovitch, M. (2011). Memory Transformation and Systems Consolidation. *Journal of the International Neuropsychological Society*, 17(05):766–780.

Yaroush, R., Sullivan, M. J., and Ekstrand, B. R. (1971). Effect of sleep on memory: II. Differential effect of the first and second half of the night. *Journal of Experimental Psychology*, 88(3):361–366.

Yu, Y.-Q., Xiong, Y., Chan, Y.-S., and He, J. (2004). In vivo intracellular responses of the medial geniculate neurones to acoustic stimuli in anaesthetized guinea pigs. *The Journal of Physiology*, 560(1):191–205.

Zandt and Visser (2013). A neural mass model based on single cell dynamics to model pathophysiology.

Zar, J. H. (1999). Biostatistical analysis. 4th. *Upper Saddle River, NJ: Prentice Hall*, 1:389–94.

Zhang, Z.-w. and Arsenault, D. (2005). Gain modulation by serotonin in pyramidal neurones of the rat prefrontal cortex. *The Journal of Physiology*, 566(2):379–394.

Żygierewicz, J., Blinowska, K. J., Durka, P. J., Szelenberger, W., Niemcewicz, S., and Androsiuk, W. (1999). High resolution study of sleep spindles. *Clinical Neurophysiology*, 110(12):2136–2147.

Żygierewicz, J., Suffczyński, P., and Blinowska, K. (2001). A model of sleep spindles generation. *Neurocomputing*, 38–40:1619–1625.